Jahresbericht
Annual Report

2024

Leibniz-Institut
für Festkörper- und
Werkstoffforschung
Dresden

Umschlagfoto: Jürgen Lösel

Impressum
Imprint

Annual Report 2024

- Preliminary Report -

Herausgegeben durch das:
Leibniz-Institut für Festkörper- und
Werkstoffforschung Dresden
Helmholtzstraße 20, 01069 Dresden, Germany

www.ifw-dresden.de

Inhaltliche Verantwortung:
Prof. Dr. Bernd Büchner

Redaktion und Gestaltung:
Patricia Bäuchler

Bildnachweise:
IFW Dresden, sofern nicht anders angegeben

Druck:
ARNOLD group, Großbeeren

Dresden, März 2025

Liebe Leserinnen und Leser,

Unser wissenschaftlicher Alltag ist geprägt vom Austausch ungleicher Sichtweisen. Selbst vermeintlich klare Messwerte lassen sich unterschiedlich interpretieren oder sich in ihrer Methodik hinterfragen. Es ist dieses interdisziplinäre und manchmal auch konträre Denken, welches uns letztlich zum Erkenntnisgewinn führt und neue Perspektiven und Handlungsfelder aufzeigt. Das geschieht, wenn wir bereit sind, kritische Nachfragen als annehmbare Option wahrzunehmen. Damit schaffen wir eine stabile Grundlage, auf der neuartige Theorien und schließlich Innovationen aufbauen können. Lassen Sie uns für eine lebenswerte Zukunft auch gesellschaftlich mit dieser Offenheit für- und miteinander agieren.
Viel Freude beim Entdecken der Themen, die uns im vergangen Jahr beschäftigt haben.

Dear readers,

Our everyday scientific life is characterized by the exchange of different points of view.
Even supposedly clear measurements can be interpreted differently or their methodology questioned. It is this interdisciplinary and sometimes contrary thinking that ultimately leads us to gain knowledge and reveals new perspectives and fields of action. This happens when we are prepared to accept critical questions as an acceptable option. In this way, we create a stable foundation on which new theories and ultimately innovations can be built.
Let us also act socially with this openness for and with each other for a future worth living.
We hope you enjoy discovering the issues that concerned us last year.

Mit herzlichen Grüßen / Best wishes

Juliane Schmidt, Kaufmännische Direktorin und Prof. Dr. Bernd Büchner, Wissenschaftlicher Direktor.
Juliane Schmidt, Administrative Director and Prof. Dr. Bernd Büchner, Scientific Director.

Foto: Jürgen Lösel

Annual Report 2024

Inhalt
Content

Foto: Caspin Ivent Mokry

Jahresrückblick 2024

Das IFW Dresden kann auf ein sehr positives Jahr 2024 zurückblicken: es bot viele neue Möglichkeiten und Chancen, die richtungsweisend sind für eine weitere erfolgreiche Entwicklung des Instituts. Dies betrifft viele Bereiche, angefangen von der Neufokussierung des Forschungsprogramms, über Investitionen in die Forschungsinfrastruktur und die Vorbereitung für die Realisierung des Neubaus, bis hin zur Etablierung neue lokaler und internationaler Kooperationen.

2024 war das erste Jahr seit fast einem Jahrzehnt, in dem das Direktorium des IFW Dresden vollzählig besetzt war. Am 1. Januar 2024 hat Frau Prof. Dr. Anjana Devi ihre Tätigkeit als neue Direktorin des IFW-Instituts für Materialchemie (IMC) aufgenommen. Im Rahmen einer gemeinsamen Berufung wurde sie als Professorin für Materialchemie an die Fakultät Chemie und Lebensmittelchemie der TU Dresden berufen. Frau Prof. Devi ist eine führende Wissenschaftlerin auf dem Gebiet der Synthese dünner Schichten mittels Präkursor-Chemie und besitzt hohe internationale Sichtbarkeit auf dem Gebiet der skalierbaren Atomlagenabscheidung (ALD). Ihr strategisches Ziel ist es, das IFW innerhalb der Leibniz-Gemeinschaft und des Technologiestandorts Sachsen als zentralen Akteur im Bereich der ALD zu etablieren und damit Grundlagenforschung, Technologieentwicklung und Hersteller miteinander zu vernetzen. Diese Themen passen perfekt zum IFW-Forschungsprogramm und bringen neue Forschungsrichtungen und Vernetzungsmöglichkeiten ein.

Review of 2024

The IFW Dresden can look back on a very positive year 2024: it offered many new possibilities and opportunities that will set the course for the further successful development of the institute. This applies to many areas, from refocusing the research program, investing in research infrastructure and preparing for the construction of the new building, to establishing new local and international collaborations.

2024 was the first year in almost a decade in which the IFW Board of Directors was fully staffed. On January 1, 2024, Prof. Dr. Anjana Devi took up her position as the new Director of the IFW Institute for Materials Chemistry (IMC). As part of a joint appointment, she was appointed Professor of Materials Chemistry at the Faculty of Chemistry and Food Chemistry at TU Dresden. Prof. Devi is a leading scientist in the field of thin film synthesis using precursor chemistry and has high international visibility in the field of scalable atomic layer deposition (ALD).
Her strategic goal is to establish the IFW as a central player in the field of ALD within the Leibniz Association and the technology location Saxony, and thus to network basic research, technology development and manufacturers. These topics fit perfectly with the IFW research program and bring in new research directions and networking opportunities.

Links: Ein starkes Zeichen für den Wert der Demokratie und friedliches Miteinander setzte am 25. Mai 2024 die Veranstaltung "Gemeinsam für Demokratie", die von Dresdens Wissenschaft und Kultur initiiert wurde. Aus vier verschiedenen Richtungen kommend, liefen die Menschen mit Transparenten gemeinsam zum Dresdner Altmarkt. Rund 2.500 Menschen beteiligten sich an diesem Fest der Demokratie.
Left: The "United for Democracy" event, initiated by Dresden's science and culture community, provided a strong signal for the value of democracy and peaceful coexistence on 25 May 2024. Participants converged on Dresden's Altmarkt, coming from four different directions and carrying banners. This event was attended by around 2,500 people.

Im Rahmen eines Direktoriums-Retreats und eine dreitägigen Programmklausur mit allen verantwortlichen Wissenschaftlerinnen und Wissenschaftlern wurde das IFW-Forschungsprogramm aktualisiert und mit Blick auf die Leibniz-Evaluierung 2028 neu ausgerichtet.
Insbesondere auf dem Gebiet der zweidimensionalen Materialien und bei der Entwicklung nachhaltiger Elektronik- und Energiewandlungstechnologien hat das IFW-Forschungsprogramm starke neue Impulse erhalten. Dies manifestiert sich unter anderem im neuen Slogan „Quantum – Function – Sustainability“, der das Wesentliche des IFW-Forschungsprogramms transportieren soll: Im Mittelpunkt stehen Materialien mit physikalischen oder chemischen Eigenschaften, die aufgrund quantenmechanischer Phänomene oder aufgrund ihrer geringen Dimensionalität noch nicht grundlegend verstanden sind und die eine zukünftige Anwendung als Funktionsmaterialien in nachhaltigen Technologien versprechen.

As part of a Board of Directors retreat and a three-day program meeting with all responsible scientists, the IFW research program was updated and realigned with a view to the Leibniz Evaluation in 2028.

The IFW research program has received strong new impetus, particularly in the field of two-dimensional materials and in the development of sustainable electronics and energy conversion technologies. This is reflected, among other things, in the new slogan “Quantum - Function - Sustainability”, which is intended to express the essence of the IFW research program: The focus is on materials with physical or chemical properties that are not yet fundamentally understood due to quantum mechanical phenomena or due to their low dimensionality and which promise future application as functional materials in sustainable technologies.

Im Januar 2024 konnte der wissenschaftliche Direktor des IFW Dresden, Professor Bernd Büchner, die neue Direktorin des IFW-Instituts für Materialchemie, Frau Professorin Anjana Devi, im Haus begrüßen. Ihr Arbeitsbereich umfasst sechs unterschiedliche Arbeitsgruppen, die sich sowohl intern als auch extern durch eine starke interdisziplinäre Zusammenarbeit auszeichnen. Ihre Forschung konzentriert sich auf die Synthese und Untersuchung dünner Schichten und der Methode der Atomlagenabscheidung (ALD). Anjana Devi hält zeitgleich die Professur für Materialchemie an der Technischen Universität Dresden.
In January 2024, the Scientific Director of the IFW Dresden, Professor Bernd Büchner, welcomed the new Director of the IFW Institute of Materials Chemistry, Professor Anjana Devi, to the Institute. Her department consists of six different research groups, which are characterised by strong interdisciplinary cooperation both internally and externally. Her research focuses on the synthesis and characterisation of thin films and atomic layer deposition (ALD). Anjana Devi also holds the Chair of Materials Chemistry at the University of Technology in Dresden.

Foto: Jürgen Lösel

Als Leibniz-Institut erhält das IFW Dresden eine Grundfinanzierung in Höhe von etwa 35 Millionen Euro pro Jahr von Bund und Ländern. Zusätzlich eingeworbene Drittmittel stellen nicht nur eine wesentliche Erweiterung dieses Budgets dar, sondern sind ein wichtiger Maßstab für unsere Leistungs- und Wettbewerbsfähigkeit. Mit der weiteren Steigerung der Drittmitteleinwerbungen und dem Erreichen der Marke von 15 Millionen Euro für die Jahresscheibe 2024 haben wir diese erneut unter Beweis gestellt. Darüber hinaus spiegeln die Drittmittelprojekte auch unsere Forschungsschwerpunkte und strategischen Kooperationen wider. Besonders hervorzuheben ist die Bewilligung des deutsch-ukrainischen Exzellenzzentrums für Quantenmaterialien GU-QuMat im Rahmen einer BMBF-Ausschreibung. Das Projekt Gu-QuMat wurde gemeinsam mit drei weiteren Projekten für die Förderung von deutsch-ukrainischen Exzellenzkernen ausgewählt. Diese sollen die Ukraine gezielt beim Wieder-

As a Leibniz Institute, the IFW Dresden receives basic funding of around 35 million euros per year from the federal and state governments. Additional third-party funding not only represents a significant expansion of this budget, but is also an important benchmark for our performance and competitiveness. We have once again demonstrated this by once again increasing our third-party funding and reaching the EUR 15 million mark for the 2024 annual funding round. In addition, the third-party funded projects also reflect our research priorities and strategic collaborations. Particularly noteworthy is the approval of a German-Ukrainian Center of Excellence for Quantum Materials GU-QuMat as part of a BMBF call for proposals. The Gu-QuMat project was selected together with three other projects for the funding of German-Ukrainian cores of excellence. These are intended to provide Ukraine with targeted support in rebuilding a functioning science system and will be funded by the

Gemeinsames Leibniz Lab in Kiew: Das Projekt GUQuMat wird vom IFW Dresden in Zusammenarbeit mit der Akademischen Universität Kiew geleitet und vom Bundesministerium für Bildung und Forschung (BMBF) gefördert. Quantentechnologien sind ein Schlüsselelement der Forschungsstrategien der EU, Deutschlands und der Ukraine. Mit dem Projekt soll zudem ein Beitrag zum Wiederaufbau und der Stabilisierung digitaler Infrastruktur in der Ukraine geleistet werden. Das Projekt umfasst Forschung, Bildung und Innovation im Bereich der Quantenmaterialien für Zukunftstechnologien.
Joint Leibniz Lab in Kyiv: The GUQuMat project is led by IFW Dresden in partnership with Kyiv Academic University and funded by the German Federal Ministry of Education and Research (BMBF). Quantum technologies are a key element of EU, German and Ukrainian research strategies and fit into the digitalisation agenda of the Ukrainian Recovery Plan. The project includes research, education and innovation in quantum materials for future technologies.

Foto: A. Kordyuk

aufbau eines funktionierenden Wissenschaftssystems unterstützen und werden vom BMBF für vier Jahre mit 2,5 Millionen Euro gefördert.
Im Rahmen des Leibniz-Wettbewerbs war das IFW 2024 mit dem Antrag auf eine Leibniz Junior Research Group erfolgreich. Frau Dr. Shu Zhang wird ab 2025 eine Nachwuchsgruppe zum Thema „Quantentransport in quasi-zweidimensionalen magnetischen Systemen“ aufbauen und leiten.

Eine wichtige strategische Säule unserer Drittmittelaktivität ist unser Engagement im Exzellenzcluster „Complexity and Topology in Quantum Matter” an der TU Dresden und an der Universität Würzburg (ct.qmat), das von 2019 bis 2025 im Rahmen der Exzellenzstrategie des Bundes gefördert wird. Das IFW hat sich intensiv in den Fortsetzungsantrag für ct.qmat eingebracht und an der Konzeption und Darstellung des Antrags mitgewirkt. Darüber hinaus ist das IFW maßgeblich an der Beantragung eines der neuen Exzellenzcluster der TU Dresden beteiligt: Der Clusterantrag „Responsible Electronics in Climate Change era“ (REC2) wird von Prof. Vaynzof koordi-

BMBF for four years with 2.5 million euros.
The IFW was successful in the Leibniz competition in 2024 with its application for a Leibniz Junior Research Group. From 2025, Dr. Shu Zhang will set up and lead a junior research group on the topic of “Quantum transport in quasi-two-dimensional magnetic systems”, which is based at the IFW's Theory Institute.

An important strategic element of our third-party funding activities is our involvement in the Cluster of Excellence “Complexity and Topology in Quantum Matter” at TU Dresden and the University of Würzburg (ct.qmat), which is being funded from 2019 to 2025 as part of the German government's Excellence Strategy. The IFW was involved intensively into the follow-up application for ct.qmat and played a significant role in the conception and presentation of the application. Furthermore, the IFW is heavily involved in the application for one of the new Cluster of Excellence at TU Dresden: The cluster proposal “Responsible Electronics in Climate Change era” (REC2) is

Im September fand die Sommerschule „Advanced Materials“ statt. Diese wurde von der Hochschule für Technik und Wirtschaft Dresden, dem Leibniz-Institut für Polymerforschung und dem IFW Dresden ausgerichtet. Gemeinsam möchten wir zukünftig die Ausbildung von Fachkräften auf dem Gebiet neuer Materialien vorantreiben. Ziel ist die Entwicklung neuer Lehrformate, bei denen die Einrichtungen ihre jeweiligen Kompetenzen einbringen.
The Advanced Materials Summer School took place in September. It was organized by the University of Applied Sciences Dresden, the Leibniz Institute of Polymer Research and the IFW Dresden. Together we want to promote the training of specialists in the field of new materials in the future. The aim is to develop new teaching formats in which the institutions contribute their respective expertise.

Foto: Sven Döring

niert, die seit 2023 eines der fünf Institute des IFW leitet. Im Jahr 2024 hat dieser Antrag erfolgreich die Hürde der Vorentscheidung genommen. Wir blicken nun gespannt auf die Bekanntgabe der Förderentscheidung zu den Exzellenzclustern am 22. Mai 2025 und hoffen sehr, dass die beiden Clusteranträge mit IFW-Beteiligung von jeweils drei PIs erfolgreich sein werden. Unabhängig von der Förderentscheidung zeigen diese Antragsaktivitäten, wie eng das IFW mit der TU Dresden verbunden ist und wie stark beide Einrichtungen von dieser Zusammenarbeit profitieren können.

Das IFW pflegt langjährige und intensive Kooperationsbeziehungen, sowohl mit lokalen als auch mit internationalen Partnern. Besonders eng und vielfältig ist die Zusammenarbeit mit der TU Dresden und der Bergakademie Freiberg, mit denen uns gemeinsame Berufungen verbinden. 2024 ist zu diesem Kreis eine weitere Hochschule dazugekommen: Mit der HTW Dresden wurde ein gemeinsames Berufungsverfahren für eine W2-Professur „Angewandte Forschungstechnik“ gestartet, um ab 2025 die Leitung des Bereichs

coordinated by Prof. Vaynzof, who has headed one of the five IFW institutes since 2023. In 2024, this application successfully passed the preliminary decision hurdle. We are now looking forward to the announcement of the funding decision on the Clusters of Excellence on May 22, 2025 and very much hope that the two cluster applications with IFW participation from three PIs each will be successful. Regardless of the funding decision, these application activities show how closely the IFW is linked to TU Dresden and how much both institutions can benefit from this collaboration.

The IFW maintains long-standing and very close cooperative relationships with both local and international partners. In particular, there are diverse and close collaborations with the TU Dresden and the TU Bergakademie Freiberg, including joint appointments to professorships with management functions at the IFW. In 2024, another university was added to this circle: A joint appointment procedure was launched with HTW Dresden for a W2 professorship “Applied Research

Die Sommerschule "Advanced Materials" hinterließ besonders durch den praktischen Anteil bei den Studierenden einen positiven Eindruck. Die gemeinsame Sommerschule soll als Angebot für Studierende verstetigt werden und damit zu einem strukturierten Zusammenwirken der Leibniz-Institute und der Hochschule für Technik und Wirtschaft Dresden beitragen.
The Advanced Materials Summer School left a positive impression on the students, especially due to the practical component. The joint Summer School is to become a permanent offer for students and thus contribute to a structured cooperation between the Leibniz Institutes and the Dresden University of Applied Sciences.

Foto: Sven Döring

Forschungstechnik am IFW neu zu besetzen. Außerdem wurde erstmalig eine einwöchige Sommerschule gemeinsam mit dem IPF und der HTW zum Thema „Advanced Materials“ organisiert, bei der Studierende der HTW die Forschungsthemen und Arbeitsmöglichkeiten an den beiden materialorientierten Leibniz-Instituten IPF und IFW kennenlernen konnten.

Die Ausbildung des wissenschaftlichen Nachwuchses bleibt ein sehr wichtiges Anliegen unserer Arbeit am IFW Dresden. An fast allen wissenschaftlichen Projekten und den daraus resultierenden Publikationen sind Promovierende und Studierende beteiligt. 2024 wurden 24 Promotionen erfolgreich abgeschlossen, acht davon haben die bestmöglichen Note - summa cum laude – erreicht und wurden mit der Tschirnhaus-Medaille des IFW Dresden ausgezeichnet.

Zahlreiche Seminare, Kolloquien, Workshops und Tagungen haben den wissenschaftlichen Austausch am IFW belebt, ebenso wie die interne Programm-

Technology” to fill the position of Head of Research Technology Department at IFW from 2025. In addition, a one-week summer school was organized for the first time together with the IPF and the HTW on the topic of “Advanced Materials”, where students from the HTW were able to get to know the research topics and work opportunities at the two materials-oriented Leibniz Institutes IPF and IFW.

The training of young scientists remains a very important aspect of our work at the IFW Dresden. PhD students and undergraduates are involved in almost all scientific projects and the resulting publications. In 2024, 24 doctorates were successfully completed, eight of which achieved the highest possible grade - summa cum laude - and were awarded the IFW's Tschirnhaus Medal.

Numerous seminars, colloquia, workshops and conferences have stimulated scientific exchange at the IFW, as has the internal program retreat

Zum erfolgreichen Abschluss des europäischen Doktoranden-Trainingsnetzwerks BIOREMIA blicken wir dankbar auf vier Jahre Koordination zurück. Gemeinsam mit 17 Partnerinstitutionen aus 12 Ländern Europas förderte das Netzwerk die fachspezifische Ausbildung von wissenschaftlichen Nachwuchs auf dem Gebiet der biomedizinischen Materialforschung. Das Förderprogramm bot den 15 Teilnehmenden neben herausragenden Forschungsbedingungen durch zahlreiche Workshops auch umfassende Möglichkeiten, den Anforderungen an moderne und vernetzte Wissenschaft gerecht zu werden.
With the successful completion of the European Doctoral Training Network BIOREMIA, we look back with gratitude on four years of coordination. Together with 17 partner institutions from 12 European countries, the network promoted the professional training of young scientists in the field of biomedical materials research. The funding program offered the 15 fellows not only excellent research conditions through numerous workshops, but also extensive opportunities to meet the requirements of modern and networked science.

klausur zur intensiven Diskussion des IFW-Forschungsprogramms. 2024 hat sich auch das internationale Tagungsgeschäft weiter belebt. Das IFW hat mehrere Tagungen organisiert, darunter den International Workshop on Microprinting in Bad Schandau, den International Workshop on Novel Superconducting Materials im IFW sowie Kick-off Meetings zu neuen Netzwerkprojekten. Auch jenseits des wissenschaftlichen Austauschs gab es zahlreiche Möglichkeiten für soziales Miteinander und interkulturellen Austausch. Dazu gehören die Techniker-Schule, der IFW-Sommer-Gesundheitstag, Sportevents wie z.B. die Teilnahme an der REWE-Team-Challenge oder ein neues Hochschulsportangebot, die Familienweihnachtsfeier und das Dezemberkolloquium. Ein Novum 2024 war das Angebot offener Labore in Form eines IFW-weiten Adventskalenders.

Im Bereich der Öffentlichkeitsarbeit und Nachwuchswerbung sind wir weiterhin sehr aktiv. Im Jahr

for intensive discussion of the IFW research program. The international conference business also continued to pick up in 2024. The IFW organized several conferences, including the International Workshop on Microprinting in Bad Schandau, the International Workshop on Novel Superconducting Materials at the IFW and kick-off meetings for new network projects. Beyond scientific exchange, there were also numerous opportunities for social interaction and intercultural exchange.
These included the Technician School, the IFW Summer Health Day, sporting events such as participation in the REWE Team Challenge or a new university sports program, the family Christmas party and the December colloquium. A novelty in 2024 was the offer of open labs in the form of an IFW Advent calendar.

We continue to be very active in the area of public relations and recruiting young talent. In 2024, we have particularly increased our activities in guided

Mit einem selbst gestalteten Stromkreis (Kinder-)Augen zum Leuchten bringen, Strukturen der Zukunft kennenlernen, Eindrücke im virtuellen Fullerenlabor sammeln oder Schleuderbilder mit dem SpinBike herstellen: Zur Dresdner Langen Nacht der Wissenschaften war in unserem Institut wieder für jeden etwas Passendes dabei. Über 1.500 Besuchende durften wir an diesem Abend unter dem Motto "United by Science" in unserem Haus begrüßen.
Make (children's) eyes light up with a self-designed electric circuit, get to know the structures of the future, gather impressions in the virtual fullerene laboratory or create spinning pictures with the SpinBike: There was something for everyone at our institute during the Dresden Science Night. We welcomed more than 1.500 visitors to our institute that evening under the motto "United by Science".

2024 haben wir insbesondere unsere Aktivitäten bei Führungen für Schulklassen und Lehrerfortbildungen im Bereich der Quantenphysik verstärkt. Darüber hinaus haben wir uns wieder an übergreifenden Veranstaltungsformaten mit umfangreichen Programmen beteiligt, wie der Dresdner Langen Nacht der Wissenschaften, dem Girls'Day, der Juniordoktor-Kampagne und der Leibniz-weiten Reihe „Book a scientist“. Zudem konnten wir sowohl zum sächsischen Wissenschaftsfestival SPIN2030 als auch am Tag des Offenen Regierungsviertels in Dresden mit zahlreichen Gästen ins Gespräch kommen und unsere aktuelle Forschung vorstellen. Einmal mehr zeigte sich, dass die direkte Kommunikation mit der Gesellschaft sehr willkommen und gefragt ist.

In 2024 haben wir die Vorbereitungen für den Start unseres gemeinsamen Neubauprojektes mit der TU Dresden weiter vorangetrieben. Dank des unermüdlichen Wirkens des Bauherrenteams konnte die Entwurfsplanung fristgerecht Ende September 2024 eingereicht werden. Inzwischen liegt der Prüfbericht dazu vor, so dass in 2025 die nächsten Schritte bis hin zum Baubeginn folgen können.

Alles in allem war 2024 ein sehr erfolgreiches Jahr, in dem wir mit Neubesetzungen, Initiativen und Investitionen aktuelle Chancen genutzt und wichtige Weichen gestellt haben. Wir danken allen Mitarbeiterinnen und Mitarbeitern, Gremienmitgliedern, Partnern und Förderern, die dazu beigetragen haben, ganz herzlich.

tours for school classes and teacher training in the field of quantum physics.
In addition, we once again took part in overarching event formats with broad programs, such as the Dresden Science Night, the Girls'Day, the Juniordoctor campaign and the Leibniz-wide event “Book a scientist”.
We also had the pleasure of speaking to numerous guests at the Saxon Science Festival SPIN2030 and at the Open Government Quarter Day in Dresden, where we presented our latest research. Once again, it was clear that direct communication with society is very welcome and in demand.

In 2024, we pushed ahead with preparations for the start of our joint new building project with TU Dresden. Thanks to the tireless work of the building team, the design planning was submitted on time at the end of September 2024. The review report has now been submitted, meaning that the next steps up to the start of construction can follow in 2025.

All in all, 2024 was a very successful year in which we took advantage of current opportunities and set an important path with new appointments, initiatives and investments.
We would like to thank all employees, board members, partners and funding bodies who have contributed to this success.

Entwurfszeichnung des gemeinsamen Neubaus der Technischen Universität Dresden und des IFW Dresden. Das Baufeld befindet sich im direkten Umfeld des derzeitigen Institusgeländes an der Nöthnitzer Straße im Dresdner Süden. Die Entwurfsvorlage stammt von : AWB Architekten, Dresden.
Design drawing of the joint new building of the Technische Universität Dresden and the IFW Dresden. The construction site is located in the immediate vicinity of the current institute premises on Nöthnitzer Straße in the south of Dresden. The design was submitted by AWB Architekten, Dresden.

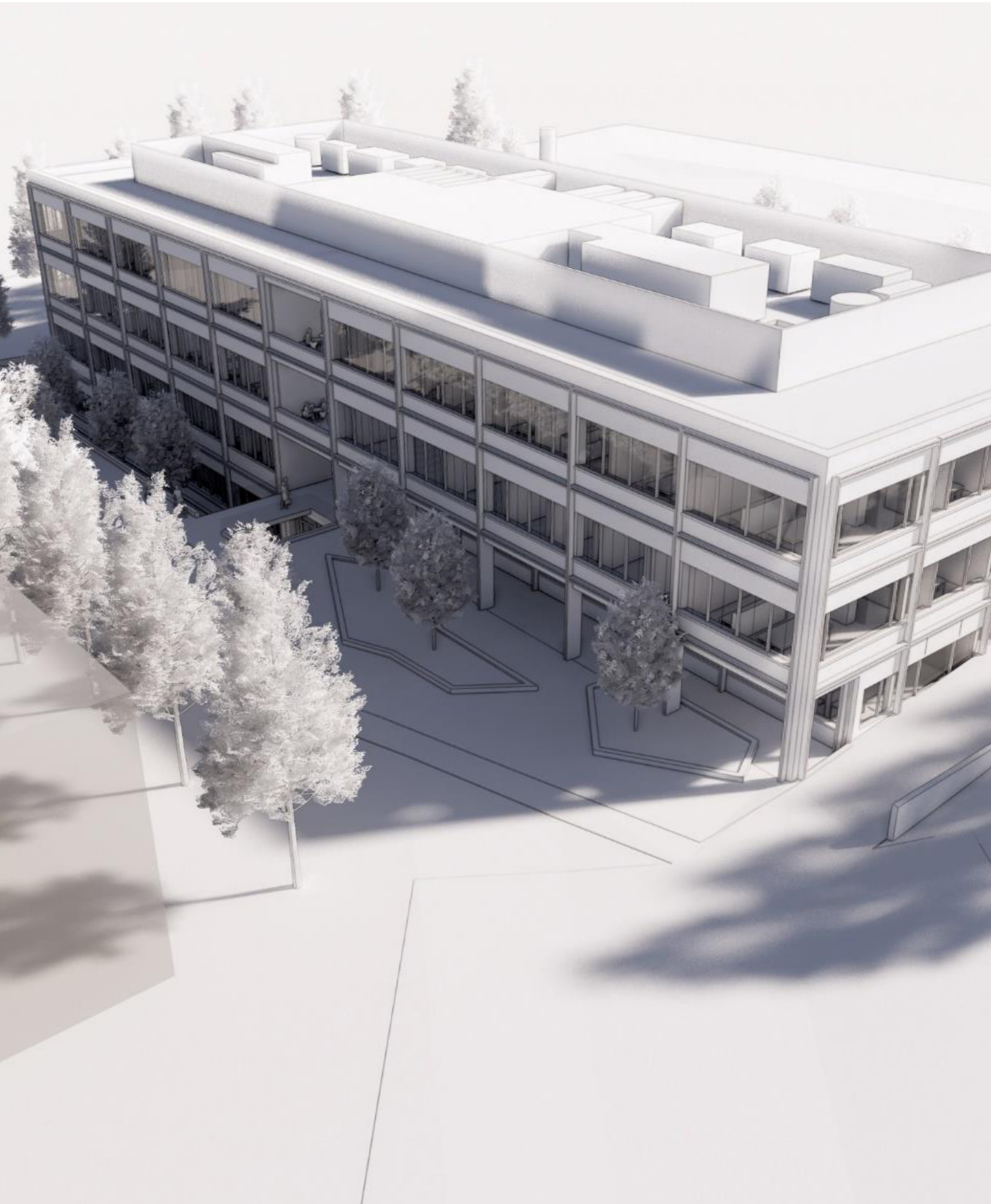

Unser Forschungsprogramm

Dem Unerforschten auf der Spur

Das IFW Forschungsprogramm bringt die Disziplinen, Methoden und Kompetenzen der fünf IFW-Institute zusammen.
Bei aller Breite und Interdisziplinarität gilt für all unsere Forschungsaktivitäten, dass sich Wissenschaftler*innen mit noch unerforschten Eigenschaften neuer Materialien beschäftigen. Das Ziel dabei ist, neue Funktionalitäten und Anwendungen für zukunftsfähige Technologien zu erschließen und herauszuarbeiten.

Our Research Program

On the track of the unexplored

The IFW research program brings together many disciplines, methods and competences of the five IFW institutes.
Despite its breadth and interdisciplinarity, all IFW research activities have in common that scientists are investigating still unresearched properties of matter with the aim of developing new functionalities and applications.

quantum
function
Sustainability

quantum
Quantenmaterialien

Quantenmaterialien sind Stoffe, die besondere Quantenphänomene zeigen. Diese werden von unkonventionellen Spin-Wechselwirkungen, elektronischen Korrelationen, Elektron-Photon-Wechselwirkungen und / oder topologischen Bandstrukturen verursacht. Beispiele sind Supraleitung und Magnetismus. Auch in nanoskaligen Systemen spielen Quanteneffekte eine wichtige Rolle.

function
Funktionsmaterialien

Funktionsmaterialien können auf Grund ihrer physikalischen und chemischen Eigenschaften bestimmte Aufgaben erfüllen: zum Beispiel den Strom leiten, elektromagnetische Wellen einer bestimmten Frequenz filtern, ein magnetisches Feld abschirmen oder Energie speichern.

Sustainability
Nachhaltigkeit als Voraussetzung für die Anwendung

Die Umwelt- und Klimaverträglichkeit neuartiger Materialien wird zunehmend zur unabdingbaren Voraussetzung für ihre Anwendung in neuen Technologien. Umgekehrt haben neue Materialien und neue Synthesewege aus sich heraus ein großes Potential, um einen verantwortungsvolleren Umgang mit Energie und Ressourcen zu befördern. In jedem Fall ist ein grundlegendes Verständnis der beteiligten chemischen und physikalischen Prozesse die Voraussetzung für Innovationen in eine nachhaltige Technologie.

quantum
Quantum Materials

Quantum materials are solids showing peculiar quantum phenomena related to unconventional spin interactions, electronic correlations, electron-photon interactions and/or topological band structures. Examples are superconductivity and magnetism. Quantum effects have also a strong influence in materials with spatial extension constraint to the nanometer scale, like nanoparticles, thin films or nanotubes.

function
Functional Materials

Functional materials exhibit special physical, mechanical or chemical properties which enable them to fulfil a specific function in devices, e.g. conducting electric current, filter acoustic waves of a certain frequency, shielding magnetic fields or storing energy.

Sustainability
Prerequisite for Application

The environmental and climate compatibility of new materials is increasingly becoming an indispensable prerequisite for their use in new technologies. Conversely, new materials and new synthesis methods have great potential in themselves to promote a more responsible use of energy and resources. In any case, a fundamental understanding of the chemical and physical processes involved is the prerequisite for innovations in sustainable technology.

Unsere Forschungsgebiete

Die Mission des IFW Dresden besteht darin, Grundlagenforschung und anwendungsorientierte Forschung und Entwicklung auf dem Gebiet der Festkörper und Werkstoffe zu betreiben. Kernelemente der Forschungsaktivitäten sind experimentelle und theoretische Untersuchungen von Phänomenen, die sich auf der Ebene von Elektronen, Atomen, Molekülen und Nanostrukturen abspielen. Die Arbeiten reichen von der Charakterisierung physikalischer und chemischer Materialeigenschaften bis hin zur Entwicklung neuer Materialien und elektronischer Bauelemente mit neuen Funktionalitäten für eine nachhaltige Zukunft.

Forschungsgebiet 1:
Funktions-Quanten-Materialien

Forschungsgebiet 2:
Materialien für nachhaltige Anwendungen

Forschungsgebiet 3:
2D-Materialien und topologische Zustände

Forschungsgebiet 4:
Vom Material zu neuen Technologien

Our Research Areas

The mission of IFW is to pursue fundamental as well as application-oriented research and development in the field of solid-state matter and materials science. Key elements of the research activities are both experimental and theoretical studies of phenomena that take place at the level of electrons, atoms, molecules and nanostructures as well as the characterization of physical and chemical material properties. This includes also application-oriented research up to the development of new materials and devices based on investigated physical effects and on new functionalities for a sustainable future.

Research Area 1:
Functional quantum materials

Research Area 2:
Materials for sustainable applications

Research Area 3:
2D materials and topological states

Research Area 4:
From materials to novel technologies

Unsere fünf IFW-Institute
Our five IFW Institutes

Institut für Festkörperforschung - Institute for Solid State Research (IFF)
Director: Prof. Dr. Bernd Büchner
Das IFF beschäftigt sich mit materialorientierter Festkörperforschung mit den besonderen Schwerpunkten Quantenmaterialien und nanoskalige Substanzen.
The IFF does research in the field of material-oriented experimental solid state physics with a special focus on quantum materials and nanoscale substances.

Institut für Metallische Werkstoffe - Institute for Metallic Materials (IMW)
Director: Prof. Dr. Kornelius Nielsch
Das IMW befasst sich vor allem mit thermoelektrischen, magnetischen und supraleitenden Materialien, funktionellen Dünnschichten sowie mit Metallphysik.
Main research topics of IMW are thermoelectric, magnetic and superconducting materials, functional thin films and metal physics.

Institut für Materialchemie - Institute for Complex Materials (IMC)
Director: Prof. Dr. Anjana Devi
Die Forschungsaktivitäten des IMC fokussieren sich auf die Chemie funktioneller Materialien mit Schwerpunkt bei nanoskaligen und 2D-Materialien, Strukturanalytik sowie Legierungsdesign und Prozesstechnologien.
The research activities of the IMC are concerned with the chemistry of functional materials with a focus on nanoscale and 2D materials, structural analysis as well as alloy design and process technologies.

Institut für Neuartige Elektronik-Technologien - Institute for Emerging Electronic Technologies (IET)
Director: Prof. Dr. Yana Vaynzof
Das IET konzentriert sich auf die Entwicklung von Materialien und Geräten für neue elektronische und optoelektronische Technologien.
The IET focuses on the development of materials and devices for emerging electronics and optoelectronic technologies.

Institut für Theoretische Festkörperphysik - Institute for Theoretical Solid State Physics (ITF)
Director: Prof. Dr. Jeroen van den Brink
Die Forschung am ITF konzentriert sich auf die theoretischen Aspekte der Physik der kondensierten Materie und der Materialwissenschaften.
The ITF focuses on theoretical aspects of condensed matter physics and materials science.

Forschung aktuell

Current **Research** Topics

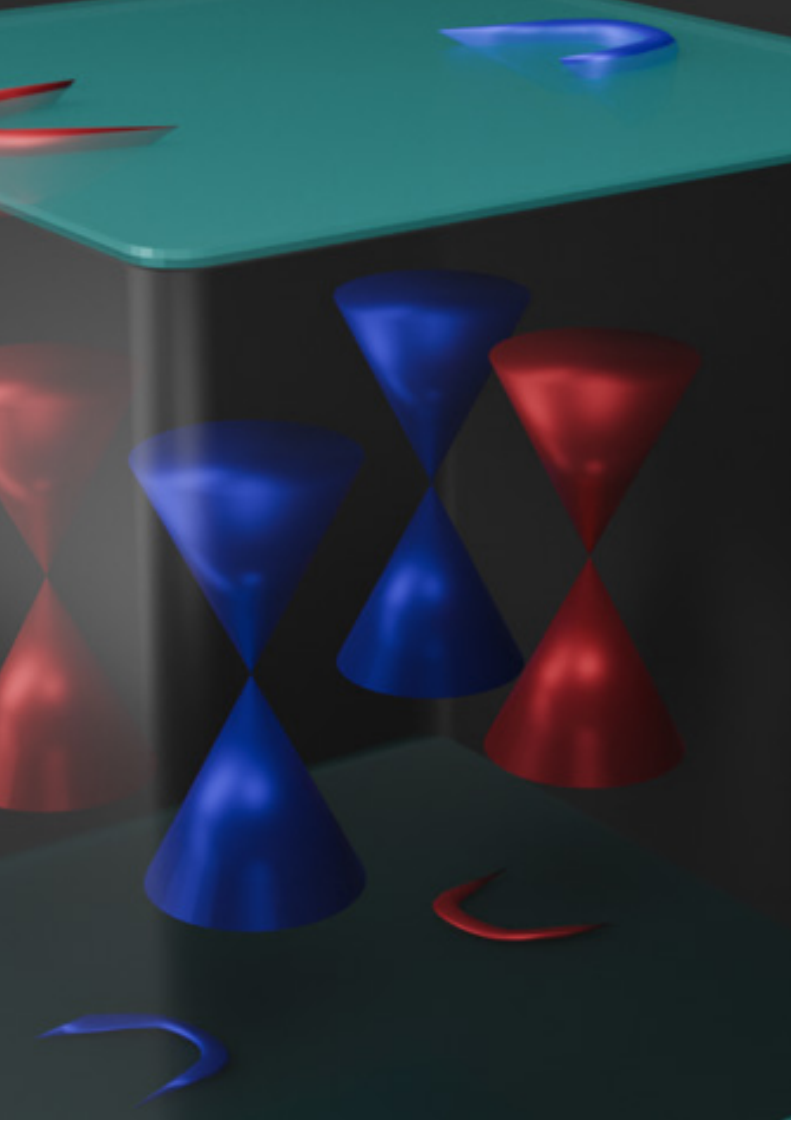

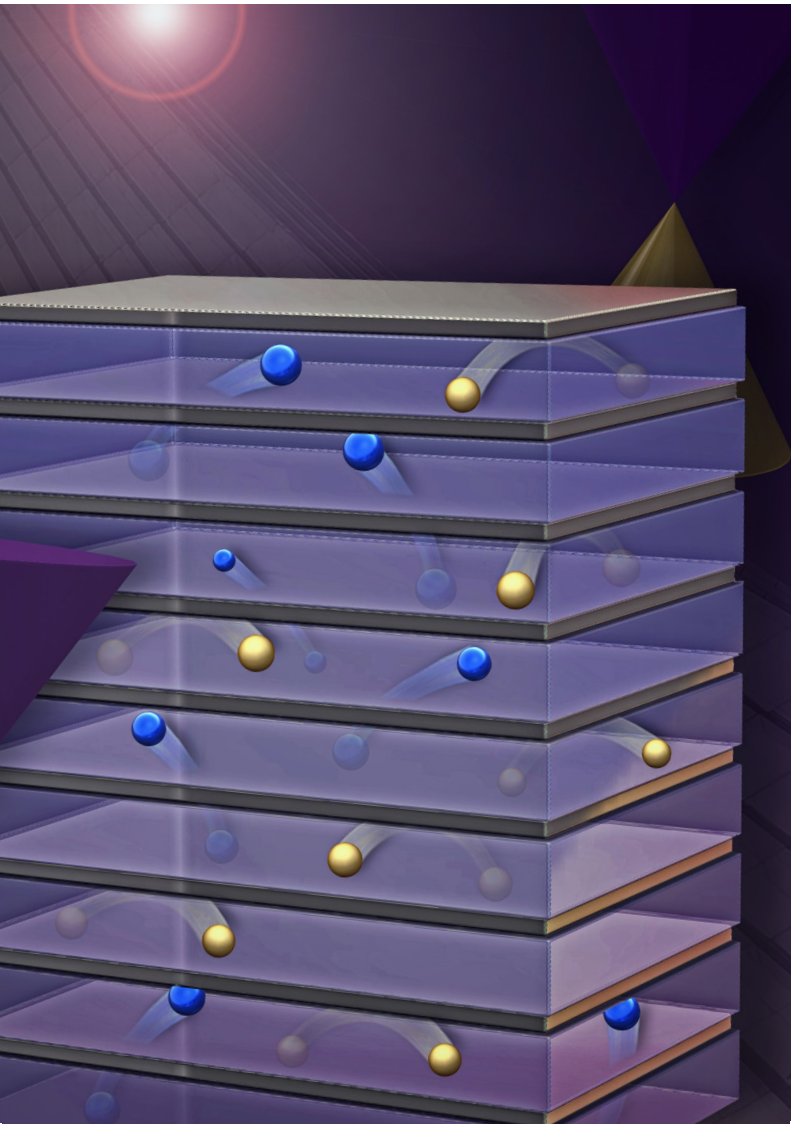

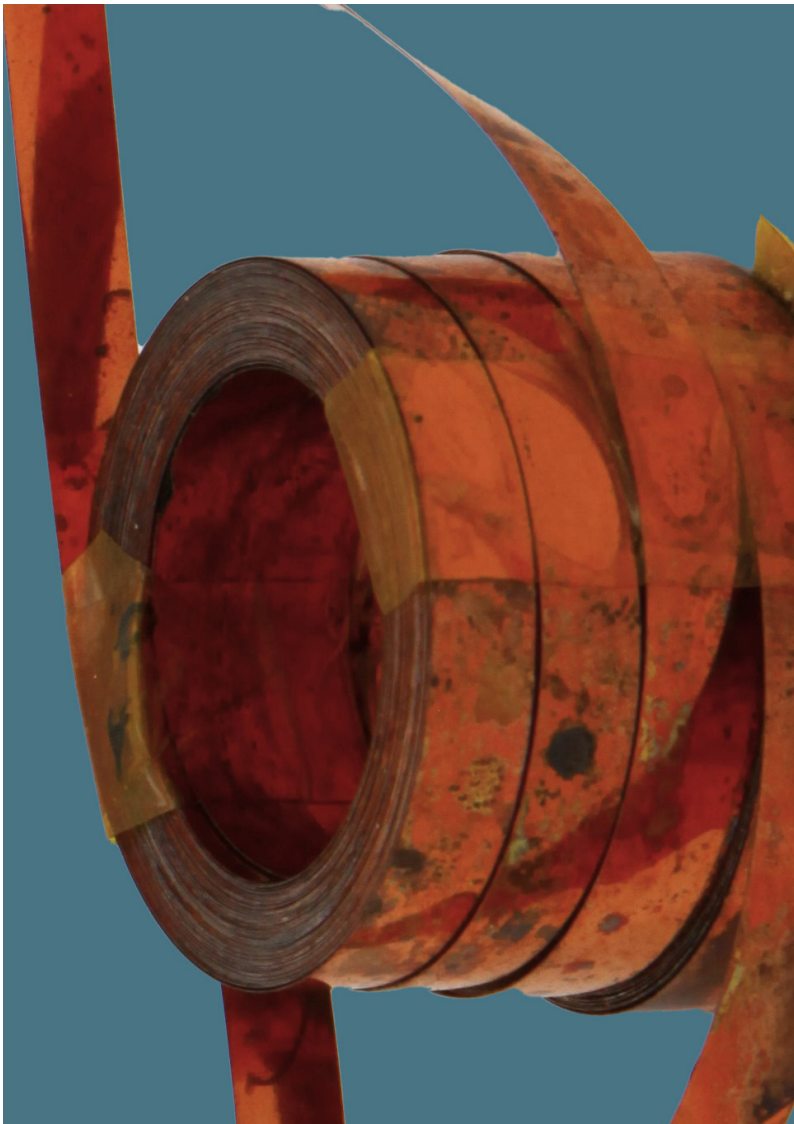

Current Research Topic 1

Superconducting arcs

Sergey Borisenko, Andrii Kuibarov, Oleksandr Suvorov, Riccardo Vocaturo, Alexander Fedorov, Rui Lou, Klaus Koepernik, Jeroen van den Brink and Bernd Büchner

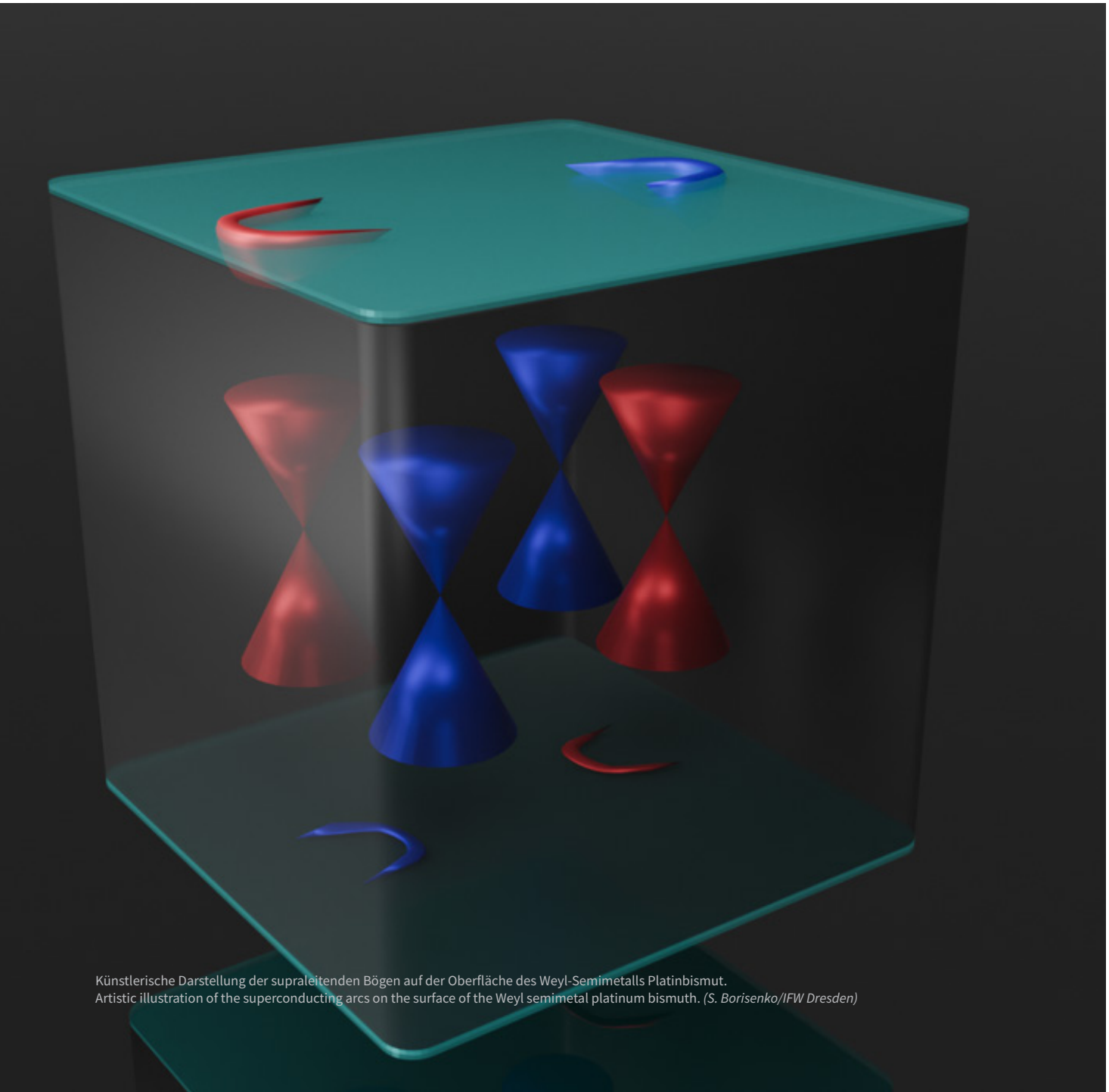

Künstlerische Darstellung der supraleitenden Bögen auf der Oberfläche des Weyl-Semimetalls Platinbismut.
Artistic illustration of the superconducting arcs on the surface of the Weyl semimetal platinum bismuth. *(S. Borisenko/IFW Dresden)*

Topologische Supraleitung ist eine Schlüsselkomponente für die Erzeugung von Majorana-Fermionen, die für die Quanteninformatik von großer Bedeutung sind.
Da es schwierig ist, topologische Supraleiter in der Materialmasse zu finden, haben Forschende versucht, die durch die Umgebung induzierte Supraleitung zu nutzen, aber auch dieser Ansatz ist anfällig und nicht einfach umsetzbar. Weyl-Semimetalle sind ebenfalls vielversprechende Materialien, wobei sich die meisten Forschungen auf ihre Volumensupraleitung konzentriert haben. Dabei wurde die Möglichkeit der Supraleitung in ihren topologischen Oberflächenzuständen, den sogenannten Fermi-Arcs, übersehen. In einer Studie haben wir Experimente und Berechnungen eingesetzt, um topologische Fermi-Arcs auf gegenüberliegenden Oberflächen des Weyl-Materials Platinbismut ($PtBi_2$) zu identifizieren.
Wir fanden heraus, dass diese Oberflächenzustände bei etwa 10 Kelvin supraleitend werden. Die von uns beobachteten Kohärenzspitzen sind die stärksten und schärfsten Signale, die jemals in Photoemissionsexperimenten von festen Materialien aufgezeichnet wurden. Unsere Ergebnisse deuten darauf hin, dass Supraleitung in $PtBi_2$ nur an der Oberfläche auftritt, was das Material zu einer potenziellen Plattform für die Aufnahme von Majorana-Fermionen macht.

Topological superconductivity is a key ingredient for creating Majorana fermions, which are important for quantum computing. Since finding bulk topological superconductors has been difficult, researchers were looking into using proximity-induced superconductivity, but this approach can be fragile and hard to implement. Weyl semimetals could also be promising candidates, but most research has focused on their bulk superconductivity, overlooking the possibility of superconductivity in their topological surface states, called Fermi arcs. In this study, we used experiments and calculations to identify topological Fermi arcs on opposite surfaces of the Weyl material Platinum bismuth ($PtBi_2$). We found that these surface states become superconducting at about 10 Kelvin. Notably, the coherence peaks we observed are the strongest and sharpest signals ever recorded in photoemission experiment from solid materials. Our results suggest that superconductivity in $PtBi_2$ occurs only at its surface, making it a potential platform for hosting Majorana fermions.

The possibility of intrinsic superconductivity of the arcs themselves, which is related to the topology of the band structure with Weyl nodes, was practically not considered earlier. Although the arcs cannot support superconductivity in time-reversal-breaking Weyl semimetals[1], the non-centrosymmetric variants remain an option. Indeed, the superconductivity associated with the Fermi arcs of such systems was only recently predicted theoretically[1,2].
Trigonal $PtBi_2$ has recently been shown to be a type I Weyl semimetal that has been reported to exhibit superconductivity[3,4], making it an attractive candidate for topological superconductivity. Scanning tunneling spectroscopy experiments observed typical spectra of superconducting gaps[5], but their size implied much stronger superconductivity, not consistent with the earlier findings, calling for more detailed studies of the electronic structure.
The electronic structure of trigonal $PtBi_2$ has already been investigated experimentally and theoretically. The material crystallises in the trigonal space group and exposes two different surfaces during cleaving, which we refer to as A and B in the following. The band structure is mainly formed by the hybridisation of the Bi 6p, Pt 5d and Pt 6s states. Two groups of Weyl points are located in momentum space near the M points and have an energy of 47 meV above the Fermi level. To provide a basis for resolving the three-dimensional (3D) band structure, we recorded angle-resolved photoemission spectroscopy (ARPES) data covering at least the first 3D Brillouin zone and an energy of about 1 eV, using photon energies from 15 to 43 eV.
This allowed us to identify points of high symmetry along the kz direction and determine the value of the inner potential. All features in theory and experiment looked very similar and were only slightly shifted in energy or momentum, with no signs of strong renormalisation or similar phenomena. The experimental confirmation of the main features of the band structure and the Weyl points near the Fermi level implies that $PtBi_2$ is indeed a Weyl semimetal.

To achieve a higher energy and momentum resolution, we recorded Fermi surface maps from both terminations with the lower photon energy of 17 eV. They show mostly the same pattern if the intensity fluctuations are taken into account. The number of localised features could be clearly distinguished in

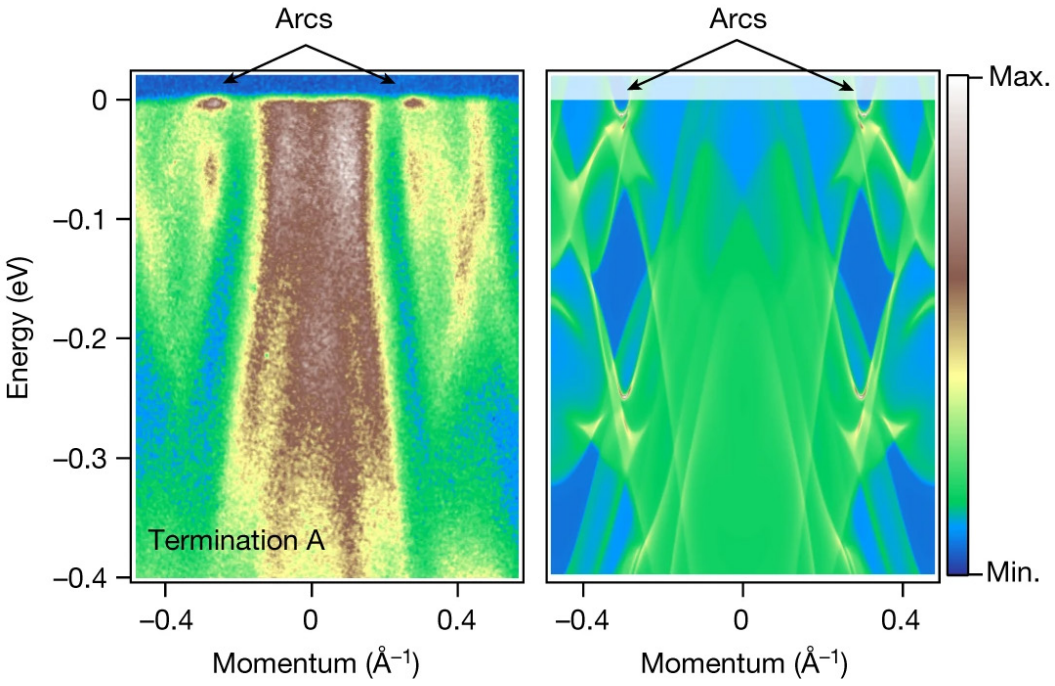

Abb. 1: In der Studie nachgewiesene schärfste Energieverteilungskurve. Derartig deutliche Peaks wurden bisher nie in einem Festkörper-Photoemissionsexperiment nachgewiesen.
Fig. 1: One of the narrowest and strongest EDCs (energy distribution curve) detected in the present study. Such significant peaks have never before been detected in a solid-state photoemission experiment.

the map of termination B, at about 3/4 of the ΓM distance and at equivalent locations. These features have been overlooked in previous ARPES studies. Since the calculated bulk continuum does not contain similar electronic states in this region, we assumed that they originate from the surface. The detected intensity spots, which we identified as surface states, are in remarkable agreement with the results of calculations that account for the presence of the surface. Since $PtBi_2$ is a Weyl semimetal, the presence of topological Fermi arcs that differ for endpoints A and B is expected. In an ideal type I Weyl semimetal, the position of the start and end points of the arcs should be identical, as they are the projections of the Weyl points. The Weyl points, non-degenerate intersections of the bands in 3D k-space, can hardly be recognised directly with ARPES due to the finite resolution, but the corresponding Fermi arcs have been repeatedly observed experimentally in different materials.

Figure 1 shows a comparison of the intensity distribution along the paths that run through the arcs. The arcs are very close to the Fermi level and can be easily distinguished from the regions that are blurred by the kz resolution of the bulk dispersions. Considering the discrepancies in the experimental and theoretical 3D band structure, we do not expect exact agreement between the calculated Fermi arcs and the ARPES data, but the observed agreement proves not only that the experimental features are indeed the topological Fermi arcs, but also that $PtBi_2$ is a Weyl semimetal.

To investigate the detected intensity spots in the maps of the Fermi surface in more detail, we performed ARPES experiments with a laser setup. Due to the low kinetic energy of the photoelectrons (about 1.7 eV), the part of the Brillouin zone that is accessible in these experiments is very limited. We focussed on detecting at least one arc. With this effort, the arc is better resolved but still very localised, both in terms of momentum and energy. We estimate that the momentum expansion is of the order of 0.04 Å-1, which is in excellent agreement with theory.

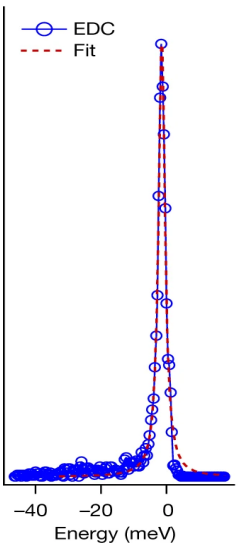

Abb. 2: Experimentelle und berechnete Energie-Impuls-Intensitätsdiagramme für Anschluss A.
Fig. 2: Experimental and calculated energy-momentum intensity plots for termination A.

The most striking feature of the arc states is their energy distribution. In Figure 2 we show the energy distribution curve (EDCs) corresponding to the surface Fermi arc. The sharpness and peak-to-background ratio of the EDC representing the Fermi arc are unprecedented. We have routinely observed peaks with a FWHM of less than 3 meV and a peak-to-background ratio of about 50 in numerous cleaves of many samples. As far as we know, such a sharp peak has never been observed in a solid-state photoemission experiment.
We then observed further appearances of the arcs in the momentum-energy plots from different cleaves and different terminations. The sharpness and flatness maintained the robust properties of the feature in all our experiments at the lowest temperatures.
We found that the arc states for A and B surfaces are supported by the strongly and weakly dispersing bulk states, respectively, exactly as expected from theory. A direct comparison with the calculations, taking into account the presence of topological surface states, showed a remarkable agreement with the experiment: bulk- and surface-related dispersions were detected not only qualitatively but also quantitatively. Despite the clear agreement between the laser ARPES data and the density functional theory calculations, there was one detail that remained unexplained - the striking flatness of the surface band without any signature of Fermi level crossings (Fig.1).

The record-breaking sharpness of the arc EDCs strongly resembled the coherence peaks in ARPES data of superconductors. To determine whether the electronic states in question exhibit other characteristic features of superconductivity, we performed temperature-dependent measurements. Comparison of the spectra recorded at different temperatures emphasised their flatness at the lowest temperature. The arcs lost significantly in spectral weight and gained in scattering - exactly as is to be expected when the system transitions to the normal state.

We have also reproducibly observed another particular aspect of the behaviour in the superconducting state. When the arcs are measured at the highest resolution, the typical backbending of the dispersion from the side where the states are closest to the Fermi level was clearly seen. Our measurements from the shifts of the peak positions at kF give TcA = 14 ± 2 K and TcB = 8 ± 2 K, while the corresponding superconducting energy gaps are 1.4 ± 0.2 meV and 2 ± 0.2 meV, respectively.
Remarkably, the average value of the gap closely matched the gap values determined by STM. [5] The rather unusual sizable zero conductance observed by Schimmel et al. [5] now has a very natural explanation in terms of a bulk contribution that is not gapped. As follows from our ARPES data, the integrated contribution of the states associated with the bulk can easily reach a noticeable fraction of the signal from the surface (Fig. 2) despite the dominant intensity of the arcs.

$PtBi_2$ thus turns out to be a stoichiometric Weyl semimetal with possible pure surface superconductivity, opening up a wealth of possibilities to manipulate topological and superconducting phases in a single material. For example, by varying the thickness of the single crystal, a tunable Josephson junction can be obtained that is inherently topological due to the Weyl semimetal forming the weak junction. Topological superconductivity at the surface can also generate Majorana states at the edges.
Further studies are needed to clearly identify and control both higher Tc superconductivity and possible Majorana states at surfaces and edges of $PtBi_2$ single crystals and nanostructures.

References

[1] M. Sato & Y. Ando Rep. Prog. Phys. 80, 076501 (2017)
[2] M. M. Sharma et al. Sci. Tech. 35, 083003 (2022)
[3] A. Veyrat A. et al. Nano Lett. 23, 1229–1235 (2023)
[4] G. Shipunov et al. Phys. Rev. Mater. 4, 124202 (2020)
[5] S. Schimmel et al. Nat Commun 15, 9895 (2024)

Funding

Deutsche Forschungsgemeinschaft (DFG)
Alexander von Humboldt Foundation
SFB 1143 and Dresden-Würzburg Cluster of Excellence project ct.qmat
BMBF: project UKRATOP

Cooperation

Helmholtz Zentrum Berlin

Current Research Topic 2

Non-Hermitian topological ohmmeter

Viktor Könye, Kyrylo Ochkan, Anastasiia Chyzhykova, Jan Carl Budich[1], Jeroen van den Brink, Ion Cosma Fulga, and Joseph Dufouleur

Die Messung großer elektrischer Widerstände ist ein wesentlicher Bestandteil gängiger Anwendungen wie etwa der Isolationsprüfung, leidet jedoch unter einem grundlegenden Problem: Je größer der Widerstand, desto unempfindlicher ist ein herkömmliches Ohmmeter. Wir haben ein konzeptionell anderes Ohmmeter aus Operationsverstärkern und Widerständen entwickelt, indem wir die topologischen Eigenschaften nicht-hermitescher multiterminaler elektronischer Systeme ausnutzen, die auf Störungen exponentiell reagieren können. Die Genauigkeit des Geräts steigt exponentiell mit der Anzahl der Anschlüsse und kann eine Standardmessung um mehr als eine Größenordnung übertreffen, was den Weg zu einer hochpräzisen nicht-hermitischen Messung ebnet.

Measuring large electrical resistances forms an essential part of common applications such as insulation testing but suffers from a fundamental problem: the larger the resistance, the less sensitive is a canonical ohmmeter. We developed a conceptually different ohmmeter made of operational amplifiers and resistances by exploiting the topological properties of non-Hermitian multiterminal electronic systems that can have an exponential response to perturbations. The accuracy of the device increases exponentially with the number of terminals and can outperform a standard measurement by over an order of magnitude, paving the way toward non-Hermitian high-precision sensing.

Abb. 1: Zusammengesetztes System mit Widerständen und Operationsverstärkern.
Fig. 1: Real system realized on a bredboard with resistances and operational amplifiers.

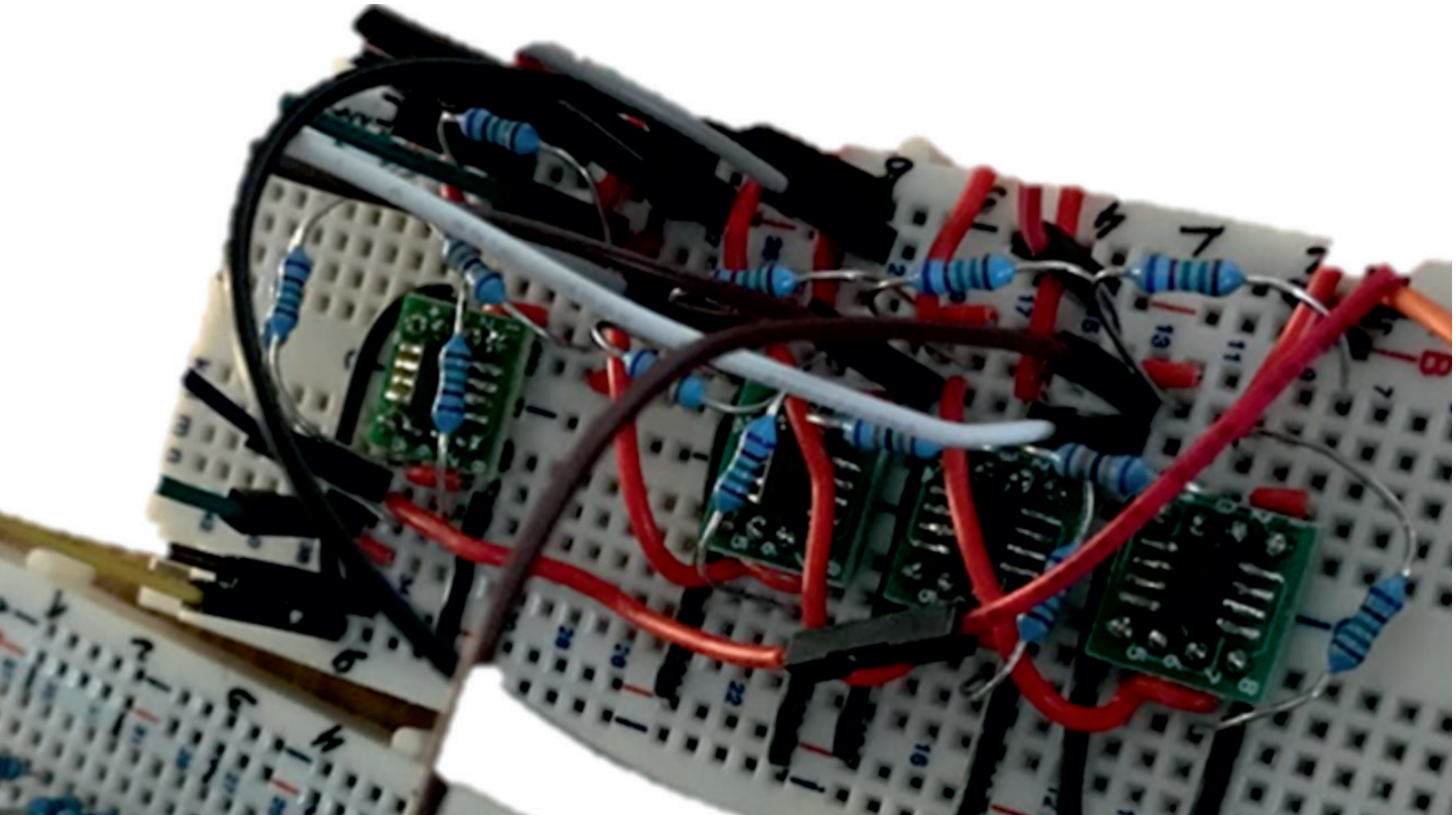

A linear system is a system whose response to an excitation is a linear function of the excitation. The properties of these systems can therefore be very simply described by a matrix that relates the excitation to the response. Linear systems are often described by Hermitian matrices. In this case, Weyl's inequalities tell us that the spectrum of the matrix cannot vary by more than the perturbation applied to it, satisfying the general physical intuition that small causes produce small effects. However, when this matrix is non-Hermitian, we can find systems whose spectrum response grows exceptionally with the dimension of the matrix.

In the case of the non-Hermitian electronic system we are studying here, the excitation is constituted by a set of currents applied to terminals and the response is a set of voltages measured at these different terminals. The current vector is made up of all the currents injected (excitation) and a voltage vector made up of all the voltages read (response). The matrix linking these two vectors is the resistance matrix, which is simply the inverse of the conductance matrix. We built our Ohmmeter taking advantage of the high sensitivity of non-Hermitian systems to an excitation.
Following the method we have recently developed in another recent work [2], we have translated the exceptional sensing properties of a non-Hermitian quantum system into exceptional performances of our ohmmeter for measuring very high resistance by building an electronic circuit whose conductance matrix exactly mimics the Hamiltonian of the non-Hermitian system previously studied by theorists [3]. Our systems and its electronic scheme are depicted in Figure 2. We have shown that the properties of our ohmmeter are very robust against any fluctuations of the system parameters (fluctuating value of the resistances or fluctuating characteristics of the operational amplifiers for instance) because they are protected by a non-trivial topology.

Unlike the standard method, we consider here a multiple-source device the sensitivity of which increases exponentially with the number of terminals. Our system consists of a chain of electronic elements A and electronic elements B (Fig. 2), elements A and B being connected to terminals where a current can be injected and a voltage read. The open chain, i.e. without any element connecting the first terminal to the last, corresponds to the system without any perturbation. The perturbation is caused by a large resistor connecting the first terminal to the last. We first show that the sensitivity of our Ohmmeter, defined as the variation of the spectrum to any perturbation of the system, increases exponentially with the number of terminals in the system. To this aim, we measure the variation of the smallest eigenvalue of the conductance matrix $|\Delta g_0|$ when a large resistor R is connecting the two ends of the chain. As expected, and similarly to standard system, this variation is found to decrease when R increases. Importantly, in contrast to standard model, $|\Delta g_0|$ increases also exponentially with the number of sites, in excellent agreement with our theoretical predictions (Figure 3).

A standard method to measure large resistances is the constant-voltage method, where a known (large) voltage is sourced and the current flowing through the device under test (DUT) is measured. Such a current vanishes as the resistance R of the DUT increases and high-precision measurements of infinitesimal currents are required to achieve a decent measurement of resistances above the mega-ohm regime, setting the limit of the resistance measurement's precision. In order to compare the performance of the non-Hermitian ohmmeter with a standard measurement, we measure the relative accuracy K for a standard set-up and for our non-Hermitian ohmmeter.
K is the ratio between the resistance noise-to-signal ratio ε_R (the finale absolute precision of the device) and the voltage noise-to-signal ratio ε_V (the absolute precision of the voltage measured). Again, K shows the same trend as a function of R for all measurements but can be exponentially increased for a larger number of terminals of the

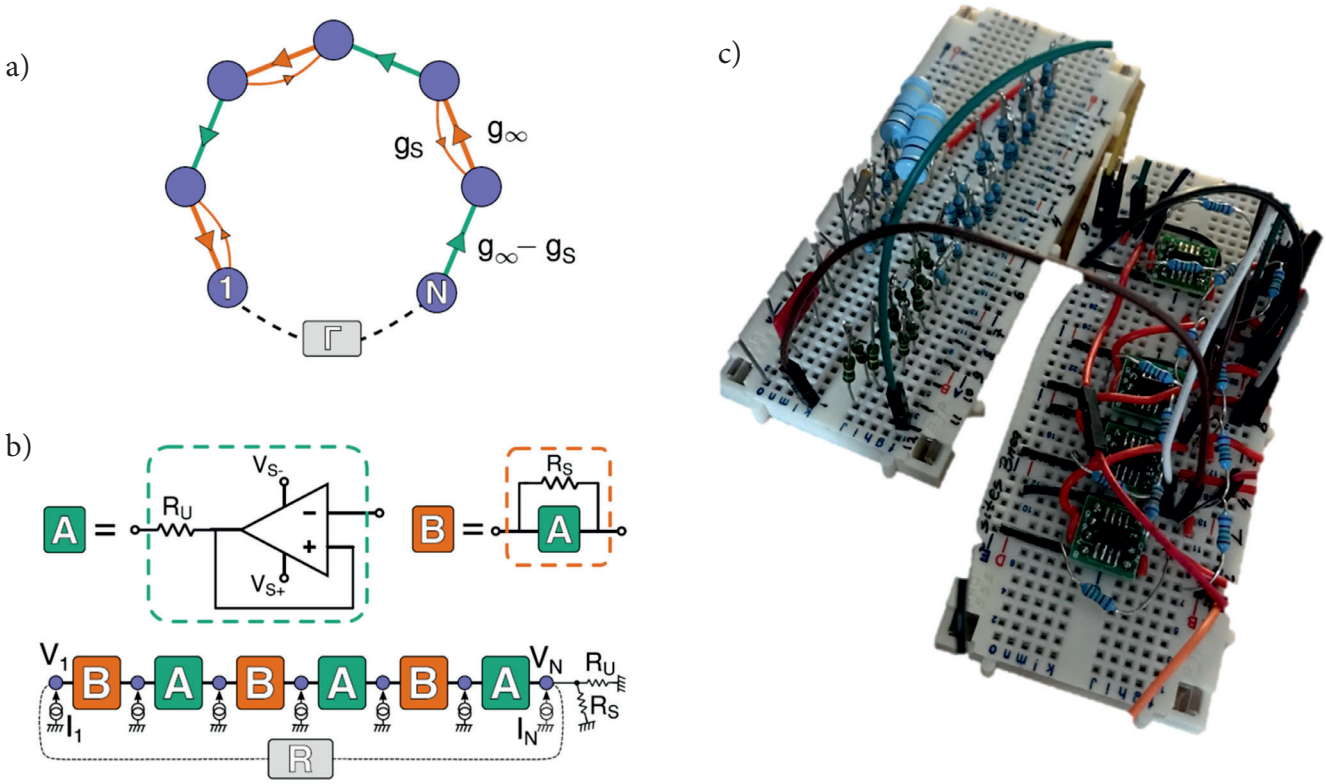

Abb. 2: a) Prinzip des nicht-hermiteschen elektronischen Systems mit nicht-reziproken Verbindungen (Pfeile) zwischen den Terminalen. Die Störung (zu messende Größe) wird durch eine Verbindung Γ zwischen dem ersten und dem letzten Terminal dargestellt. b) Die elektronische Schaltung, deren Leitwertmatrix die Hamiltonian des in [3] untersuchten nicht-hermiteschen Systems nachbildet. c) Reales System mit Widerständen und Operationsverstärkern.
Fig. 2: a) Principle of the non-Hermitian electronic system with non-reciprocal connections (arrows) between terminals. The perturbation (quantity to be measured) is the represented by a connection Γ between the first and the last terminal. b) The electronic circuit the conductance matrix of which mimic the Hamiltonian of the non-Hermitian system studied in [3]. c) Picture of the real system realized on a bredboard with resistances and operational amplifiers.

non-Hermitian device. Thus, we observe that the relative accuracy of the non-Hermitian ohmmeter outperforms that of the simple single-terminal measurement starting at $N = 7$ and becomes one order of magnitude larger at $N = 9$ (Figure 4).

Our work positions the topological device as a thrilling new option in sensor engineering and has led to a patent application [4]. Its principle can be extended to various measurement of large impedances or on-chip measurement using the properties of the quantum Hall effect edge states instead of the active operational amplifiers, opening the way to more highly precise measurement of large impedance quantum devices.

References

[1] V. Könye et al., Phys. Rev. Applied 22, L031001 (2024)
[2] K. Ochkan et al., Nature Physics 20, 395–401 (2024)
[3] J. C. Budich and E. J. Bergholtz, Phys. Rev. Lett. 125, 180403 (2020)
[4] V. Könye et al., Patent number EP4394400A1

Funding

Leibniz Association
German Research Foundation DFG
Würzburg-Dresden Cluster of Excellence on Complexity and Topology in Quantum Matter – ct.qmat.

Cooperations

Technische Universität Dresden, Germany
Max Planck Institute for the Physics of Complex Systems, Germany

Abb. 3: a) Veränderung des niedrigsten Eigenwerts der Leitwertmatrix in Abhängigkeit von der Störung 1/*R* bei unterschiedlicher Anzahl von Terminalen. Es wird ein exponentieller Anstieg der Reaktion in Abhängigkeit von der Anzahl der Terminalen beobachtet.
Die Punkte zeigen die experimentellen Daten während die Linien die theoretischen Erwartungen darstellen.
b) Experimentelle und theoretische Empfindlichkeit in Abhängigkeit von der Anzahl der Terminalen.
Fig. 3: a) Variation of the lowest eigenvalue of the conductance matrix as a function of the perturbation 1/*R* for different number of terminals. An expeonential increase of the response is observed as a function of the number of terminals. The points are the experimental data and the lines are the theoretical expectations.
b) Experimental and theoretical sensitivity as a function of the number of terminals.

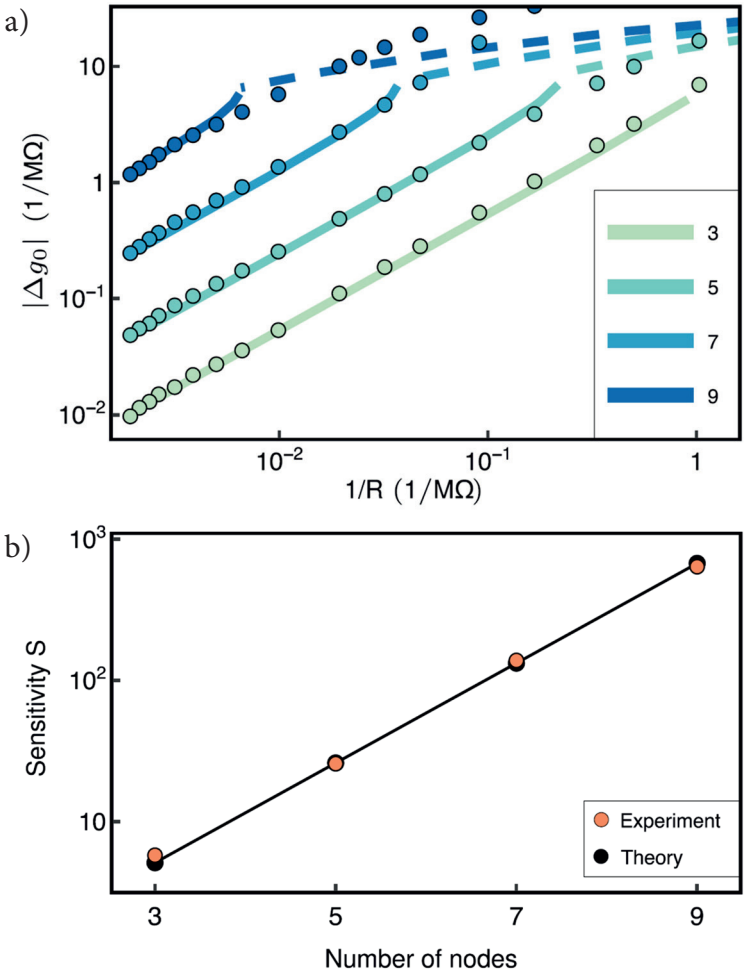

Abb. 4: Die relative Genauigkeit unseres Systems, gemessen als Funktion von *R* und für eine unterschiedliche Anzahl von Terminalen. Ein direkter Vergleich mit einem Standard-Ohmmeter unter Verwendung desselben Voltmeters und derselben Stromquelle ist ebenfalls dargestellt. Bei 7 Terminalen ist unser Ohmmeter genauer als das Standard-Ohmmeter und bei 9 Terminalen übertrifft es das Standardsystem um mehr als eine Größenordnung.
Fig. 4: The relative accuracy of our system measured as a function of *R* and for different number of terminals. A direct comparison with a standard ohmmeter using the same voltmeter and current source is also shown. For 7 terminals, our ohmmeter is more accurate than the standard one and it outperforms the standard system by more than an order of magniture for 9 terminals.

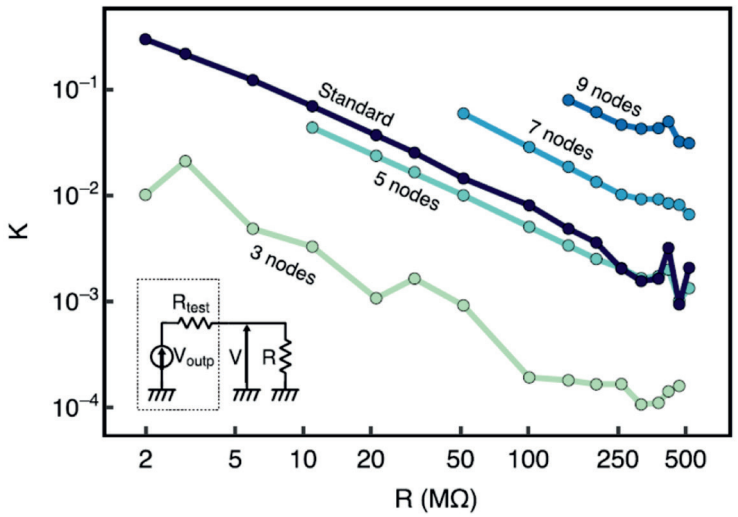

Current Research Topic 3

Dynamic phase-enabled steering of topological states in composite waveguide arrays

Min Tang, Chi Pang, Christian N. Saggau, Haiyun Dong[1], Ching Hua Lee[2], Ronny Thomale[3], Sebastian Klembt[3], Ion Cosma Fulga, Jeroen van den Brink, Yana Vaynzof, Oliver G. Schmidt[4], Jiawei Wang[5], and Libo Ma

In der Optik spielt die Topologie eine entscheidende Rolle, die durch die Berry-Phase charakterisiert wird. Die dynamische Phase, die grundlegende Eigenschaften in Wellensystemen bestimmt, ist damit jedoch nicht verflochten, da beide Phasen verschiedene Ursprünge haben. In dieser Arbeit nutzen wir die dynamische Phase, um die kontrollierte Anregung des topologischen Zustands in einem zusammengesetzten Su-Schrieffer-Heeger Wellenleitergitter zu ermöglichen, das eine Brücke zwischen der topologischen geometrischen Phase und der dynamischen Phase des Lichts schlägt. Unsere Forschung eröffnet einen neuen Ansatz zur Manipulation topologischer Zustände in photonischen Verbundbauteilen mit Potenzial für Anwendungen, bei denen die dynamische und geometrische Phase eine zentrale Rolle bei der Steuerung des Lichtflusses in topologischen On-Chip-Bauteilen spielen.

Topology has been known to play a significant role in optics, which is characterized by the topological Berry phase. The dynamic phase, determining a series of fundamental properties in wave systems, is known to not intertwine with any topological Berry phase as they have different origins. Here, we utilize the dynamic phase to realize the controllable excitation of the topological state in a composite Su-Schrieffer-Heeger waveguide lattices, which builds a bridge between the topological geometric phase and the dynamic phase of light. Our research provides a new knob for the manipulation of topological states in composite photonic devices, holding great potential for broad applications where the dynamic phase and geometric phase play crucial roles in regulating light flow in on-chip topological devices.

Abbildung: KI-generiert mit Adobe Firefly.

Topology, as a mathematical concept addressing invariant properties under continuous deformation, has been applied in physics to describe the characteristics of wavefunctions under a certain evolution in a parameter space. As a key quantity in topological physics, the geometric phase (Berry phase) [1] not only has theoretical significance but also leads to observable phenomena. In photonics, topology plays a crucial role in revealing intriguing properties such as topological robustness and one-way transmission [2], resulting in vibrant development in applications such as lasers [3], filters [4], and beam splitters [5]. Interference is a fundamental phenomenon in wave systems, ranging from classical optics, acoustics to wavefunctions in quantum mechanics. While optical interference in topological states has been studied to highlight the robustness of edge modes [6], the interference between topological edge modes in composite photonic structures remains largely underexplored. This gap presents exciting opportunities for advancing the manipulation of topological states in photonic devices.

In our recent study, we explored the excitation and transition between bulk and non-trivial topological states using dynamic-phase-steered interference in a carefully designed composite Su-Schrieffer-Heeger (c-SSH) waveguide array, as shown in Figure 1. The c-SSH system comprises two SSH waveguide arrays symmetrically positioned on either side of a central waveguide. Laser light is coupled into this system through two input waveguides, which enable precise control of the dynamic phase difference of the input light, facilitating the excitation of topological modes. This approach offers a new pathway for controlling topological states in photonic devices, paving the way for applications in regulating light flow in on-chip systems.

Utilizing the advanced micro-nano photonic device fabrication capabilities at IFW, we fabricated the c-SSH waveguide array, with its cross-sectional structure schematically illustrated in Figure 2a. In this system, K_c represents the coupling strength between the central waveguide and its adjacent waveguides, while K_a and K_b denote the alternating coupling strengths in the left and right waveguide arrays. All constituent waveguides share identical geometrical parameters and the same propagation constant.

In our designed c-SSH waveguide array, the condition $K_a < K_b$ is consistently satisfied by maintaining $d_a > d_b$, where d_a and d_b are the alternating waveguide gaps in the lattice (see Fig. 2a). This configuration guarantees the existence of topological states localized within the SSH array. The central waveguide, highlighted by a red dashed box, couples with the SSH waveguide arrays on either side.
The antisymmetric topological zero mode (TZM) arises in the c-SSH system, representing a combination of topological edge states that satisfy specific phase relationships.

As depicted in Figure 2b, the c-SSH waveguide arrays are integrated with several on-chip functional optical components, including multimode interference couplers, unbalanced injection arms, and a waveguide taper. This integrated photonic device uniquely enables simultaneous control over both the dynamic phase and the topological phase.

To characterize the light propagation behavior in the c-SSH waveguide array, a wavelength-tunable Ti:sapphire laser (Equinox) was end-fired into the cleaved facet of the taper waveguide assisted by fiber-port coupler and polarization controller. To image light-scattering patterns from the top view of the waveguide arrays, a 24x high-magnification zoom lens system was used together with an 8 MP monochrome CCD camera (S805MU2).

Figure 3 presents the experimental results of mode field distributions at the end facets of the waveguide array, where the dynamic phase difference $\Delta\varphi$ is tuned by adjusting ΔL and the wavelength λ. When ΔL=0 µm, $\Delta\varphi$ is strictly equal to 0, resulting in the destructive interference of TZMs, as illustrated in Figure 1. Under this condition, the TZM vanishes, and only bulk modes are excited across the spectral range of 780 to 800 nm.

Introducing a path length difference, such as ΔL=10 µm, generates a wavelength-dependent dynamic phase difference as light propagates through the unbalanced arms. In Figure 3b, a TZM emerges at λ_{b1} due to the constructive interference of TZMs under the condition $\Delta\varphi = \pi$. In contrast, at λ_{b2}, where $\Delta\varphi = 2\pi$ (equivalent to 0), only bulk modes are formed, and the TZM is absent.

By further increasing the path length difference to ΔL=30 µm, more periods of dynamic phase difference from 0 to π are observed within the same spectral range, as shown in Figure 3c. Consequently, additional transition periods between TZMs and bulk modes appear, marked from λ_{c1} to λ_{c3}. These experimental results closely match the simulations shown in the top panel of Figure 3, validating the effective control of topological modes by modulating the dynamic phase difference.

These findings highlight the ability to selectively excite either topological or bulk modes by simply changing the dynamic phase difference at the same wavelength. Moreover, the dynamic phase difference could be further tuned by applying external magnetic or electric fields if the waveguides are fabricated using responsive materials [7]. This capability significantly broadens the potential applications of these systems for controlling and utilizing topological states in on-chip photonic devices.

In summary, we have proposed and demonstrated a method for the tunable excitation of a topological zero mode with a non-trivial geometric phase by adjusting the dynamic phase difference in composite topological waveguide arrays. This approach enables the selective excitation of either bulk or topological modes, depending on whether the dynamic phase difference induces constructive or destructive interference in the topological non-trivial state within the composite system. Our experimental and theoretical analyses are in excellent agreement, underscoring the validity of this technique. To the best of our knowledge, this represents one of the simplest and most effective methods for controllable excitation of topological states in photonic lattices, establishing a direct link between the geometric and dynamic phases of light. Furthermore, this work lays a solid foundation for future investigations into mode control in non-Hermitian topological systems, where the direction of light flow can be manipulated by tuning the dynamic phase.

References

[1] M. V. Berry, Proc. R. Soc. Lond. A 392 (1984) 45
[2] Z. Wang, et al. Nature 461 (2009) 772
[3] Y. Zeng, et al. Nature 578 (2020) 246
[4] Y. Kang, et al. Nat. Commun. 9 (2018) 3029
[5] G. J. Tang, et al. Phys Rev B 102 (2020) 174202
[6] A. Blanco-Redondo, et al. Science 362 (2018) 568
[7] D. M. Wu, et al. Adv. Mater. 30 (2018) 1703912

Funding

Würzburg-Dresden Cluster of Excellence ct.qmat
German Research Foundation

Cooperations

[1] Institute of Chemistry, Chinese Academy of Sciences, Beijing, China
[2] National University of Singapore
[3] Universität Würzburg, Germany
[4] Technische Universität Chemnitz, Germany
[5] Harbin Institute of Technology, Shenzhen, China

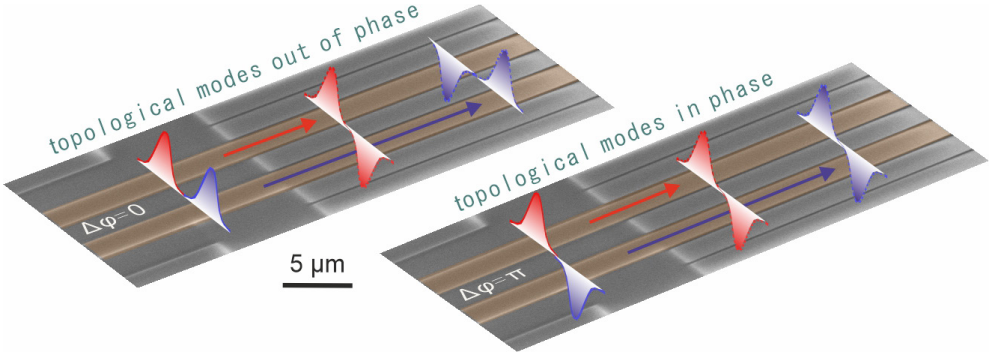

Abb. 1: Richtige dynamische Phasendifferenzen in zwei Eingangslichtstrahlen führen zu destruktiven (Außer Phase) und konstruktiven (Phasengleich) Interferenzen von topologischen Nullmoden (TZMs) in einem zusammengesetzten photonischen Gitter.
Fig. 1: Proper dynamic phase differences in two input light beams lead to destructive (out of phase) and constructive (in phase) interferences of topological zero modes (TZMs) in a composite photonic lattice.

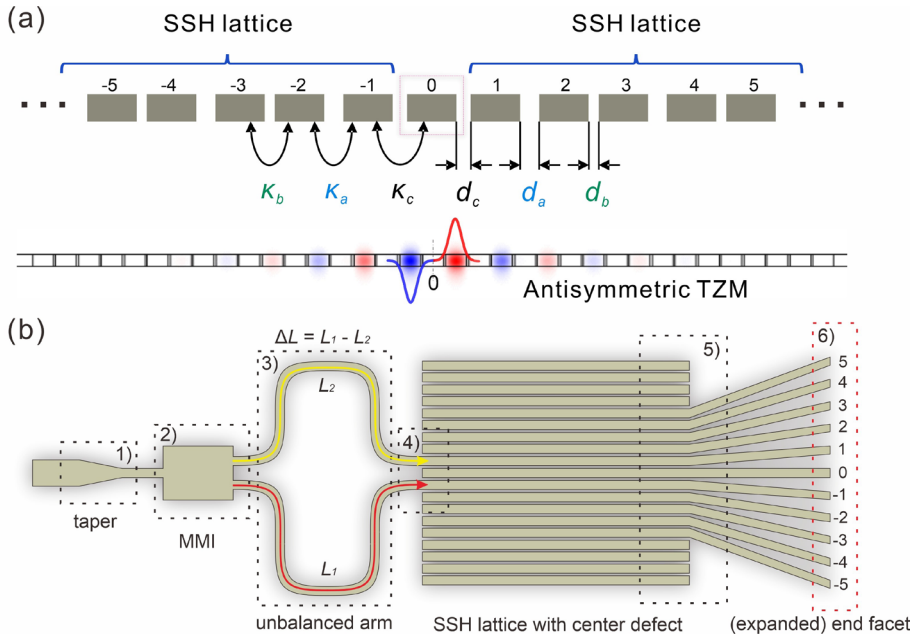

Abb. 2a) Schematische Darstellung eines zusammengesetzten Wellenleiterarrays (Querschnitt) mit einem zentralen Defekt (j = 0). Die numerische Simulation zeigt einen antisymmetrischen TZM im zusammengesetzten SSH-Gitter. 2b) Schematische Darstellung des entworfenen Musters, das besteht aus: 1) verjüngtem Eingangs-Wellenleiter,
2) 1×2 MMI-Koppler, 3) unausgeglichenen Armen, 4) Einspeiseregion in das Wellenleiterarray, 5) Endfläche des Wellenleiterarrays und 6) erweiterter Endfläche.
Fig. 2a) Schematic diagram of a composite waveguide array (cross-section) with a central defect (j = 0). Numerical simulation shows an antisymmetric TZM in the composite SSH lattice.
2b) Schematic diagram of the designed sample consists of 1) tapered input waveguide, 2) 1×2 MMI coupler, 3) unbalanced arms, 4) injection region to the waveguide array, 5) end facet of the waveguide array, and 6) expanded end facet.

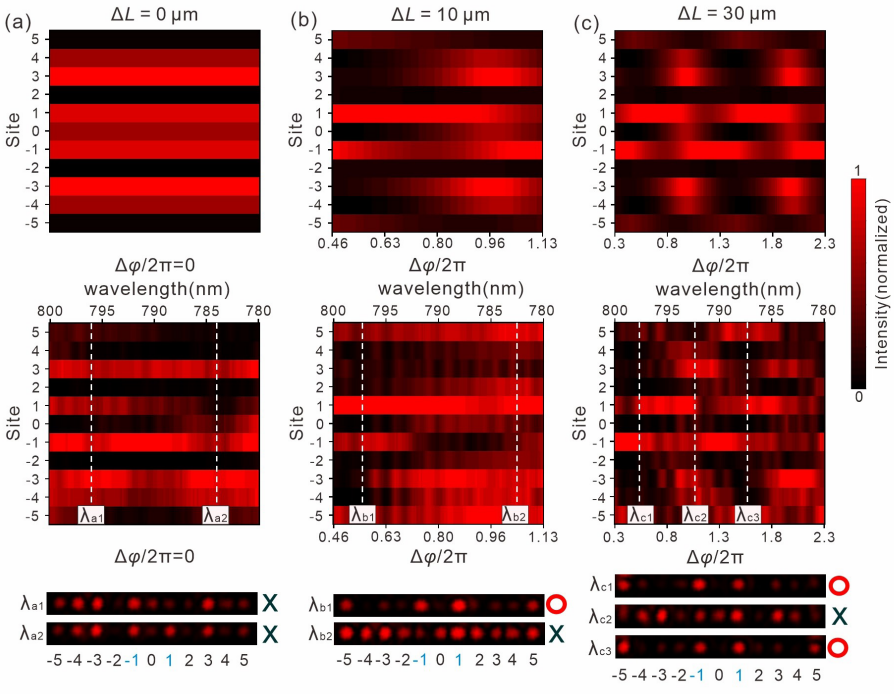

Abb. 3: Simulations- (oberes Feld) und experimentelle (mittleres Feld) Ergebnisse der Modenfeldverteilungen in Hohlleiterstellen (0 bis ±5) in Abhängigkeit von der Phasendifferenz Δφ/2π für die Fälle (a) ΔL = 0 µm, (b) 10 µm und (c) 30 µm. Unten: Die an den Endfacetten des Wellenleiters aufgezeichneten Modenverteilungen zeigen typische Bulk- (mit schwarzen Kreuzen gekennzeichnet) und TZM-Moden (mit roten Kreisen gekennzeichnet), die den in den mittleren Feldern durch gestrichelte Linien markierten Fällen entsprechen.
Fig. 3: Simulation (top panel) and experimental (middle panel) results of the mode field distributions in waveguide sites (0 to ±5) versus the phase difference Δφ/2π for the cases of (a) ΔL = 0 µm, (b) 10 µm, and (c) 30 µm. Bottom panel: mode distributions recorded from the waveguide end facets show typical bulk (labeled with black crosses) and TZM (labeled with red circles) modes, corresponding to the cases marked by dashed lines in the middle panels.

Current Research Topic 4

Implementation of HTS coated conductor tapes in superconducting magnetic bearings

Tilo Espenhahn, Anke Kirchner, Mostafa Baloochi, Johannes Saske, Kornelius Nielsch, and Ruben Hühne

Im Rahmen aktueller DFG-Projekte wird der Einsatz von hochtemperatursupraleitenden Bandleitern in supraleitenden Magnetlagern untersucht. Die höhere Stromtragfähigkeit, bessere Verfügbarkeit und größere mechanische Flexibilität dieser Bandleiter ermöglicht eine weitere Verbesserung der Lagereigenschaften für unterschiedliche Anwendungen. Dabei muss aber die zusätzliche Anisotropie der Leitergeometrie berücksichtigt werden. Erste Untersuchungen zeigen, dass sowohl Bandstapel als auch supraleitende Spulen die derzeit genutzten Massivsupraleiter und Permanentmagnete in diesen Lagern ersetzen können. Eine weitere Optimierung der Anordnung kann dabei neue Anwendungsszenarien für diese Lager eröffnen.

Within the scope of currently running DFG projects we investigate the application of coated conductors based on high-temperature superconductors for superconducting magnetic bearings. The higher current-carrying capacity, better availability and greater mechanical flexibility of such coated conductors might enable a further improvement of the bearing properties for various applications. However, the additional anisotropy of the conductor geometry itself must be taken into account. Initial investigations show that both tape stacks and superconducting coils might replace bulk superconductors and permanent magnets used so far in these bearings. It is expected that a further optimization opens new pathways for the application of such bearings.

Abb. 1: Ausschnitt einer supraleitenden nahtlosen Testspule. Durch die Fertigung ohne Kontaktstellen werden Ohm'sche Verluste vollkommen vermieden.
Fig.1: Detail of a seamless superconducting test coil. Ohmic losses are completely eliminated by manufacturing without contact points.

Application of high-temperature superconductors in magnetic bearings

Since the discovery of high temperature superconductivity (HTS) in cuprates with critical temperatures above the boiling point of liquid nitrogen (77 K), major efforts are devoted to the realization of energy-efficient devices based on these materials. This includes power systems like motors, cables, fault current limiters as well as ultra-high field magnets and levitation-based applications. One particular example of levitation-based devices is a superconducting magnetic bearing (SMB).
The basic setup of such a superconducting bearing is shown in Figure 2a. In this case, a strong ferromagnet - typically $Nd_2Fe_{14}B$ permanent magnets – is levitating above a high temperature superconductor, which is cooled below its critical temperature in a cryostat. *RE*$Ba_2Cu_3O_{7-x}$ compounds (*RE*BCO, *RE* = Y, Gd or other rare earth elements) are commonly used as superconducting material for such applications. Such parallel arrangement is used for components in high-speed ring spinning machines developed in cooperation with groups at TU Dresden [1,2]. Alternatively, concentric setups might be used as shown in Figure 3.

So far, bulk materials are used in such SMB setups, which are produced by melt texturing of compacted powders and subsequent heat treatment with post-oxidation. A major disadvantage of this established method is the lack of scalability of the manufacturing process due to the high time and material costs. An alternative industrial fabrication path for HTS materials is the coating of metallic templates by physical or chemical methods resulting in a highly textured superconducting layer. Such *RE*BCO coated conductors have higher critical current densities in magnetic fields compared to bulk materials, better thermal and mechanical stability, and greater flexibility with respect to the device geometry. These advantageous physical and mechanical properties as well as the greater availability make coils or stacks of such coated conductors attractive for replacing *RE*BCO bulks in superconducting magnetic bearings.

However, the anisotropy of the conductor tapes itself, i.e., the distribution of the superconductor in layers of a few micrometer separated by significantly thicker metal substrates, is a major challenge for the application of tape stacks and coils in levitation systems. Different approaches are studied currently at IFW Dresden to tackle this technological challenge.

Development of HTS tape stacks

In a first project, HTS tapes stacks are prepared from pieces of superconducting *RE*BCO tapes, which were originally developed for current transport in cables, to study, if they are suitable as replacement for typically used bulks in SMBs [3]. As the tapes are characterized by a significantly higher critical current density compared to bulk material, high trapped fields and levitation forces are expected with an effective flux pinning inside the superconductor. Therefore, stacks with different height were prepared and compared to bulk samples having the same size (see Fig. 2b). In all cases, improved properties were measured with increasing sample height up to a thickness of about 8 mm.
A further increase of the bulk or stack height did not lead to any further improvement of the properties for the configurations studied. For tape stacks, a strong anisotropy of the levitation properties was found. In vertical direction, the levitation forces of tape stacks are even slightly higher than for bulk samples of the same geometry, when the superconducting layers are aligned perpendicular to the magnetic field direction. However, the lateral forces are almost absent for this configuration. The opposite behavior is observed, when the tape stack is rotated by 90° around the in-plane direction. Consequently, it is important to arrange the tape stacks as a set with their superconducting layer parallel and perpendicular to the magnetic field in rotationally symmetric SMBs to ensure a high stability in all directions.

In general, there are different ways to realize an optimized configuration. At one hand, one can use a combination of tape stacks with vertical and lateral alignment (see right image in Figure 2b for an example). This results in a significantly improved lateral stiffness; however, by sacrificing some of the vertical stability. At the other hand, the magnetic field distribution might be adjusted with regard to the stack alignment. Instead of a single permanent magnet, magnet configuration as flux collector arrangements or Hallbach arrays having strong magnetic field gradients in the superconducting area are studied currently.

Design of a fully superconducting magnetic bearing

Alternatively, *RE*BCO coated conductors might be wound to small coils in order to realize of a fully superconducting magnetic bearing. In this case, also the arrangement of permanent magnets, which creates the magnetic field for levitation, is replaced by such coils. The major advantage is that significantly higher magnetic fields might be realized in particular at low temperatures. To study this in detail, a fully superconducting magnetic bearing with a coaxial design was developed in the framework of a DFG funded project. The basic setup of such a bearing is shown in Figure 3a. Numerical simulations were used in the design phase to estimate the levitation forces and to determine the temperature distribution during operation. Based on the coated conductor tape data of different suppliers these simulations yielded a magnetic field of about 0.5 T at 77 K in the centre of the coils independent of the tape material used. Larger differences were observed for lower temperature, which correlate with the temperature dependence of the critical current density of the respective conductors. In this case, fields of up to 4 T might be realized at 20 K using such a coil configuration. Based on these results, the final coil setup for the rotor and stator was designed and realized as shown in Figure 3b and c. Preliminary tests verified the results of the simulations at 77 K. The study will be extended to lower temperatures using an electrical cooling system integrated in this setup.

Study of jointless coils

Whereas the prototype of the fully superconducting magnetic bearing was realized with shortcutted stator coils using a soldering technique, it would be beneficial to use jointless coils to avoid the losses at the resistive joint.
To test this approach, jointless coils with an inner diameter of 20 mm were prepared from 12 mm wide coated conductor tapes as shown in Figure 4a [4]. The tapes were slit along the length except of both ends and wound by a wind and flip technology into four pancake coils connected in series. Afterwards, the prepared coils were charged contact-free with a superconducting dynamo. A clear dependence on the magnet size and frequency was found for the charging characteristics. A maximum magnetic field of about 0.3 T at 77 K was imprinted in one of these coils (Fig. 4b). It is expected that an improvement of the dynamo configuration will lead to an enhanced charging behavior resulting in even higher fields. A slight decay of the magnetic field was observed after charging, which might be explained with a superconducting resistance in the vicinity of the critical current. Furthermore, a degradation of the coils was found over time indicated by some delamination at the cutted edges, which reduced the maximum achievable magnetic field after a few weeks. Therefore, protective layers are required to avoid such a degradation, which will be tested within the recently granted project extension.

Conclusion

Our studies indicate that *RE*BCO coated conductor material has the potential to replace bulk elements as well as permanent magnets in superconducting magnetic bearings. Therefore, it is crucial to optimize the arrangement of the superconductor as well as the magnetic field configuration and to study the interactions of both components with numerical simulations. This will enable the design of such bearings for special application scenarios.

References

[1] M. Hossain et al., Text. Res. J. 95 (2020) 951-968.
[2] M. Baloochi et al. Eng. Res. Express 6 (2024) 035524.
[3] A. Kirchner et al., Materials 17 (2024) 4516.
[4] M. Espenhahn et al., Supercond. Sci. Technol. 37 (2024) 095021.

Funding

DFG HU1726/9, HU1726/10, ES594/2

Cooperations

Technische Universität Dresden, Germany
IFW Research Technology

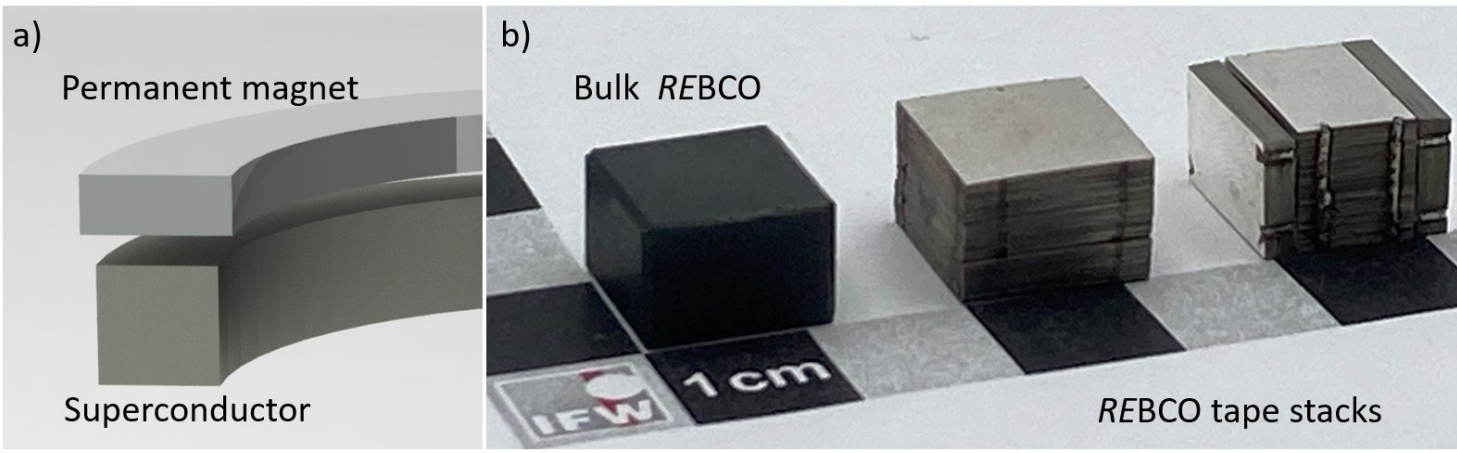

Abb. 2: a) Schematische Darstellung der parallelen Anordnung eines supraleitenden magnetischen Lagers, wie es beim Ringspinnen verwendet wird; b) Supraleitendes Massivmaterial und Bandstapel aus 145 Einzellagen, die Höhe beträgt jeweils 8 mm [4].
Fig. 2: a) Schematic setup for a superconducting magnetic bearing with parallel arrangement used in ring spinning; b) Superconducting bulk and tape stacks made from 145 single tapes; the height is always 8 mm [4].

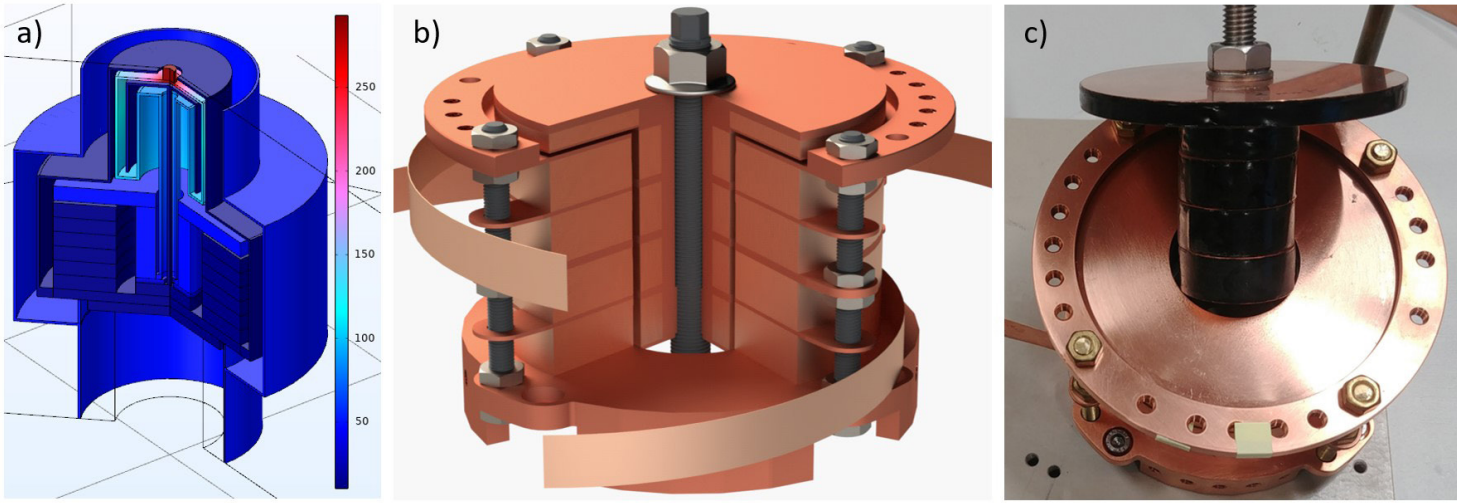

Abb. 3: a) Schematischer Aufbau eines komplett supraleitenden Lagers, zusätzlich wurde die Temperaturverteilung im Lager nach der Abkühlung simuliert;
b) schematischer Querschnitt durch die Anordnung der supraleitenden Spulen des Lagers; c) fertiges Lager mit herausgehobenem Rotor.
Fig. 3: a) Setup for a fully superconducting bearing with simulated temperature distribution after cool down; b) Schematic cross section of the coil setup for the bearing;
c) image of the realized bearing with lifted rotor.

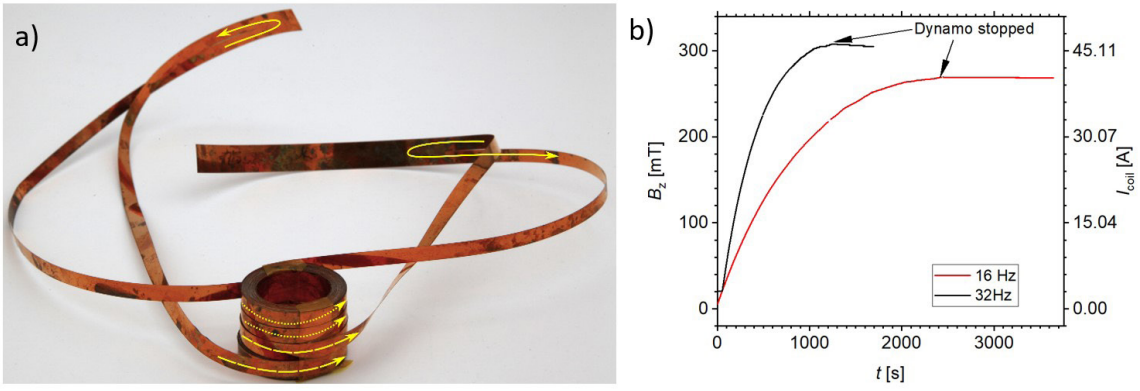

Abb. 4: a) Endlose supraleitende Testspule; b) Messung der Ladecharakteristik der Spule bei 77 K in Abhängigkeit der Magnetpassagefrequenz eines supraleitenden Dynamos [4].
Fig. 4: a) Jointless superconducting test coil; b) Measurement of the loading characteristics at 77 K in dependence of the magnet frequency for a superconducting dynamo [4].

Current Research Topic 5

Altermagnets: A new materials class for spintronics

Andy Thomas, Ruben Gonzalez, Heike Schlörb, Dominik Kriegner[1], Helena Reichlova[1], Sabine Wurmehl, Christian Blum, Bernd Büchner, Oleg Janson, Toshihiro Sato, Volodymyr Kravchuk, and Jeroen van den Brink

Jeder kennt die kleinen Ferromagnete, mit denen wir am Kühlschrank unsere Merkzettel befestigen. In dieser Materialklasse richten sich benachbarte magnetische Momente parallel aus. Darüber hinaus existiert eine weitere Materialklasse, die sogenannten Antiferromagnete, welche benachbarte Momente jeweils entgegengesetzt (antiparallel) ausrichtet. Dadurch verschwinden allerdings auch viele Eigenschaften, die für eine technische Anwendung vorteilhaft sind. In der jüngsten Vergangenheit wurde nun mit den Altermagneten eine weitere Materialklasse vorhergesagt und auch schon in Experimenten bestätigt. Diese Materialklasse verbindet viele der für Anwendungen vorteilhaften Eigenschaften von Ferromagneten und Antiferromagneten und zeigt darüber hinaus auch ganz neue, einzigartige Phänomene.

We are probably all familiar with the small ferromagnets that we use to attach our sticky notes to the fridge. In this class of materials, neighboring magnetic moments align in parallel. In addition, there is another class of materials, the so-called antiferromagnets, which align neighboring moments in opposite directions (antiparallel). However, this also eliminates many properties that are advantageous for technical applications.
In the recent past, another class of material has been predicted in the form of altermagnets and has already been confirmed in experiments. This class of materials combines many of the properties of ferromagnets and antiferromagnets that are advantageous for applications and also exhibits completely new, unique phenomena.

Abb. 1: Bild einer typischen Probe für temperatur- and magnetfeldabhängige Messungen. Ein kleines Probensubstrat wurde mit rotem Lack auf den Chipträger geklebt und kann mit bis zu 32 Aluminiumdrähten kontaktiert werden. In der Mitte ist schwach die Hallbar der eigentlichen Struktur zu sehen.
Fig. 1: Image of a typical sample for temperature and magnetic field-dependent measurements. A small sample substrate was mounted to the chip carrier with red glue and can be contacted with up to 32 aluminum wires. The Hall bar of the actual structure can be faintly seen in the center.

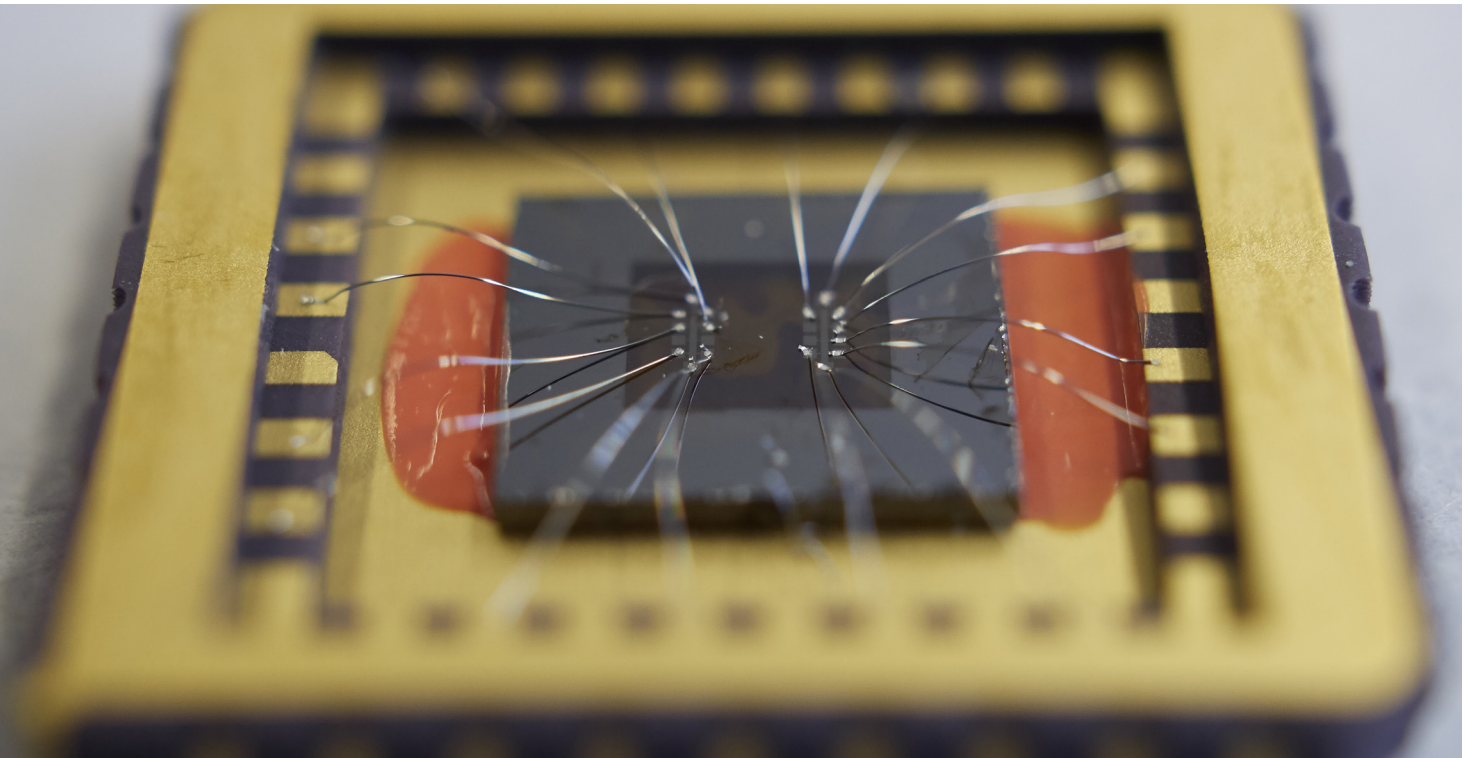

First, we have to ask ourselves: What distinguishes altermagnets from ferro- and antiferromagnets? This is based on a somewhat abstract concept of comparing crystal and spin symmetries. If we only consider two neighboring spins and we limit our example to collinear orientations, we have two basic options: spins can be aligned either parallel, i.e., in the same direction, or antiparallel, i.e., in opposite directions. These configurations correspond to the commonly known ferromagnets and antiferromagnets, respectively. Importantly, in an antiferromagnet, flipping all spins by 180 degrees does not typically alter its physical properties due to its symmetry.

However, when we also account for the lattice structure and the positions of non-magnetic atoms, the scenario changes. In certain crystal structures, the 180-degree spin rotation can result in distinct physical properties, allowing us to differentiate between these configurations. This breaks the conventional symmetry of antiferromagnets and gives rise to a new class of materials known as altermagnets.

The field of altermagnetism is an emerging field which promises exciting new research directions, in particular, in the field of spintronics. Spintronics is short for spinelectronics, which is a compound word that denotes *electronics utilizing the spin*. Generally, this refers to the spin of the electrons that can be used in addition to its charge, which enables new possibilities for functionalities and, eventually, devices. In the past, there are several applications for spintronic devices that successfully made their way into large scale, mainstream applications: giant- (GMR) and tunnel-magnetoresistance (TMR). Most prominently, both effects are used in read heads of magnetic hard disk drives.

The main goal of altermagnetic research with regard to spinelectronics will be the implementation of altermagnetic materials in similar devices. Due to their particular symmetries altermagnets show robust and large spin dependent electronic properties which makes them ideal candidates for spintronic devices. In order to understand the potential of this, we have to take a step back and look at some of the limitations of devices based on ferromagnetic materials. Namely, there are two possible drawbacks that are inherently connected to the use of ferromagnets. First, ferromagnetic materials are affected by stray fields, i.e. other magnets can alter or even destroy the information encoded in a ferromagnetic material. Secondly, ferromagnetic materials can only operate of up to GHz frequencies. Both drawbacks could possibly be addressed utilizing altermagnetic materials. Altermagnets are predicted to operate at THz frequencies and are much more resistant to external stray fields, similar to conventional antiferromagnets.

But before we can think about GMR and TMR devices, we have to look at more fundamental properties of materials for spintronics. The main feature that altermagnets and ferromagnets can provide - and antiferromagnets cannot - are spin polarized bands. In other words, the current flowing in a particular direction will consist of more up than down spins or vice versa. In a ferromagnet, this will be isotropic, i.e. the same for all current directions. However, in certain altermagnets, it is spin up polarized for one particular current direction and spin down polarized if the electrical current direction is rotated by 90 degrees. Please note that the net magnetization of the material will still be zero, because there is the same amount of up and down spins.

The particular symmetry of altermagnets lead to other physical properties unexpected in compensated collinear magnets, such as the presence of a spontaneous Hall effect. The Hall effect describes the generation of a voltage (the Hall voltage) perpendicular to both, the applied electrical current and magnetic field. If the material can give rise to a Hall effect even without an external magnetic field, it is called a spontaneous Hall effect. Therefore, a strong experimental hint for altermagnetism, is the observation of a spontaneous Hall effect and concurrently zero net magnetization in a collinear magnet.
The vibrant field of altermagnetism has been spawned by theoretical research, and some of our activities pertain to theory and numerical calculations. One of such theory projects demonstrates that in a particular layer with a honeycomb structure, interactions between electrons can not only induce altermagnetism, but give rise to the anomalous Hall effect [1]. This result is noteworthy, because, as mentioned in the previous paragraph, the anomalous

Hall effect is usually associated with ferromagnets. This discovery was achieved through advanced computer simulations using the quantum Monte Carlo method, which allowed us to study the behavior of interacting electrons in complex systems with high precision. Revealing the pivotal role of electronic correlations in altermagnets provides a new perspective and opens exciting avenues in this rapidly growing field.

In another theory project, we showed that thermal spin fluctuations in films of d-wave altermagnets gives rise to piezomagnetism: there is a coupling between mechanical strain and magnetic polarization [2]. The induced magnetic moment is perpendicular to the film and its direction (up or down) is determined by direction of the stress application relative to the crystallographic axes. This remarkable result has been proven by direct numerical spin-lattice simulations of two different magnetic models, namely the Heisenberg model of rutiles, e.g. RuO_2, MnF_2, and the checkerboard model. Another interesting prediction of this work - *anisotropic thermal spin conductivity driven by magnetic fluctuations* - awaits experimental verification, i.e., we predict the generation of the spin-polarized current in response to the applied temperature gradient.

The first challenge for experiments is to identify materials that are altermagnetic. To this end, first-principles calculations based on density functional theory proved useful: the electronic structure of altermagnets must contain the so-called band splitting between the bands of spin-up and spin-down electrons. While the bare presence of such splitting may be apparent, a quantitative analysis is not straightforward. To tackle this problem, we developed several measures of spin splitting, and applied them to more than 60 known materials that were potentially altermagnetic [3]. In this way, we identified several candidate materials with a particularly large spin splitting and detailed the mechanism of their spin splitting.

Once the materials are identified, they can be synthesized in the IFW Dresden as well. One of the previously known materials is CrSb. CrSb crystals were grown by high-temperature-solution growth also sometimes referred to as flux growth. For this method, the precursors of the target material and an appropriate solvent are placed in a crucible (something like a closed cooking pot). In the present case, both precursors are metals, viz. Chromium and Antimony, with Sb excess as a solvent. At room temperature, all constituents are solid. Upon heating to 1100°C, all ingredients melt or, in other words, the precursors are dissolved in the flux and our container holds now a liquid. This high temperature is dwelled for 24 hours and then slowly cooled. During this process, the solubility of the solute is decreasing again and CrSb crystals nucleate and grow. As the content of our crucible is solid at room temperature, we need to separate the flux from the crystals at high temperature, above the melting point. This is done by a centrifugation process at 750°C yielding mm-sized metallic and shiny CrSb single crystals.

Finally, experiments will be done with some of the candidate materials. In order to do these experiments, Hall bar structures are prepared, for example, from the single crystals via focussed ion beam cutting. A typical experiment investigates the field, temperature and angular dependence of the resistance and the Hall effect. A spontaneous Hall effect was observed in MnTe [4] and Mn_5Si_3 [5] although only a vanishingly small net magnetic moment was found as well. As mentioned before, this is a strong experimental hint for altermagnetism. Furthermore, the anomalous Hall effect in Mn_5Si_3 was shown to be anisotropic with the Néel vector orientation, which provides further systematic support to consider epitaxial thin films of Mn_5Si_3 as an altermagnetic candidate material [6]. Additionally, we experimentally demonstrated the altermagnetic arrangement of magnetic moments with respect to crystal symmetries in thin films of Mn_5Si_3 [7]. Finally, we found an anisotropic magnetoresistance in MnTe which is linked to both the relative orientation of current and magnetic order, as well as crystal and magnetic order. Altermagnetism is manifested as a three-fold component in the transverse magnetoresistance which arises due to the anomalous Hall effect [8].

Overall, theory, materials synthesis and experiments are working hand in hand on this exciting topic in the emerging field of altermagnetism.

References
[1] T. Sato et al., Phys. Rev. Lett. 133, 086503 (2024).
[2] K. V. Yershov et al., Phys. Rev. B 110, 144421 (2024).
[3] Y. Guo et al., Mater. Today Phys. 32, 100991 (2023).
[4] R. D. Gonzalez Betancourt et al., Phys. Rev. Lett. 130, 036702.
[5] H. Reichlova et al., Nature Comm. 15 (2024) 4961.
[6] M. Leiviskä et al., Phys. Rev. B 109 (2024) 224430.
[7] J. Rial at al., Phys. Rev. B 110, L220411 (2024).
[8] R.D. Gonzalez Betancourt et al., NPJ spintronics 2 (2024) 45.

Funding
Deutsche Forschungsgemeinschaft
Japan Society for the Promotion of Science (JSPS)
CRC 1143
Cluster of Excellence ct.qmat

Cooperations
[1] Institute of Physics, Czech Academy of Sciences, Czech Republic
Univ. Grenoble Alpes, CNRS, CEA, Grenoble INP, IRIG-SPINTEC, France
Aix Marseille Université, CINaM-CNRS/Polytech, France
Max-Planck-Institut für Physik komplexer Systeme, Germany

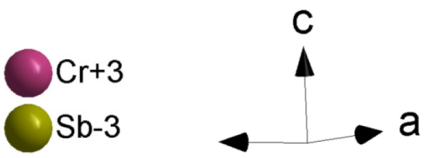

Abb. 2: Die hexagonale Kristallstruktur von CrSb. Die wissenschaftliche Klassifizierung lautet: Prototyp NiAs; Raumgruppe $P6_3/mmc$.
Fig. 2: The hexagonal crystal structure of CrSb. Its scientific classification is: prototype NiAs; spacegroup $P6_3/mmc$.

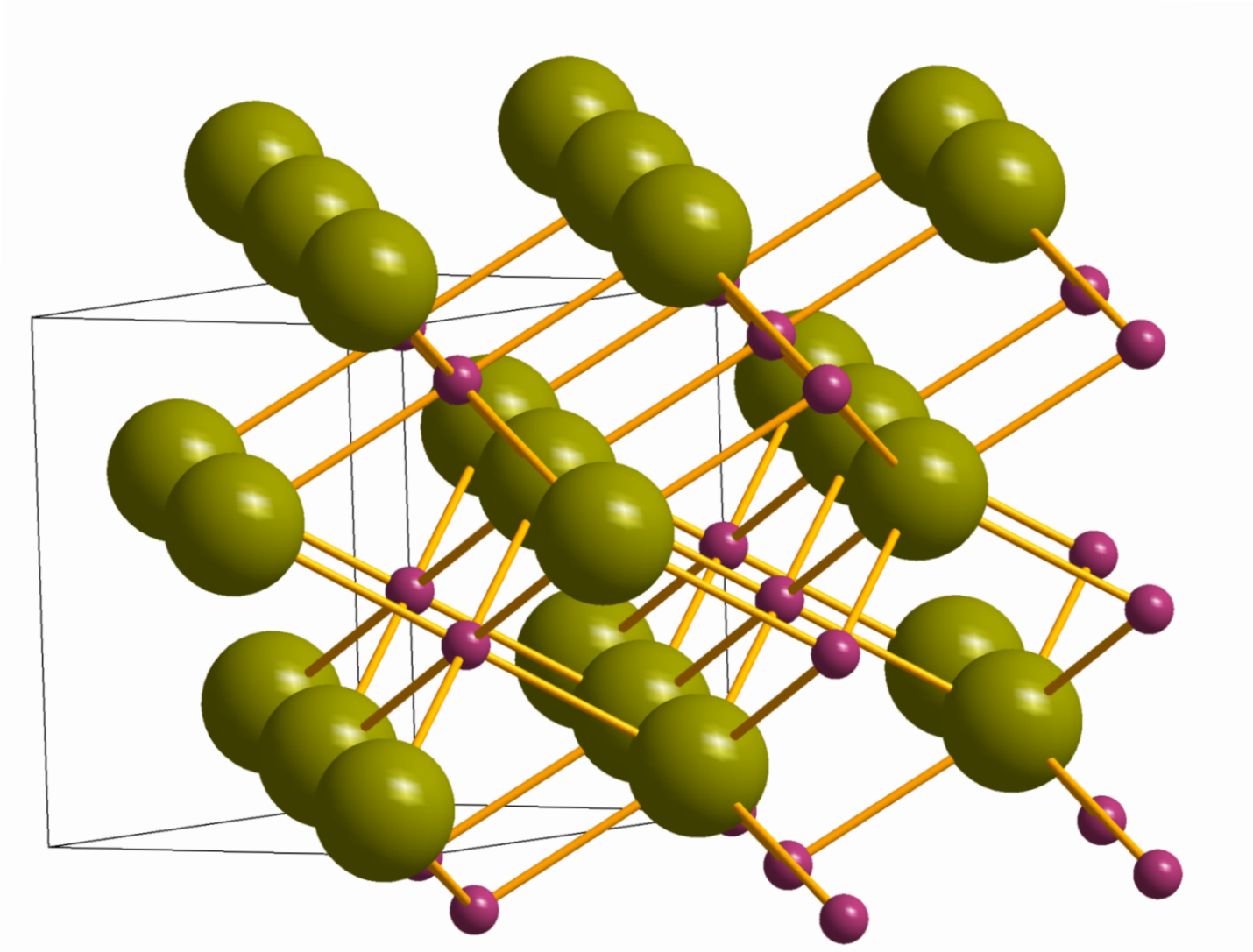

Current Research Topic 6

Probing solidification and phase transformations in metals with high-speed imaging and synchrotron X-ray diffraction

Ivan Kaban and Shilei Liu

Die Synchrotron-Röntgendiffraktometrie (XRD) ist eine leistungsfähige Methode für in situ Untersuchungen der Phasenbildung und -umwandlung unter Gleichgewichts- und Nichtgleichgewichtsbedingungen. Mit Hilfe der mobilen elektromagnetischen Schwebeschmelzanlage des IFW Dresden und der zeitaufgelösten Röntgendiffraktometrie am Deutschen Elektronen-Synchrotron DESY in Hamburg wurden kürzlich Erstarrung und Phasenumwandlungen in Fe-Co-Basislegierungen in Abhängigkeit von der Unterkühlung der Schmelze und dem Legieren mit Nickel und Molybdän entschlüsselt. Erstmals wurde dabei die Keimbildung von δ-Ferrit mit einer Lebensdauer von weniger als einer Millisekunde und die Umwandlung in Austenit nachgewiesen.

Synchrotron X-ray diffraction (XRD) is a powerful tool for in situ studies of phase formation and transformations occurring at equilibrium and non-equilibrium conditions. By using the mobile electromagnetic levitation facility of IFW Dresden and time-resolved XRD at the German Electron Synchrotron DESY in Hamburg recently, the solidification and phase transformations in Fe-Co-based alloys depending on the melt undercooling and alloying with nickel and molybdenum have been revealed. A direct evidence on the nucleation of δ-ferrite with a life time less than one millisecond and transformation to austenite has been obtained for the first time.

Abb. 1: Aufbau des elekromagnetischen Levitators des IFW Dresden an der Beamline P21.1 (Synchrotronstrahlungsquelle PETRA III) am DESY in Hamburg durch Mitarbeiter der IFW-Forschungstechnik.
Fig. 1: Installation of the IFW Dresden electromagnetic levitator at the beamline P21.1 (synchrotron radiation source PETRA III) at DESY in Hamburg by IFW research technicians.

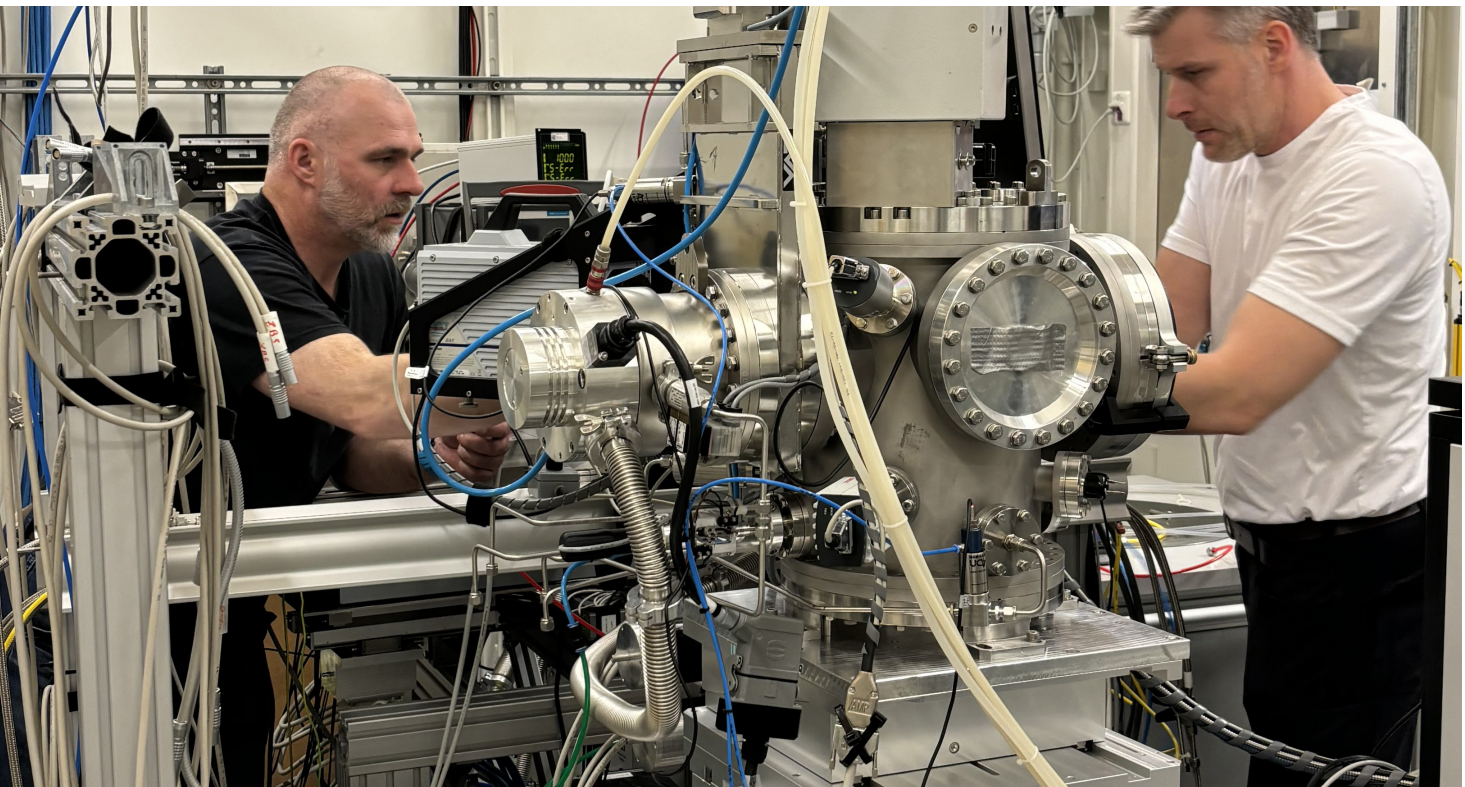

Phase formation during solidification and solid state phase transformations play crucial role in determining microstructure and properties of metallic alloys. Therefore, profound knowledge of these phenomena is fundamental to tailoring material properties and designing manufacturing technologies. For example, two-step solidification of austenitic stainless steels through nucleation of metastable ferrite (δ phase) and subsequent transformation to stable austenite (γ phase) is essential for the resistance to hot cracking in casting, welding and additive manufacturing. The appearance of the so-called double recalescence is not only dependent on alloy composition but on processing and solidification conditions as well [1,2].
Recently the solidification and phase transformations in $Fe_{60}Co_{25}Ni_{10}Mo_5$ and $Fe_{63}Co_{26}Ni_{11}$ alloys (at.%) have been investigated in situ by using electromagnetic levitation (EML), high-speed video and high-energy synchrotron X-ray diffraction [3]. The study has been carried out by researchers from IFW Dresden in collaboration with colleagues from the Institute of Materials Physics in Space (German Aerospace Center DLR, Köln) and Synchrotron Radiation Source PETRA III (German Electron Synchrotron DESY, Hamburg).

$Fe_{60}Co_{25}Ni_{10}Mo_5$ is a newly developed maraging alloy with excellent mechanical properties resulting from the complex microstructure containing austenite, martensite and Mo-rich nano-precipitates [4]. It is worth to explore its solidification, phase formation and microstructure evolution in detail. $Fe_{60}Co_{25}Ni_{10}Mo_5$ alloy is also interesting as it can be considered as a derivative of the binary $Fe_{60}Co_{40}$ where the nucleation and growth competitions between δ and γ phases are known to take place during solidification from undercooled liquid state [5]. The ternary composition has been chosen in order to clarify the role of the alloying elements Ni and Mo.

The samples of about 1.2 g weight were studied by using the EML facility of IFW Dresden, which was installed at the Swedish Materials Science Beamline P21.1 at PETRA III, DESY Hamburg (Fig. 1). The electromagnetic levitation enabled a crucible-free heating and cooling of metallic samples, including melting and solidification, inside the induction coil in a high-purity He atmosphere. The high-energy XRD in transmission geometry provided in situ probing the structure and phase constitution during the sample processing. The energy and the size of the monochromatic X-ray beam were respectively 101.5 keV and 1×1 μm². Two-dimensional diffraction patterns were collected with hybrid-pixel detector EIGER2 X 4M from DECTRIS AG. Noise-free single-photon counting allowed obtaining high quality XRD data at the acquisition rate up to 1000 Hz. The XRD patterns were calibrated by using LaB_6 standard powder and converted to one-dimensional intensities as a function of diffraction angle 2θ. The temperature of levitated samples was measured with the high-speed pyrometer from Dr. Mergenthaler GmbH & Co. KG. The pyrometer was operated in a single-colour mode (spectral range 1.65 – 2 μm) in the temperature range between 618 and 3273 K. The pyrometer data was corrected by using the liquidus temperature T_l measured by differential scanning calorimetry (DSC) as reference. The solidification was recorded with the high-speed camera (HSC) FASTCAM SA5 775K-M3 from Photron Ltd. at a rate of 30.000 frames per second (fps).

A two-dimensional contour plot of the XRD intensities for the $Fe_{60}Co_{25}Ni_{10}Mo_5$ sample measured at the detector frequency of 1000 Hz during one heating-cooling cycle and a corresponding time-temperature curve are presented in Figure 2a. Since the measurement ended at 1035 K upon cooling, it has been repeated with the frequency of the X-ray detector reduced to 10 Hz. The contour plot elucidating the behaviour of the sample during cooling to room temperature is also shown in Figure 2a. The positions of Bragg peaks for the body-centred cubic (bcc) and face-centred cubic (fcc) lattices are indicated on the right-hand side of the graph. The full *T(t)* line shows the data acquired by the pyrometer. The dashed line down to room temperature is a linear projection outside the operation range of the pyrometer.

Similar to a phase analysis of the as-cast sample (not shown), strong reflexes of the main bcc phase (α-ferrite) and weak reflexes of the minor fcc phase (γ-austenite) have been identified on the XRD intensities captured during initial heating up to about 1040 K. Only positions of the peaks shift to smaller 2θ values due to the thermal expansion in this

temperature range. The steep temperature increase to ~1114 K coincides with the onset of the transformation from bcc to fcc taking place during the observed temperature arrest. The endothermic event is also related to the ferromagnetic-to-paramagnetic transition occurring almost simultaneously with the structural transformation.

Once formed, the high-temperature fcc phase remains stable until melting at T_l = 1734 K. Then the molten sample is heated up to 1861 K and cooled down to the nucleation temperature T_n = 1554 K, which is 180 K below the liquidus. The XRD intensities measured from the liquid exhibit two broad diffuse peaks characteristic for disordered substances. A single XRD pattern showing the liquid structure right before crystallisation is plotted in Figure 2b, t = 56.788 s. It is worth mentioning that the pattern taken 1 ms later reveals the coexistence of the three phases – liquid, bcc and fcc – at the very beginning of solidification, t = 56.789 s. As the life time of the metastable δ phase (bcc) is less than 1 ms, only reflexes of the fcc phase can be identified on the next XRD pattern, t = 56.790 s.
Upon further cooling, the solid $Fe_{60}Co_{25}Ni_{10}Mo_5$ sample exhibits a reverse transformation from austenite to α-ferrite, onset denoted by a dashed vertical line in Figure 2a. The γ→α transformation starts at significantly lower temperature (≈660 K), compared to α→γ on heating (≈1040 K). It keeps going until room temperature with a minor fraction of the fcc phase remaining untransformed.
The microstructural analysis of the solidified samples suggests that the large hysteresis of the α–γ transformation observed in the heating-cooling cycles for the $Fe_{60}Co_{25}Ni_{10}Mo_5$ alloy can be explained by microsegregation of Mo to the α/γ interface hindering its mobility.

The solidification of the $Fe_{60}Co_{25}Ni_{10}Mo_5$ alloy with δ→γ transformation revealed by in situ XRD correlates with the sample behaviour recorded by the high-speed video camera, as shown by the image sequence in Figure 3. Due to a higher temperature of rapidly growing solid it appears brighter on a dark background of undercooled liquid or primary crystalline phase and can be distinguished clearly. In all experiments with $Fe_{60}Co_{25}Ni_{10}Mo_5$, covering the range of melt undercooling between 97 and 306 K, the formation of two crystalline phases which appeared shortly after each other was observed. Assuming that that the thermal front represents the solidification front, HSC video data has been used for determination of the growth velocity and delay time for the δ→γ transformation at different undercoolings. Further details on the experiments, data analysis and interpretation, including thermodynamic considerations and available models, have been given in the work [3] submitted for publication.

Summary
Using the mobile electromagnetic levitation facility of IFW Dresden, the solidification of undercooled $Fe_{60}Co_{25}Ni_{10}Mo_5$ and $Fe_{63}Co_{26}Ni_{11}$ melts, competition of stable and metastable phases, and phase transformations upon heating and cooling have been studied with 1 ms temporal resolution at the PETRA III synchrotron radiation source at DESY Hamburg. For the first time, nucleation of the metastable primary phase with a life time less than 1 ms could be proven directly. The delay time for the δ→γ transformation and growth velocity for the both phases have been determined as a function of undercooling by using high-speed camera records. The in situ data has been complemented by calorimetry measurements and ex situ microstructure analysis by scanning electron microscopy (SEM), energy-dispersive X-ray spectroscopy (EDX) and electron backscatter diffraction (EBSD), providing a comprehensive picture on the solidification, phase constitution and microstructure evolution. This approach can be used to study rapid solidification in additive manufacturing and other processes occurring on a short time scale.

References
[1] J.A. Brooks et al., Metall. Trans. A 14A (1983) 1271.
[2] D.M. Matson et al., JOM 69 (2017) 1311.
[3] S. Liu et al., Acta Mater. (under review).
[4] H. Kwon et al., Acta Mater. 248 (2023) 118810.
[5] C. Kreischer and T. Volkmann, Materialia 20 (2021) 101211.

Cooperations
Deutsches Elektronen-Synchrotron DESY, Hamburg, Germany
Institut für Materialphysik im Weltraum, Deutsches Zentrum für Luft- und Raumfahrt (DLR), Köln, Germany

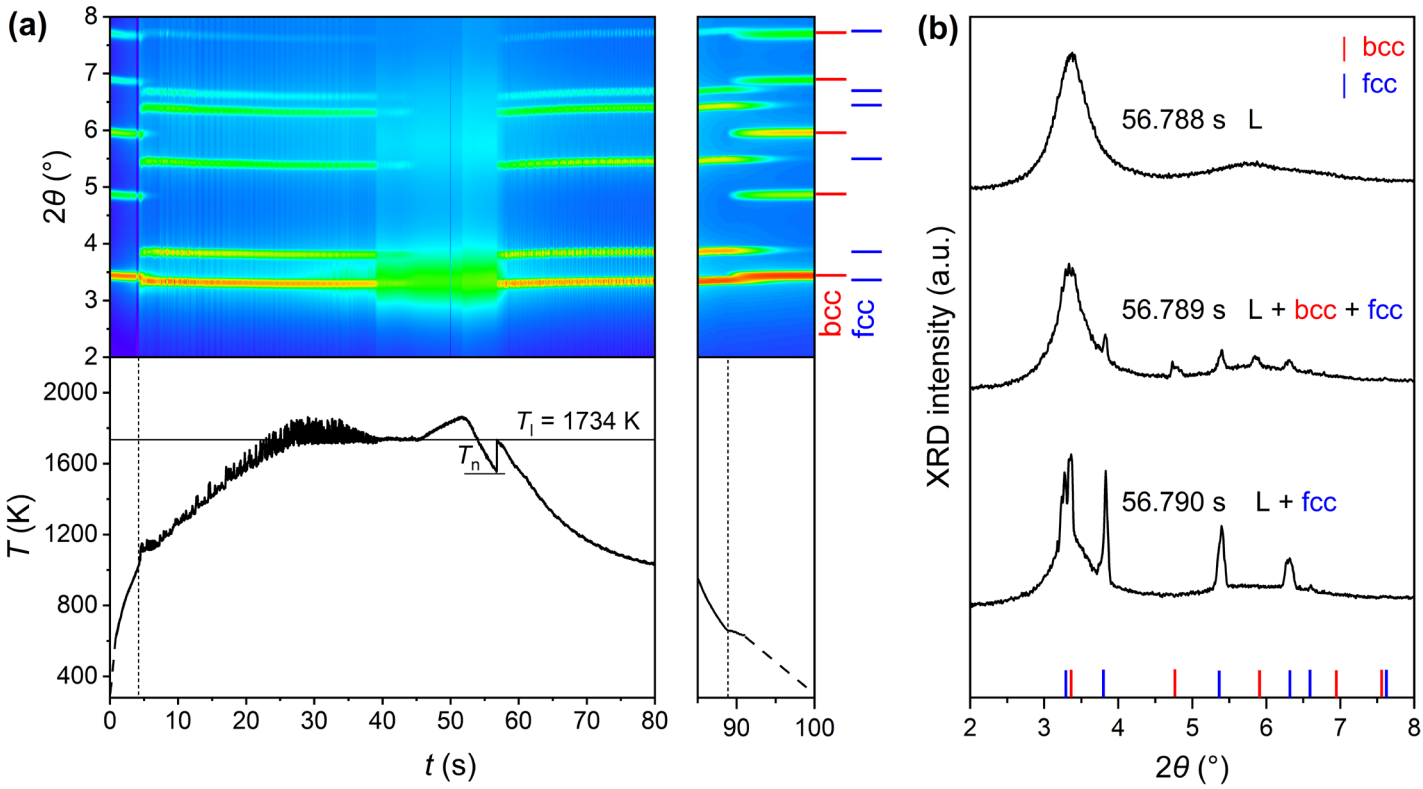

Abb. 2: a) Zeit-Temperatur Verlauf und 2D Konturdiagramm der XRD-Intensitäten für eine levitierte $Fe_{60}Co_{25}Ni_{10}Mo_5$-Probe. Durchgezogene *T(t)* Linie – gemessene Temperatur; gestrichelte *T(t)* Linien – lineare Extrapolation auf Raumtemperatur. (b) Röntgenbeugungskurven zur Erläuterung der Phasenumwandlungen während Erstarrung: i) unterkühlte Schmelze L; ii) nebeneinanderliegenden Phasen L, δ und γ; iii) nebeneinanderliegenden Phasen L and γ.
Fig. 2: a) Time-temperature curve and 2D contour plot of the XRD intensities for a levitated $Fe_{60}Co_{25}Ni_{10}Mo_5$ sample. Full *T(t)* line – temperature measured by pyrometer; dashed lines – linear projection to room temperature. (b) XRD intensities elucidating phase transformations during solidification: i) undercooled liquid L; ii) coexistence of L, bcc δ and fcc γ; iii) coexistence of L and γ.

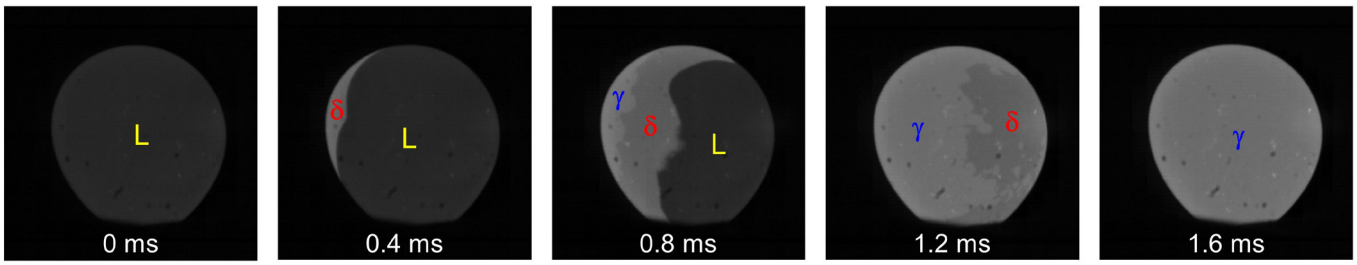

Abb. 3: Digitale Bilder zur Visualisierung der Erstarrung der $Fe_{60}Co_{25}Ni_{10}Mo_5$-Probe aus Abbildung 2. Das Video wurde mit einer Rate von 30.000 Bildern pro Sekunde aufgenommen. Nur jedes zwölfte Bild wird dargestellt.
Fig. 3: Digital images showing the solidification of the $Fe_{60}Co_{25}Ni_{10}Mo_5$ sample from Figure 2. Video data has been recorded at the rate of 30.000 fps. Each 12th frame is shown.

Current Research Topic 7

New insights into 2D magnetic Van der Waals materials

Vladislav Kataev, Rudolf Schäfer, Daria Mikhailova

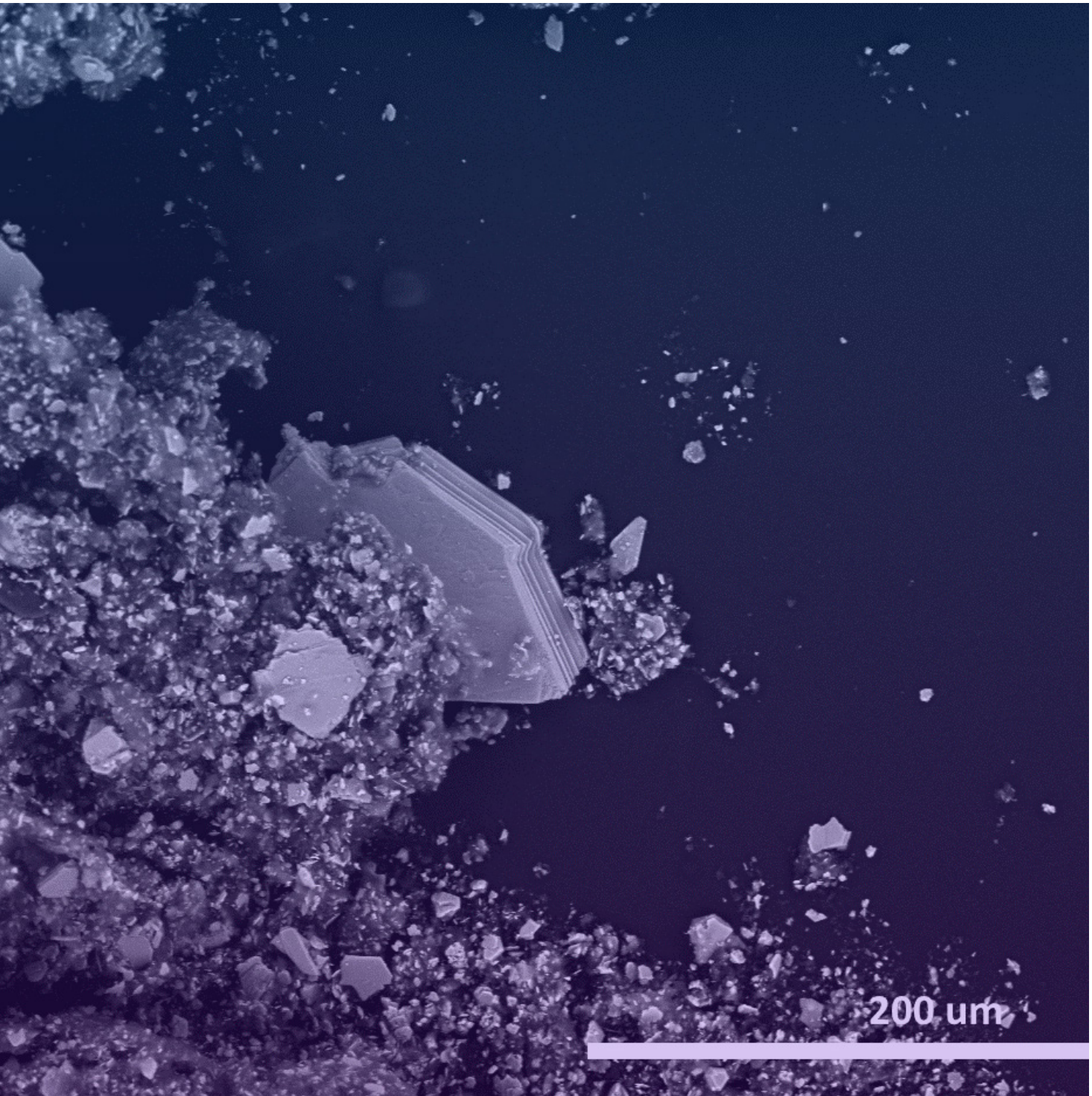

Der zweidimensionale Magnetismus ist ein breites Forschungsfeld sowohl für die Grundlagenforschung als auch für mögliche Anwendungen.
Ein wichtiger Bestandteil ist die dabei stets die magnetische Anisotropie, die für die Verringerung oder auch Verstärkung von Spinfluktuationen und damit für verschiedene Formen der magnetischen Ordnung entscheidend ist.

Wir untersuchten die drei verschiedenen Van-der- Waals-Materialien Fe_4GeTe_2, $Cr_2Ge_2Te_6$ und $NiPS_3$ im Hinblick auf folgende Aspekte:

- **Temperaturabhängigkeit der magnetischen Anisotropie und Kopplung von magnetischen und elektronischen Freiheitsgraden**
- **Hystereseeffekte in Abhängigkeit von der magnetischen Domänenstruktur und**
- **Abstimmung des gesamten Magnetismus durch Schaffung organisch-anorganischer Hybridstrukturen mit endgültiger Trennung der magnetischen Schichten.**

Im Folgenden stellen wir die drei Materialien hinsichtlich dieser Parameter vor.

Magnetism in two dimensions offers a wide range of possibilities for applications and fundamental research. An important point represents the magnetic anisotropy, which is crucial for reducing or strengthening spin fluctuations and, thus, various forms of magnetic order.

In our studies of van der Waals Fe_4GeTe_2, $Cr_2Ge_2Te_6$ and $NiPS_3$ materials, we focused on three various aspects:

- **temperature dependence of the magnetic anisotropy and coupling of magnetic and electronic degrees of freedom,**
- **hysteresis effects in dependence on the magnetic domain structure, and**
- **tuning of the entire magnetism via creating organic-inorganic hybrid structures with ultimate separation of magnetic layers**

In the following, we will present the three materials in terms of these parameters.

Links: REM-Aufnahme von $NiPS_3$-Kristalliten.
Left: SEM picture of $NiPS_3$ crystals.

Material Fe_4GeTe_2

Surprising magnetic anisotropy of the quasi-2D van der Waals ferromagnet Fe_4GeTe_2

The isolation of graphene in 2004 - a monolayer of carbon exfoliated from bulk graphite - has opened a vast new field of research on two-dimensional (2D) materials culminated by the Nobel Prize in physics in 2010 to Andre Geim and Konstantin Novoselov. Graphite belongs to a broad class of materials which are composed of 2D atomic layers held together by weak electrostatic van der Waals (vdW) forces. By now, many other 2D insulating, conductive and superconducting vdW compounds have become known. They have outstanding physicochemical, electronic and optical properties that are extremely interesting for technological applications. More recently, the focus of the 2D research was extended to magnetic vdW compounds offering new magneto-electronic and magneto-optical functionalities. In particular, in the mono- or few-layer form they can be used as a magnetic part of spintronic devices. For that, especially beneficial would be a combination of metallic conductivity and a high ferromagnetic ordering temperature TC. The latter property requires the presence of significant magnetic anisotropy to stabilize magnetic order in the 2D limit.

In the quest for new vdW magnets interesting for novel applications the teams from IFW Dresden, TU Dresden and S. N. Bose National Centre for Basic Sciences in Calcutta joined their efforts in investigating the newly discovered vdW ferromagnet Fe_4GeTe_2 which features a high, nearly room-temperature value of $T_C \approx 270$ K, high transport spin polarization and a large anomalous Hall effect. The Indian partners focused on the studies of electronic properties of Fe_4GeTe_2, colleagues from TU Dresden determined the crystal structure, and scientists from IFW Dresden concentrated on the exploration of the ferromagnetic spin dynamics by multi-frequency high-field electron spin resonance (ESR) spectroscopy.

Fe_4GeTe_2 showed a puzzling effect of spin reorientation, i.e., changing the direction of the sample's magnetization from in-plane to the out-of-plane orientation at the temperature $T_{SR} \sim 110$ K. ESR measurements (Fig. 1a) solved this puzzle. They reveal an unusually strong temperature dependence of the intrinsic magnetic anisotropy (Fig. 2a) that is caused by the coupling of spin and orbital momenta of electrons and by an extrinsic, weakly temperature dependent anisotropy given by the plate-like shape of the material.
The former forces the magnetization vector to orient normal to the plane at $T < T_{SR}$ while the latter turns it into the plane at $T > T_{SR}$ (Fig. 1b,c).

A comparison of the ESR results with measurements of electrical resistivity, magnetoresistance and the Hall effect (Fig. 2) suggests an inherent coupling between magnetic and electronic degrees of freedom in Fe_4GeTe_2 providing important clues for the functionalization of this ferromagnet for the use in magneto-electronic devices.

Reference

[1] Adv. Funct. Mater. 2024, 34, 2402551.
https://doi.org/10.1002/adfm.202402551

Funding

Deutsche Forschungsgemeinschaft (DFG)
Indian Ministry of Science and Technology
S.N. Bose National Centre for Basic Sciences.

Cooperations

TU Dresden
S. N. Bose National Centre for Basic Sciences, India

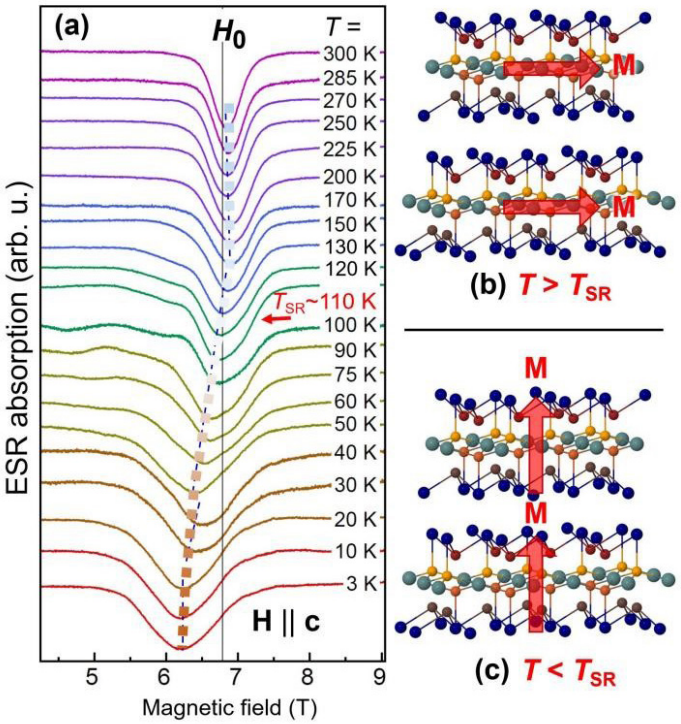

Abb.1: (a) Durch Absenken der Temperatur unter T_c verschiebt sich das ESR-Signal aufgrund der magnetischen Anisotropie von der paramagnetischen Position H_0. Die Verschiebung ist positiv bei $T > T_{SR}$ und ändert das Vorzeichen zu negativ bei $T < T_{SR}$. Dies entspricht der Umkehrung der magnetischen Vektoren M der FM-geordneten Atomebenen von Fe_4GeTe_2 von der Richtung in der Ebene zur Richtung außerhalb der Ebene, wie in (b) und (c) dargestellt.

Fig. 1: (a) By lowering the temperature below T_c the ESR signal shifts from the paramagnetic position H_0 due to magnetic anisotropy. The shift is positive at $T > T_{SR}$ and changes its sign to negative at $T < T_{SR}$. This corresponds to the flip of the magnetization vectors M of the FM ordered atomic planes of Fe_4GeTe_2 from the in-plane to the out-of-plane directions as depicted in (b) and (c), respectively.

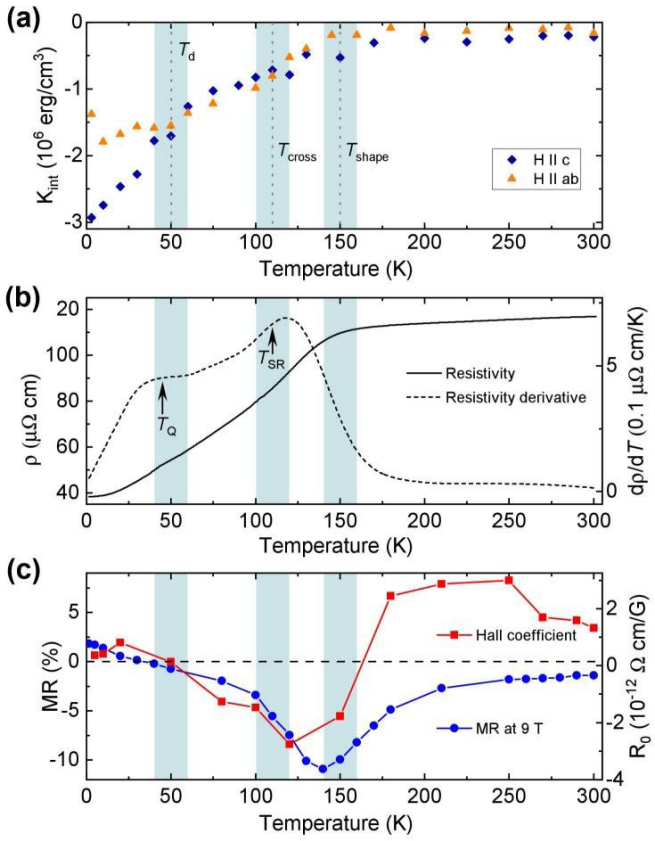

Abb. 2: (a) Die aus den ESR-Daten gewonnene magnetokristalline Energiedichte $K_{int}(T)$ nimmt unterhalb T_{shape} stark zu, was zur Umkehrung der Magnetisierungsvektoren bei T_{SR} führt (Abb. 1b,c). Charakteristische Temperaturen, bei denen die $K_{int}(T)$-Abhängigkeit ihren Charakter ändert (schattierte vertikale Balken), entsprechen denen des spezifischen Widerstands ρ(T) (b), des Magnetowiderstands MR(T) und des Hall-Koeffizienten $R_0(T)$ (c), was auf ein verflochtenes magnetisches und elektronisches Verhalten in Fe_4GeTe_2 hindeutet.

Fig.2: (a) Magnetocrystalline energy density $K_{int}(T)$ obtained from the ESR data strongly increases below T_{shape} causing the flip of magnetization vectors at TSR (Fig. 1b,c). Characteristic temperatures, where the $K_{int}(T)$ dependence changes its character (shaded vertical bars), correspond with those in the resistivity ρ(T) (b), magnetoresistance MR(T) and Hall coefficient $R_0(T)$ (c), suggesting intertwined magnetic and electronic behaviors in Fe_4GeTe_2.

Material $Cr_2Ge_2Te_6$

Wide-field MOKE Microscopy and Magnetometry on $Cr_2Ge_2Te_6$ exfoliated van der Waals flakes

As for most magnetic materials, hysteresis measurements and domain research also play crucial roles in the characterization of magnetic vdW material.
Hysteresis loops are mostly obtained by laser-based magneto-optical Kerr effect (MOKE) magnetometry or by anomalous Hall effect measurements, while for domain imaging primarily Lorentz Electron Microscopy, Nitrogen-Vacancy Microscopy and X-ray based imaging are applied [2]. Wide-field MOKE microscopy, a common imaging technique for general domain research [3], has hardly been utilized.

Using $Cr_2Ge_2Te_6$ (CGT) flakes in the 10 nm thickness range and applying our cryo-Kerr setup at a temperature of 5 K, we have explored the potential of this method for the characterization of low-dimensional crystals. Besides its capability of domain imaging, in a MOKE microscope also hysteresis loops can be measured by plotting the Kerr intensity at selectable sample areas as a function of magnetic field. Pinched loops with a shoulder when deceasing the field from saturation are typically measured on our flakes (Fig. 3) whereas magnetic domains could not be seen.

By domain theory we could show that in CGT flakes perpendicularly magnetized band domains with periods around 200 nm are expected. Such domains could not be seen in our cryo-Kerr microscope due to insufficient resolution in the 500 nm regime. However, their existence can be indirectly derived from the mentioned shoulders in the hysteresis loops.

The band domain pattern is the zero-field ground state for CGT flake thicknesses above approx. 7 nm. We have determined this thickness from the initial susceptibility of the recorded hysteresis loops.

Below that thickness, equilibrium band domains are not expected to exist, which can be deduced indirectly from the disappearance of the shoulder in the hysteresis loops. From the critical thickness a specific domain wall energy of $2.7 \cdot 10^{-4}$ J/m² for CGT flakes could be estimated.

We have furthermore demonstrated that an experimentally-found sign inversion of the Kerr signal for different flake thicknesses and light colors can be explained on base of a Fresnel-type magneto-optical depth sensitivity concept. Accordingly, the Kerr contrast is governed by the relative phase of the Kerr amplitude that can be freely adjusted by a rotatable compensator.
The compensator is thus the decisive optical element in MOKE magnetometry and microscopy on 2D vdW materials. It needs to be appropriately aligned to avoid a cancelation of the Kerr contrast and to maximise the Kerr signal.

We conclude that MOKE magnetometry may be seen as method of choice to measure hysteresis loops on magnetic 2D vdW flakes as it allows to select flake areas with specific thicknesses, which would not be possible by integral hysteresis techniques. This areal selection is especially easy if MOKE magnetometry is performed in a wide-field Kerr microscope. Our work was recently published in ref. [4].

References

[1] C. Gong et al., Nature 546, 265 (2017)
[2] Q.H. Wang et al., ACS Nano, 16, 5, 6960 (2022)
[3] R. Schäfer and J. McCord: Magneto-Optical Microscopy. In: Franco, V., Dodrill, B. (eds) Magnetic Measurement Techniques for Materials Characterization. Springer, Cham. (2019)
[4] I. Soldatov et al., IEEE Access, vol. 12, pp. 181025-181040, (2024)

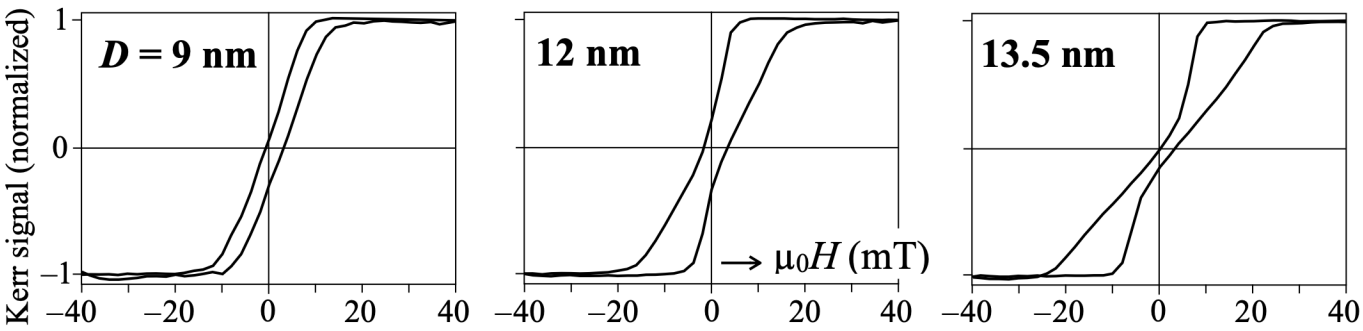

Abb. 3: Hysteresekurven einer $Cr_2Ge_2Te_6$-Flocke, gemessen in einem senkrechten Magnetfeld unter polaren Kerr-Bedingungen in Bereichen unterschiedlicher Dicke D wie angegeben. Alle Kurven wurden bei einer Temperatur von 5 K und unter Verwendung von Rotlicht gemessen. Analysator und Kompensator wurden auf ein maximales Kerr-Signal ausgerichtet.
Fig. 3: Hysteresis loops of a $Cr_2Ge_2Te_6$ flake, measured in perpendicular magnetic field under polar Kerr conditions in regions of different thickness D as indicated. All loops were measured at a temperature of 5 K and by using red light. Analyzer and compensator have been intuitively adjusted for maximum Kerr signal.

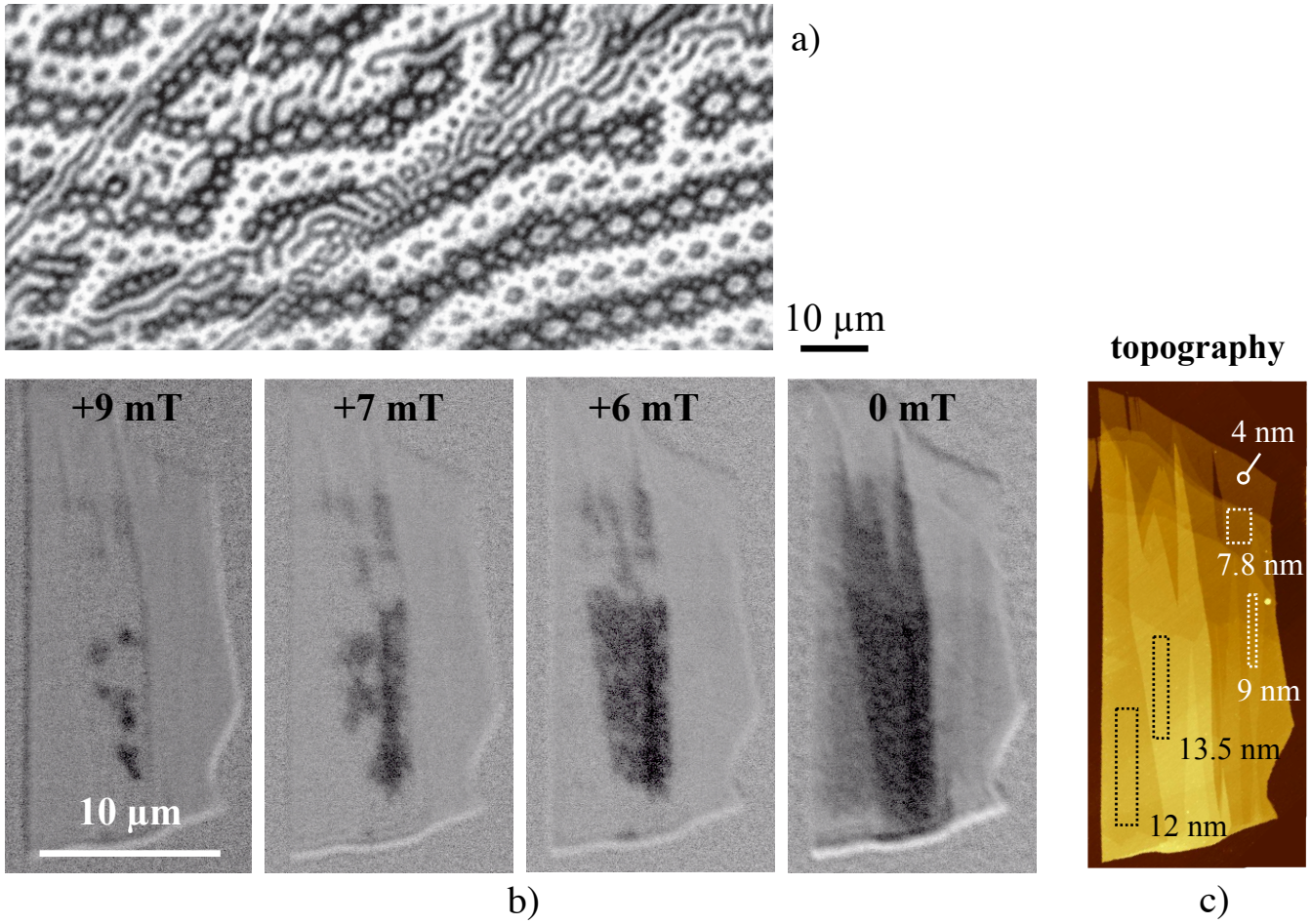

Abb. 4: (a) Typische Domänen auf einem CGT-Bulkkristall mit einer Dicke von 0,2 mm, abgebildet auf der Oberfläche senkrecht zur einfachen Achse. Zu beachten sind die Domänenverfeinerung entlang der Kratzer. (b) Domänenentwicklung bei einem abnehmenden senkrechten Magnetfeld, beobachtet durch polare Kerr-Mikroskopie. Abbildung 4c zeigt den nichtmagnetischen (topographischen) Kontrast. Alle Domänen wurden bei einer Temperatur von 5 K abgebildet.
Fig. 4: (a) Typical domains on a CGT bulk crystal with a thickness of 0.2 mm, imaged on the surface perpendicular to the easy axis. Note the domain refinement along the scratches. (b) Domain evolution at a decreasing perpendicular magnetic field, observed by polar Kerr microscopy. Image (c) shows the nonmagnetic (topographic) contrast. All domains were imaged at a temperature of 5 K.

Material $NiPS_3$

Suppressed magnetic ordering in 2D van der Waals antiferromagnet $NiPS_3$ via intercalation of organic cations

Due to their versatile anisotropic properties, van der Waals transition metal phosphorus trisulfides MPS_3 with M = Ni, Co, Fe, Mn are considered as promising materials for opto-electronic and electrocatalytic applications. In terms of fundamental physics they offer the possibility of novel ground states.

The family of MPS_3 compounds crystallizes in a $CdCl_2$-type structure, see Figure 5. In the layers, transition metal ions M, usually in the oxidation state 2+, are octahedrally surrounded by S anions, which are interconnected via P cations, containing P-P bonds. Hence, the correct presentation of the chemical formula should be $M_2P_2S_6$ with $(P_2S_6)^{-4}$ units. There are competing inter- and intra-layer magnetic interactions in the structure.
The relatively weaker van der Waals interaction between magnetic cations in neighboring layers can be controlled through change of the interlayer distance via intercalation of cations/anions. Since it is not always feasible to synthesize the desired structures using solid-state synthesis, subsequent soft chemical/electrochemical intercalation of species can be applied for tuning the resulting structural and physical properties.

$NiPS_3$ represents a quasi two-dimensional antiferromagnet with a Néel temperature of 155 K. Above this temperature, there is a broad maximum in magnetization reflecting strong short-range magnetic interactions up to 300 K. Insertion of electron-donating species into semiconducting $NiPS_3$ can result in two possibilities for the electron transfer, either to a discrete Ni atomic level, or to a molecular level of the $(P_2S_6)^{-4}$ unit.

We performed systematic structural, spectroscopic and magnetic studies of $NiPS_3$ powder after electrochemical intercalation of large *1-ethyl-3-methylimidazolium* (EMIM) cations.
More than 1 EMIM per $NiPS_3$-unit can be intercalated between host layers, leading to a significant interlayer distance expansion from 6.3 Å to 11.3 Å without noticeable rearrangements within the layers, as revealed from XRD measurements (see Fig. 5).

Surprisingly, the intercalation of EMIM cations does not lead to any changes in Ni, S and P *K*-edge XANES spectra of $NiPS_3$ (Fig. 6a) and only very little in their EXAFS spectra. It is very likely that there is an electrochemical reduction of EMIM cations to heterocyclic carbenes with their possible dimerization between host layers without any impact on the $NiPS_3$electronic structure.
However, some changes in the magnetic behavior of the hybrid organic-inorganic (EMIM)$NiPS_3$ structure were observed (Fig. 6b): with a progressive EMIM-intercalation level, the antiferromagnetic ordering vanishes while the paramagnetic contribution increases, resulting in a paramagnetic moment of 0.93 μB for $EMIM_{1.0}NiPS_3$, which is, however, lower than the spin-only theoretical paramagnetic moment of 2.83 μ_B for Ni^{2+} with a d^8 electron configuration (S = 1). The more paramagnetic-like magnetization curve for intercalated materials points to decreased interaction between $NiPS_3$-layers due to the interlayer expansion.
Using ionic liquid cations for the structural modification of van der Waals magnetic materials can provide a viable tool for a controlled tuning of magnetism without changes in the electronic structure.

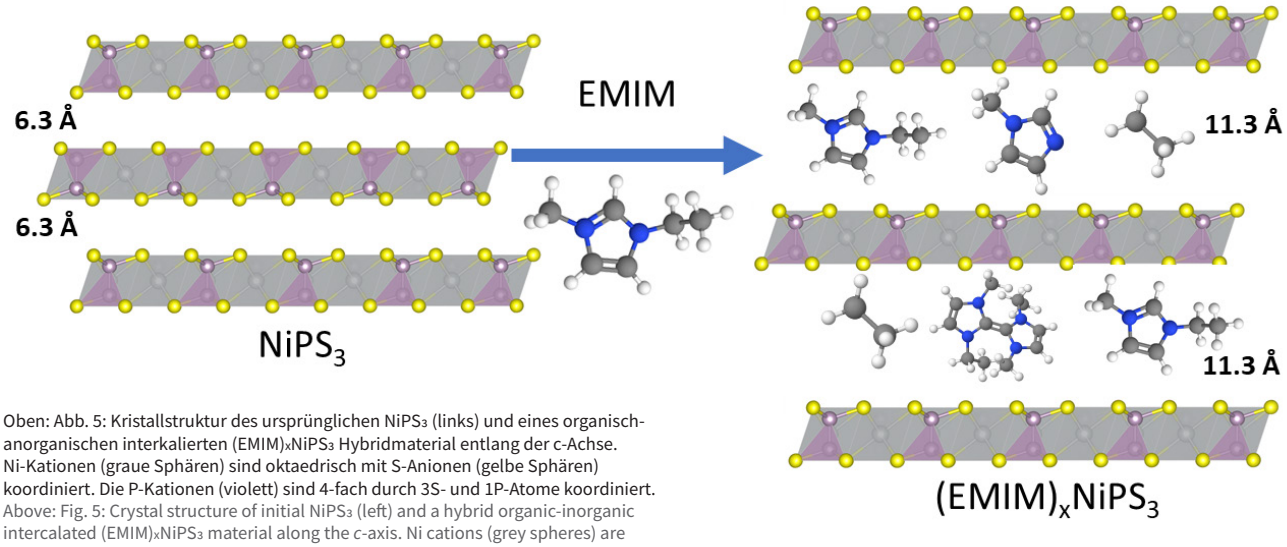

Oben: Abb. 5: Kristallstruktur des ursprünglichen $NiPS_3$ (links) und eines organisch-anorganischen interkalierten $(EMIM)_xNiPS_3$ Hybridmaterial entlang der c-Achse. Ni-Kationen (graue Sphären) sind oktaedrisch mit S-Anionen (gelbe Sphären) koordiniert. Die P-Kationen (violett) sind 4-fach durch 3S- und 1P-Atome koordiniert.
Above: Fig. 5: Crystal structure of initial $NiPS_3$ (left) and a hybrid organic-inorganic intercalated $(EMIM)_xNiPS_3$ material along the *c*-axis. Ni cations (grey spheres) are octahedrally coordinated by S anions (yellow spheres). P cations (violet) are 4-fold-coordinated by 3S and 1P atoms.

Rechts: Abb. 6: (a) Operando XAS-Daten, gemessen an der Ni K-Kante, die während der elektrochemischen Einlagerung von EMIM-Kationen in die $NiPS_3$-Struktur aufgenommen wurden, sowie die erste Ableitung des normalisierten Absorptionskoeffizienten. (b) Suszeptibilität von interkalierten $(EMIM)_xNiPS_3$-Proben, abgekühlt ohne Magnetfeld, in Abhängigkeit von der Temperatur.
Right: Fig. 6: (a) Operando Ni K-edge XAS data recorded during electrochemical intercalation of EMIM cations into the $NiPS_3$ structure, including the first derivative of the normalized absorption coefficient. (b) Susceptibility (zero-field cooling) versus temperature for intercalated $(EMIM)_xNiPS_3$ samples.

6a)

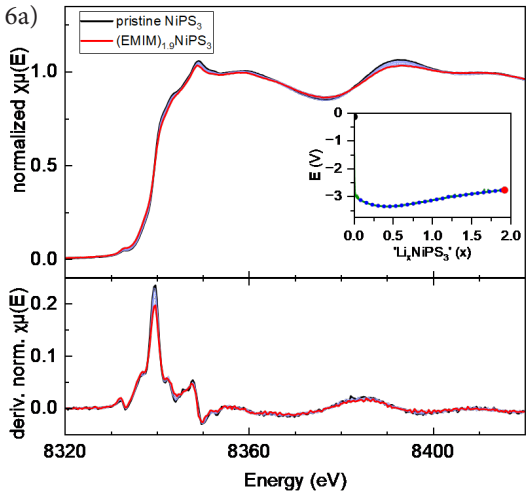

6b)

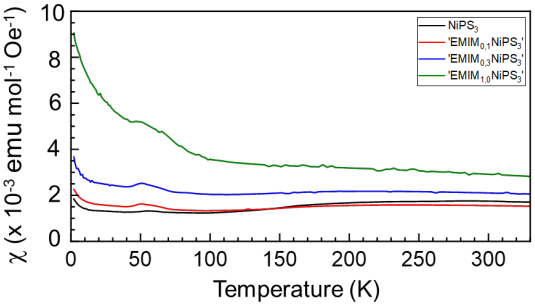

Reference

J. Mat. Chem. A, 2024, 12, 3523 - 3541
DOI: 10.1039/D3TA06196E

Funding

IFW Dresden excellence program
German Federal Ministry of Education and Research (BMBF)
German Research Foundation (DFG)

Cooperations

TU Dresden, Germany
ALBA Synchrotron, Spain
Helmholtz-Zentrum Berlin für Materialien und Energie GmbH, Germany

Current Research Topic 8

Multilayer Structures of 2D materials via Atomic Layer Deposition

Jun Yang, Amin Bahrami, Sebastian Lehmann, Daniel Wolf, Pavel Potapov, Almut Pöhl, Jaroslav Charvot[1], Tobias Ritschel[2], Mohammadreza Daqiqshirazi[2], Thomas Brumme[2], Jochen Geck[2], Filip Bureš[1], Axel Lubk, and Kornelius Nielsch

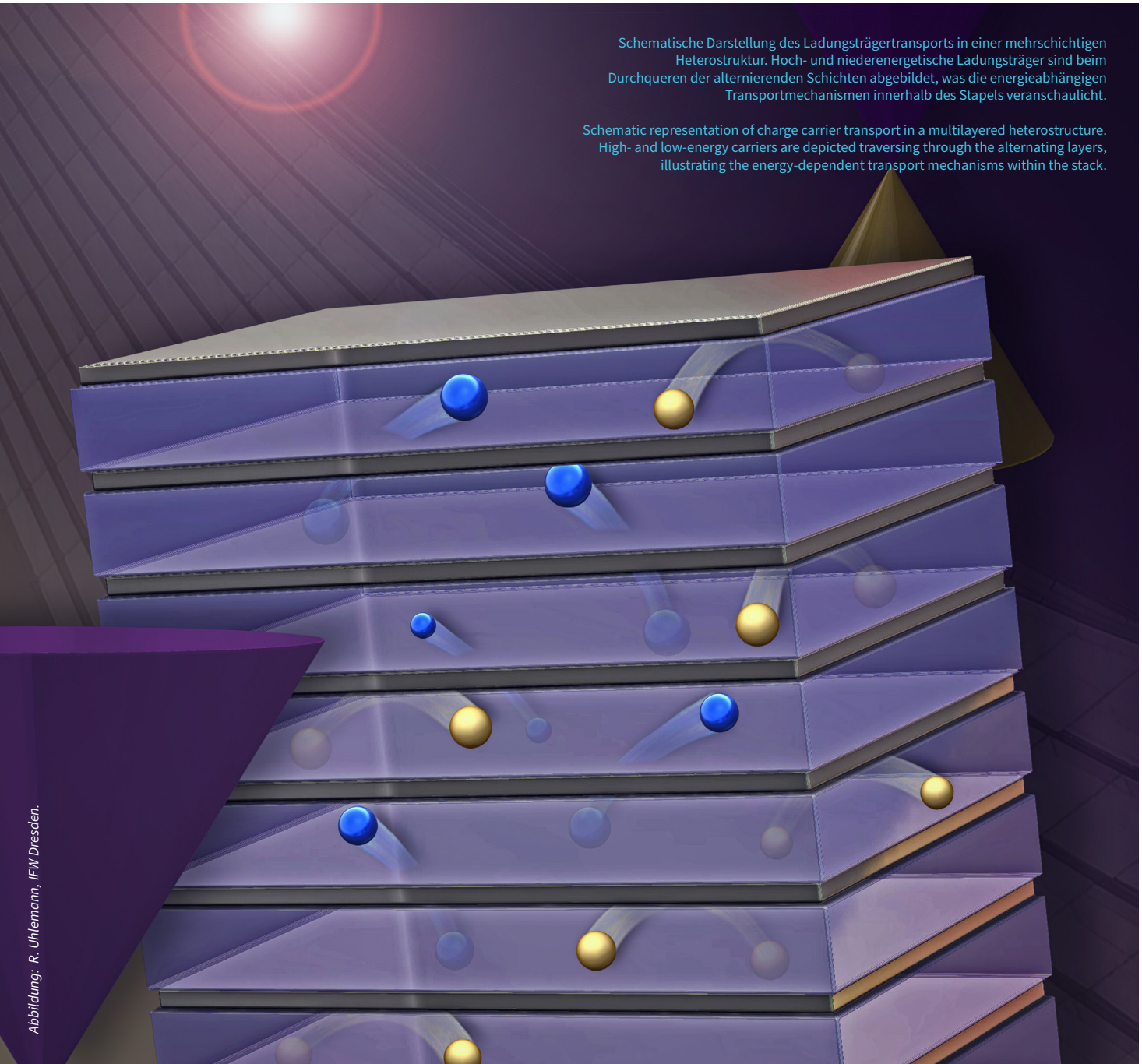

Schematische Darstellung des Ladungsträgertransports in einer mehrschichtigen Heterostruktur. Hoch- und niederenergetische Ladungsträger sind beim Durchqueren der alternierenden Schichten abgebildet, was die energieabhängigen Transportmechanismen innerhalb des Stapels veranschaulicht.

Schematic representation of charge carrier transport in a multilayered heterostructure. High- and low-energy carriers are depicted traversing through the alternating layers, illustrating the energy-dependent transport mechanisms within the stack.

Abbildung: R. Uhlemann, IFW Dresden.

In dieser Studie wurden durch Atomlagenabscheidung zweidimensionale (2D) Materialien mit gestapelten Metallchalkogenid-Architekturen synthetisiert.
Die resultierenden mehrschichtigen Dünnfilme weisen charakteristische Eigenschaften wie eine extrem niedrige thermische Leitfähigkeit und verbesserte optische Reaktionen auf. Das macht sie zu potentiellen Materialien für Anwendungen in der Nanoelektronik, Optoelektronik, Energiespeicherung und Katalyse.
Durch die strategische Kombination von geschichteten und nicht geschichteten Materialien erreichten wir eine Feinabstimmung ihrer elektronischen Eigenschaften, was die Entwicklung von Heterostrukturen mit schmalen Bandlücken und maßgeschneiderten optischen Funktionalitäten ermöglichte. Zur Charakterisierung dieser innovativen Materialien führten wir umfassende Strukturanalysen und elektronische Transportmessungen unter Verwendung speziell entwickelter mikrostrukturierter Plattformen durch.

In this study, two-dimensional (2D) materials with stacked metal chalcogenide architectures have been synthesised using atomic layer deposition.
The resulting multilayered thin films exhibit distinctive properties, including ultralow thermal conductivity and enhanced optical response, and demonstrate promising potential for applications in nanoelectronics, optoelectronics, energy storage and catalysis.
By strategically combining layered and non-layered materials, we achieved fine-tuning of their electronic properties, enabling the development of heterostructures with narrow band gaps and tailored optical functionalities. We conducted comprehensive structural analyses and electronic transport measurements using custom-designed microstructured platforms to characterize these innovative materials.

The growing demand for energy-efficient technologies in sensors, Internet of Things devices, and wearables has accelerated interest in cost-effective energy-harvesting materials. Thin-film thermoelectric (TE) devices, which convert waste heat into electrical energy, provide a promising solution. Periodic TE structures offer the flexibility to engineer electrical and thermal transport properties by manipulating interfacial features at the atomic scale. These structures demonstrate exceptional characteristics, such as extremely low thermal conductivity and the emergence of quantum phenomena, which can enhance the Seebeck coefficient. Additionally, 2D materials hold great potential for electronic devices due to their inherent compatibility with CMOS-based technologies, stemming from their relatively straightforward integration processes.
Atomic Layer Deposition (ALD) is a vapor-phase technique introduced in the 1970s by Dr. Suntola and colleagues [1]. This method utilizes sequential pulses of individual precursors to achieve self-limiting, layer-by-layer growth of atomic-scale films on substrate surfaces (Fig. 1). ALD enables the fabrication of conformal thin films with tailored properties through precise control of deposition parameters, significantly reducing the complexity of processing steps. The films produced by ALD are highly competitive for applications in micro-machines, sensors, and advanced devices across science, engineering, and technology. Despite its versatility, the use of ALD for constructing heterostructures from 2D materials remains largely unexplored, presenting an opportunity for further innovation.

In our recent work, we focused on topological insulators (TIs) due to their exceptional electrical and thermoelectric properties. A distinctive feature of TI layers is their ability to maintain high electrical conductivity and carrier mobility, even as their thickness is reduced to nanoscale dimensions. The Sb_2Te_3 films, grown at 80°C by ALD, exhibit high crystallinity with the c-axis oriented perpendicular ($\perp$) to the film plane. ALD-grown TI films demonstrate enhanced electrical conductivity compared to bulk single crystals, with carrier concentrations ranging from 10^{18} to 10^{19} cm^{-3} and carrier mobilities exceeding 100 Vs/cm^2, indicating low defect densities in these films. We conducted a detailed study of the multilayer system consisting of Sb_2Te_3 and SbO_x,

which was fabricated using an oxidant-free ALD process involving the reaction of $SbCl_3$ and $Sb(OEt)_3$ (Fig. 2a/b). Thermoelectric characterization of the highly ordered samples, performed without post-annealing using the *zT*-chip setup, revealed significant improvements in the Seebeck coefficient and electrical conductivity, alongside a notable reduction in thermal conductivity due to phonon confinement effects. The carrier mobility reached values greater than 150 Vs/cm^2, further improving when the Sb_2Te_3 layer thickness was reduced to 3 nm. High-resolution TEM imaging showed clear separation of the amorphous SbO_x and crystalline Sb_2Te_3 layers at the atomic level (Fig. 2c).

We extended this work by designing multilayered systems combining Sb_2Te_3 and Sb_2Se_3, leveraging their distinct tetrahedral and orthorhombic crystal structures. The p-type hole carrier concentration of Sb_2Te_3 films is enhanced by the Sb_2Se_3 sublayers through carrier transfer. Further thinning of the Sb_2Te_3 layers led to a significant increase in the Seebeck coefficient. The combined effect of the enhanced Seebeck coefficient and electrical conductivity in the Sb_2Te_3/Sb_2Se_3 superlattice resulted in a high power factor of up to 852 $\mu W\ m^{-1}\ K^{-2}$ at room temperature. In the Sb_2Te_3/Sb_2Se_3 system, we observed Volmer-Weber growth behavior, in contrast to the conventional monolayer-by-monolayer growth, especially for low-cycle 2D thin films. The exchange reaction at the gas-solid interface during the ALD process facilitated alloying, where exposure of the Se precursor to the Sb_2Te_3 surface led to the substitution of Te atoms with Se atoms at the interface. This process resulted in the formation of alloy clusters and atomic-scale distortions. Interestingly, the lattice thermal conductivity of the sample with a Sb_2Te_3:Sb_2Se_3 composition ratio of 2:2 nm was lower than that of the sample with a ratio of 5:5 nm (Fig. 3). This difference can be attributed to the varying phonon scattering mechanisms in the alloyed structures and the quantum confinement effects in the superlattice, which have distinct impacts on thermal conductivity.

These findings highlight the potential of ALD in fabricating high-performance 2D heterostructures with tailored electrical and thermal properties. Future work will focus on integrating organic molecular interlayers with topological insulators using a combination of molecular layer deposition and ALD. This approach will enable ultra-precise control of interlayer spacing, facilitating the integration of organic electronic functionalities and the development of advanced gas separation membranes. Additionally, the scalability of ALD will support the deposition of 2D materials on large-area and three-dimensional substrates, broadening their applicability in next-generation technologies.

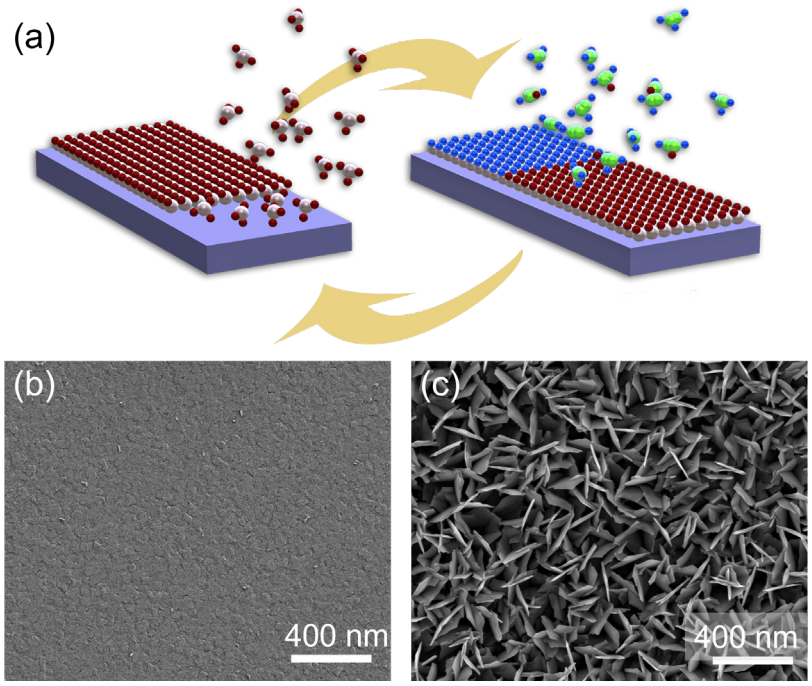

Abb. 1: (a) Schematische Illustration des ALD Prozesses. Elektronenmikroskopieaufnahmen der mittels ALD hergestellten (b) Sb_2Te_3 and (c) $Sb_2Te_{2-x}O_x$ 2D Dünnschichten.
Fig. 1: (a) Schematic illustration of the ALD process. The SEM images of ALD processed (b) Sb_2Te_3 and (c) $Sb_2Te_{2-x}O_x$ 2D thin films.

Published in

J. Yang, S. Mukherjee, S. Lehmann, F. Krahl, X. Wang, P. Potapov, A. Lubk, T. Ritschel, J. Geck, K. Nielsch, Low-Temperature ALD of SbO_x/Sb_2Te_3 Multilayers with Boosted Thermoelectric Performance. Small 2024, 20, 2306350.

J. Yang, M. Daqiqshirazi, T. Ritschel, A. Bahrami, S. Lehmann, D. Wolf, W. Feng, A. Pöhl, J. Charvot, F. Bureš, T. Brumme, A. Lubk, J. Geck, and K. Nielsch, Interfacial Distortion of Sb_2Te_3–Sb_2Se_3 Multilayers via Atomic Layer Deposition for Enhanced Thermoelectric Properties, ACS Nano 2024 18 (27), 17500-17508

References

[1] T. Suntola, Mater. Sci. Rep. 4 (1989) 261
[2] J. Yang et al., ACS Nano 18 (2024) 17500
[3] J. Yang et al., Small 20 (2024) 2306350

Funding

German Collaborative Research Centers:
Grant No.: SFB 1415

Cooperations

[1] University of Pardubice, Czech Republic
[2] Technische Universität Dresden, Germany

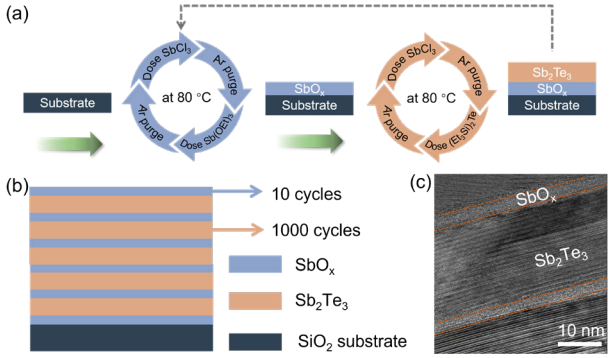

Rechts: Abb. 2: (a) Schematische Darstellung des ALD Prozesses der SbO_x/Sb_2Te_3-Heterostruktur. (b) Skizze der SbO_x/Sb_2Te_3 -Mehrschichtstruktur. (c) Typisches Querschnitts-TEM-Bild der SbO_x/Sb_2Te_3-Heterostruktur.
Right: Fig. 2: (a) Schematic illustration of the ALD process of SbOx/Sb2Te3 heterostructure. (b) Sketch of the SbO_x/Sb_2Te_3 multilayer structure. (c) The typical cross-section TEM image of SbO_x/Sb_2Te_3 heterostructure.

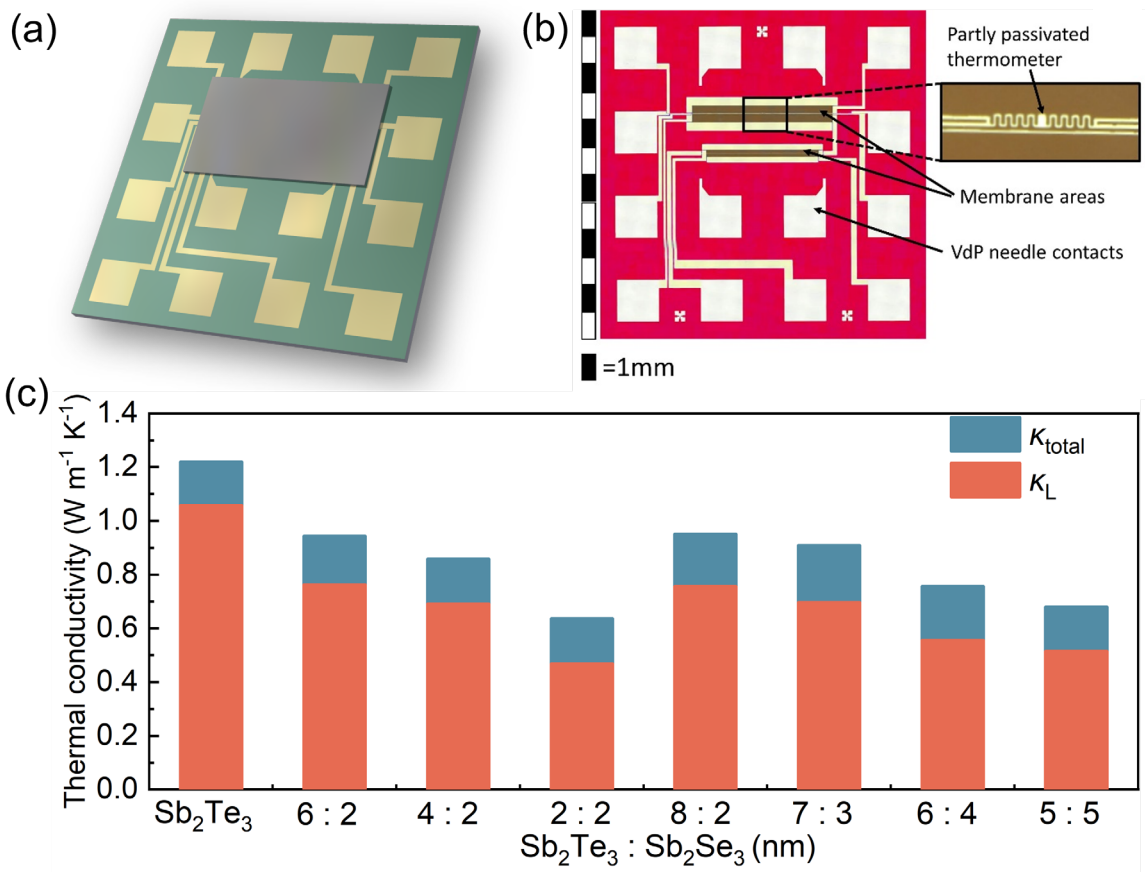

Unten: Abb. 3: Linseis TFA thermoelektrische Evaluierungsplattform (a) mit und (b) ohne Dünnschichtabscheidung. (c) Die Gesamtwärmeleitfähigkeit und die Gitter-Wärmeleitfähigkeit von Sb_2Te_3–Sb_2Se_3 Dünnschichten.
Below: Fig. 3: Linseis TFA thermoelectric evaluation platform (a) with and (b) without thin film deposition. (c) The total thermal conductivity and lattice thermal conductivity of Sb_2Te_3–Sb_2Se_3 thin films.

Current Research Topic 9

A sustainable revolution in thermoelectric technology through Atomic Layer Deposition

Pingjun Ying, Ruben Bueno Villoro[1], Amin Bahrami, Lennart Wilkens, Heiko Reith, Dominique Alexander Mattlat[1], Vicente Pacheco[2], Christina Scheu[1], Siyuan Zhang[1], Kornelius Nielsch, and Ran He

Die meisten thermoelektrischen Bauteile basieren auf Tellur, einem schwer verfügbaren und giftigen Element. Eine gute Alternative bilden magnesiumbasierte neue Materialien. Diese bedürfen allerdings einer besonderen Aufbereitung, damit sie langfristig stabil und effizient arbeiten können.

Thermoelectric components are most commonly based on tellurium, an element that is difficult to obtain and toxic. New magnesium-based materials are a good alternative, but special processing is required to ensure they remain stable and efficient in the long term.

Abbildung: Kreiert mit Adobe Firefly.

In einer Welt, in der Energieeffizienz und Nachhaltigkeit zu zentralen Prioritäten geworden sind, bietet die Thermoelektrik eine vielversprechende Lösung. Thermoelektrische Geräte wandeln Abwärme in Elektrizität um und ermöglichen eine effiziente Kühlung ohne bewegliche Teile, was sie zuverlässig und umweltfreundlich macht. Allerdings basieren die meisten kommerziellen thermoelektrischen Systeme auf Bismuttellurid (Bi_2Te_3), einem Material, das aufgrund seiner Abhängigkeit vom seltenen Element Tellur sowohl giftig als auch knapp ist. Angesichts dieser Einschränkungen haben wir bahnbrechende Fortschritte mit magnesiumbasierten (Mg-basierten) thermoelektrischen Modulen erzielt, die eine nachhaltigere Alternative darstellen.
Dieser Bericht fasst eine innovative Studie zusammen, die nicht nur das Potenzial Mg-basierter thermoelektrischer Materialien beleuchtet, sondern auch eine zentrale Herausforderung angeht: die Sicherstellung ihrer langfristigen Stabilität unter realen Bedingungen. Durch den Einsatz von Atomic Layer Deposition (ALD) als Schutzbeschichtung konnten wir bedeutende Fortschritte in der Haltbarkeit und Effizienz dieser Module erzielen und damit einen entscheidenden Schritt in Richtung nachhaltigerer Energielösungen machen.

In a world where energy efficiency and sustainability have become critical priorities, thermoelectric technology offers a promising solution.
These devices convert waste heat into electricity and enable efficient cooling without moving parts, making them reliable and environmentally friendly. However, most commercial thermoelectric systems rely on bismuth telluride (Bi_2Te_3), a material that is both toxic and scarce due to its reliance on the rare element tellurium. Recognizing this limitation, we have made groundbreaking progress with magnesium-based (Mg-based) thermoelectric modules, which offer a more sustainable alternative.
This report summarizes an innovative study that not only highlights the potential of Mg-based thermoelectric materials but also addresses a key challenge: ensuring their long-term stability under real-world conditions. By employing atomic layer deposition (ALD) as a protective coating, we achieved significant advancements in the durability and efficiency of these modules, marking a pivotal step toward more sustainable energy solutions.

Thermoelectric modules work on a simple yet powerful principle: they generate electricity by exploiting the temperature difference between two surfaces. They are used in a range of applications, from capturing waste heat in industrial processes to powering cooling systems in electronic devices. Their advantages include noiseless operation, reliability, and low maintenance requirements [1]. For decades, thermoelectric systems have been dominated by Bi_2Te_3-based materials, which are efficient at converting heat into electricity. However, these materials depend on tellurium, a toxic and extremely scarce element that is found in minute concentrations in the Earth's crust. This has created a demand for sustainable alternatives that can meet the growing need for energy-efficient technologies. Mg-based thermoelectric modules provide a compelling alternative. Composed of abundant and environmentally friendly materials such as magnesium, silver, antimony, and bismuth, these modules perform comparably to Bi_2Te_3-based systems. They are particularly well-suited for applications near room temperature, including waste heat recovery, localized cooling, and powering small devices [2]. However, their widespread use has been hindered by challenges related to durability and stability. Thermoelectric modules often operate in harsh environments where they are exposed to air, moisture, and fluctuating temperatures. Under these conditions, Mg-based materials are prone to degradation. One major issue is the formation of magnesium oxide (MgO) when the material reacts with oxygen. This leads to increased electrical resistance and reduced efficiency. Another challenge lies in the breakdown of soldering materials at contact points within the module, which further compromises performance. Addressing these problems is essential to ensuring the long-term reliability of Mg-based thermoelectric systems.
To overcome these challenges, we turned to atomic layer deposition (ALD), an advanced coating technology that offers precise and uniform protection [3]. As shown in Figure 1, ALD involves depositing an ultra-thin layer of material - as thin as a few nanometers thick - onto the surface of the thermoelectric module. This coating acts as a barrier, preventing oxygen and moisture from penetrating the material and causing damage. In this study, hafnium oxide (HfO_2) was chosen as the coating material due to its chemical stability and ability to withstand harsh

environments. We applied a 300-nanometer-thick layer of HfO_2 to Mg-based thermoelectric modules and subjected them to rigorous tests to evaluate their durability.

We conducted thermal cycling tests to simulate real-world conditions. These tests involved repeatedly heating and cooling the modules between 100°C and 250°C while monitoring their electrical resistance, as shown in Figure 2a.
Three types of modules were tested:
• Modules cycled in an argon environment: These modules showed stable performance for up to 30,000 cycles but eventually degraded due to the absence of oxygen protection.
• Modules exposed to ambient air without a coating (Fig. 2b, 2d): These modules degraded rapidly, losing significant efficiency after just 5,000 cycles due to oxidation and solder material breakdown.
• Modules coated with HfO_2 and exposed to ambient air (Fig. 2c, 2e): These modules demonstrated remarkable resilience, maintaining 93% of their original power output even after 65,000 cycles.
The results clearly show the effectiveness of the HfO_2 coating in preventing degradation. The coated modules not only retained their electrical properties but also showed no visible signs of damage, unlike uncoated modules, which developed oxidized solder materials and other defects.
To further assess the impact of degradation, we disassembled the modules after cycling and re-soldered their components (Fig. 3). We found that modules protected with HfO_2 recovered nearly all of their initial performance, while uncoated modules exhibited only partial recovery. This underscores the role of the HfO_2 coating in preserving the integrity of the module's materials and solder connections.

This study highlights the transformative potential of combining Mg-based thermoelectric materials with ALD coatings. By addressing the twin challenges of performance and durability, we have created a sustainable and high-performing alternative to Bi_2Te_3-based systems. The benefits of this innovation extend across multiple industries. In industrial settings, Mg-based modules could be used to capture waste heat from manufacturing processes, converting it into electricity and reducing overall energy consumption. In the electronics industry, these modules could power cooling systems for devices, ensuring efficiency and reliability. Moreover, the success of ALD as a protective measure opens new possibilities for improving the durability of materials in other fields, such as batteries, photovoltaics, and electronic components. The combination of Mg-based thermoelectric materials and ALD coatings represents a significant advancement in the quest for sustainable energy solutions. By leveraging abundant and environmentally friendly materials, these modules align with global efforts to reduce reliance on toxic and scarce resources. Looking ahead, further research will focus on optimizing the coating process and exploring new materials to enhance performance even further. Advancements in soldering techniques and contact materials will also play a crucial role in unlocking the full potential of this technology.
In conclusion, this study demonstrates how innovative materials and protective technologies can overcome longstanding challenges in thermoelectric systems. Mg-based thermoelectric modules, enhanced with ALD coatings, offer a path toward a greener, more energy-efficient future, paving the way for widespread adoption of sustainable energy solutions. This remarkable breakthrough underscores the power of science and technology to drive positive change, providing practical solutions to some of the world's most pressing energy challenges.

References

[1] R. He, G. Schierning, K. Nielsch, Adv. Mater. Technol., 3(4), 1700256 (2018).
[2] P. Ying, L. Wilkens, H. Reith, N. Pérez, X. Hong, Q. Lu, C. Hess, K. Nielsch, R. He, Energy Environ. Sci., 15, 2557-2566 (2022).
[3] P. Ying, R. B. Villoro, A. Bahrami, L. Wilkens, H. Reith, D. A. Mattlat, V. Pacheco, C. Scheu, S. Zhang, K. Nielsch, R. He, Adv. Funct. Mater., 34(45), 2406473 (2024).

Funding

M-ERA NET THERMOS project
ERC Starting Grant, TENTATION, 101116340
DFG, Project Number 516355940

Cooperations

[1] Nanoanalytics and Interfaces, Max-Planck-Institut für Eisenforschung GmbH, Düsseldorf, Germany
[2] Fraunhofer Institute for Manufacturing Technology of Advanced Materials, Dresden, Germany

Abb. 1: Schematisches Prinzip der Atomic Layer Deposition (ALD) und ihrer Schutzwirkung für thermoelektrische Module.
Fig. 1: A schematic of the atomic layer deposition principle and its protective power for thermoelectric modules.

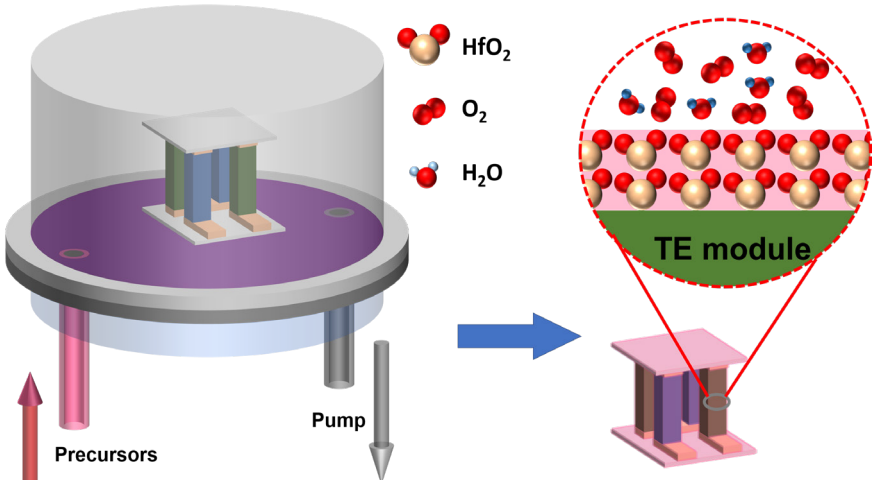

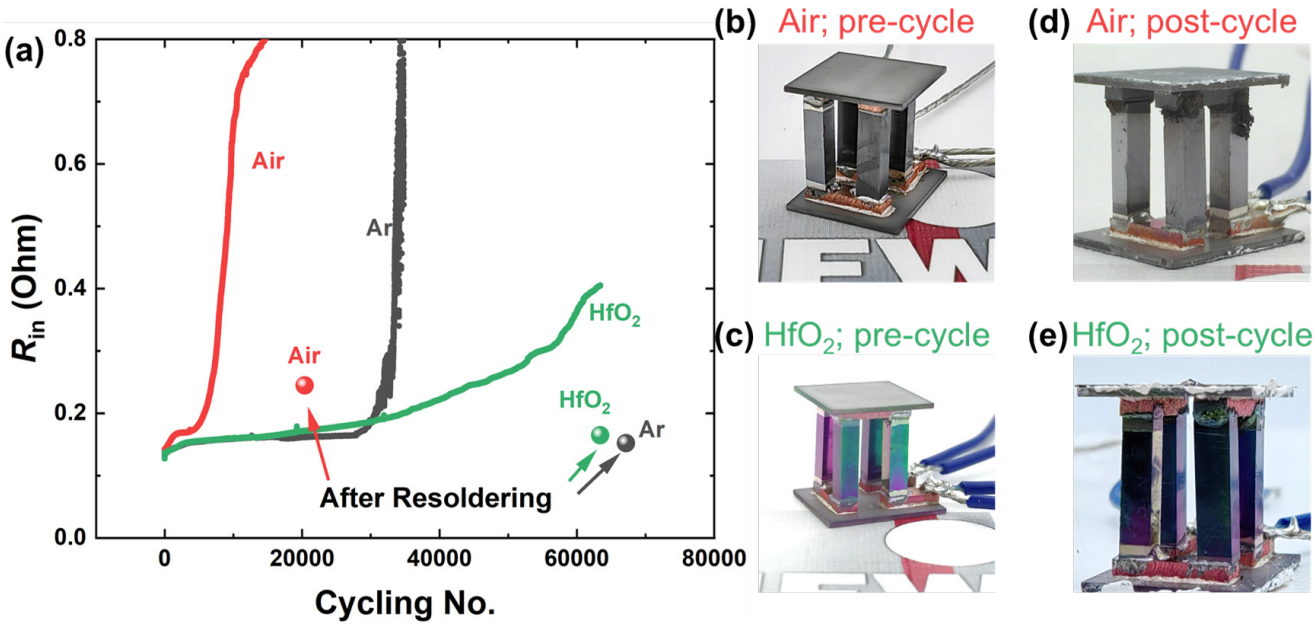

Abb. 2. (a) Veränderung des Innenwiderstands (R_{in}) der Module während des thermischen Zyklierens. Die Bilder zeigen die Module (b,c) vor und (d,e) nach dem Zyklieren. Zwei Module werden verglichen: entweder (b,d) ohne Beschichtung oder (c,e) mit HfO_2-ALD-Beschichtung. Die Kreise in (a) zeigen den Innenwiderstand neu montierter Module, bei denen die thermoelektrischen Beine nach dem Zyklieren durch erneutes Löten wiederverwendet wurden. Die Aufzeichnung des R_{in} scheiterte bei dem Modul, das in Argon (Ar) betrieben wurde, nach fast 35.000 Zyklen aufgrund eines Schaltkreisbruchs im Modul.
Fig. 2. (a) Variation of internal resistance (R_{in}) of modules upon thermal cycling. The images show the modules (b,c) before and (d,e) after cycling. Two modules are compared, either (b,d) without coating or (c,e) ALD-coated by HfO_2. The circles in (a) show the internal resistance of re-assembled modules by re-soldering the extracted thermoelectric legs from the post-cycled modules. The recording of R_{in} failed for the module cycled in Ar after nearly 35,000 times due to the in-module circuit break.

Abb. 3. (a) Veränderung der relativen Ausgangsleistung verschiedener Module (Schwarzes Quadrat: in Argon zykliert. Roter Kreis: in Luft ohne Beschichtung zykliert. Grünes Fünfeck: in Luft mit HfO_2-Schutz beschichtet) in verschiedenen Phasen (vor dem Zyklus, nach dem Zyklus und nach dem erneuten Löten). (b) Vergleich der Spannungs-Strom-Kurven (U-I) und der Ausgangsleistung (P) zwischen den in Luft zyklierenden Modulen ohne Schutz und mit HfO_2-Schutz.
Fig. 3. (a) Variations of the relative output power of various modules (Black square: cycled in Ar. Red circle: cycled in Air without coating. Green pentagon: cycled in Air with HfO_2 protection) at different stages (pre-cycle, post-cycle, and re-solder). (b) Comparisons of the Voltage-Current (U-I) curves and output power (P) between the in-air cycled modules without protection or with HfO_2 protection.

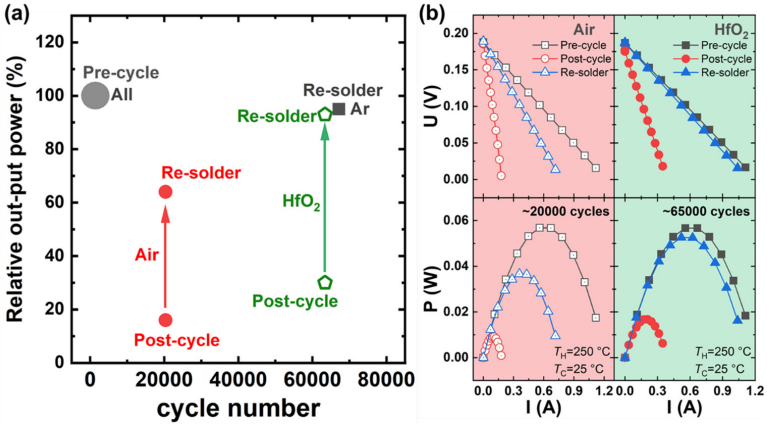

Current Research Topic 10

Molecular sieving with angstrom-scale pores

Peter Dement, Eric I. Altman[1], Anjana Devi

Bei Anwendungen wie der Meerwasserentsalzung oder der Kohlendioxidabscheidung werden Moleküle und Ionen oft durch Membranen getrennt. Die Leistung üblicher Membranmaterialien ist dickenabhängig und ermöglicht nicht gleichzeitig einen hohen Durchsatz und eine hohe Selektivität. Dies könnte durch 2D-Materialmembranen überwunden werden, sofern sie mit einer großen Anzahl gleichmäßiger Poren ausgestattet sind. Das prototypische 2D-Material Graphen wird schon lange durch Top-Down-Methoden perforiert, doch künstliche Löcher zeigen niedrige Dichten und breite Größenverteilungen. Diese Arbeit beweist, dass 2D-Siliciumdioxid dicht gepackte natürliche Poren hat, die Moleküle anhand ihrer Größe, Form und chemischen Eigenschaften unterscheiden können.

Semipermeable materials separate molecules and ions in various applications from seawater desalination to carbon dioxide capture. The performance of conventional membranes depends on the thickness and does not allow for high throughput and high selectivity at the same time. This could be overcome by 2D-material membranes provided that they are equipped with a large number of uniform pores. For a decade, the prototypical 2D material graphene was perforated by top-down methods, but artificial openings revealed low densities and broad size distributions. In this work, 2D material bilayer silica was demonstrated to have densely packed intrinsic pores that are able to distinguish molecules by their size, shape and chemical properties.

Abb. 1: Atomstruktur von zweischichtigem Siliciumdioxid mit einer hohen Dichte an natürlichen Poren im Angström-Maßstab.
Fig. 1: Atomic structure of bilayer silica featuring a high density of natural angstrom-scale pores.

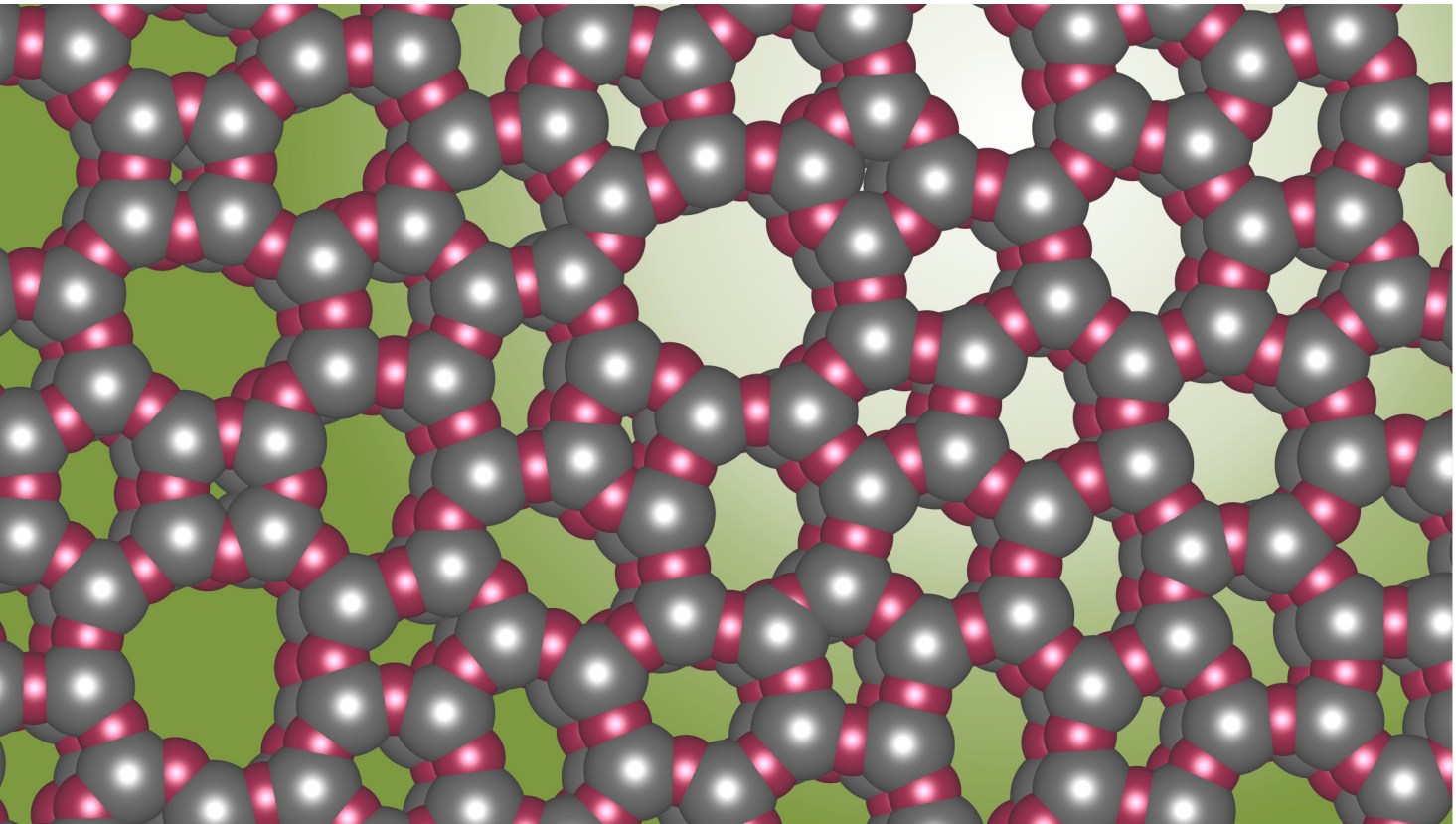

Membrane separation plays an important role in many technological settings and relies upon selective diffusion of chemical species through polymeric materials. As polymers are composed of randomly arranged long molecular chains, their free-volume elements have a broad size distribution giving rise to a selectivity-permeability trade-off. This means that the higher the throughput of a membrane, the weaker its ability to separate different substances. In contrast, chemical bonds in 2D materials spread in plane, and if there were nanoscopic openings, they could in theory enable both high-flux and size-exclusion separation. The flow rate in 2D membranes is expected to scale with the areal density of pores and the probability of particles to enter the pores. The discovery of graphene opened exciting opportunities for designing next-generation separation membranes. However, the crystal lattice of graphene is impermeable to molecules which requires the pores to be created artificially. Perforated 2D membranes attracted much attention, but removing atoms compromises the integrity of the materials and limits their porosity. Controlling the pore size at the molecular scale also appeared challenging.

The building blocks in graphene are individual carbon atoms, and this is why their hexagonal network results in a dense layer with no voids. In turn, highly open 2D polymers can be obtained from more complex polyatomic moieties forming uniform pores of around 1 nm in diameter. As fluid molecules are typically smaller than 1 nm, the intriguing 2D membrane is bilayer silica, a 2D form of silicon dioxide [1]. This material consists of medium-sized $\{SiO_4\}$ units with shared oxygen corners that constitute a 0.6-nm thin symmetric framework of two vitreous layers (Fig. 1). The structure is chemically saturated and has neither dangling bonds nor bonds to the underlying substrate. The pores in bilayer silica are log-normally distributed between four- and nine-membered rings and have long been speculated to be suitable for small molecules. The problem is that the synthetic 2D material is obtained by demanding molecular beam epitaxy on single-crystalline metals under ultrahigh vacuum conditions which hinders its characterization as a separation membrane. Nevertheless, bilayer silica is known to be stable in air and water while adsorption studies with supported sheets indirectly confirmed its intrinsic porosity.

In effort to explore mass transfer properties of bilayer silica, we developed its scalable fabrication by atomic layer deposition (ALD) on large-area metal foils and thin-film substrates instead of small single crystals [2]. The simple bottom-up procedure includes chemisorption of a volatile Si-containing precursor, and its plasma oxidation followed by high-temperature annealing in ambient atmosphere. In particular, gold thin films were found to be convenient because they exhibit excellent surface cleanliness and allow for substrate etching to transfer the 2D material onto holey supports. The oxide growth was studied in detail as a function of the deposition temperature and the number of cycles in a custom-designed ALD reactor (see Fig. 2). With the help of vibrational spectroscopy and transmission electron microscopy, the process was optimized to yield defect-free suspended bilayer silica sheets [3]. It was demonstrated that elevated substrate temperature favored homogeneous surface coverage and six ALD cycles were necessary to complete the 2D phase at 240°C. At lower temperature and larger amounts of silicon dioxide deposited, there were 3D nanoparticles emerging that endangered mechanical strength of the material.

Membrane characteristics are determined upon measuring the number of permeating particles across a material placed between two media of different concentration or pressure. The novel processing approach enabled us to conduct pioneering transport experiments with free-standing bilayer silica membranes and shed light on their functional performance [3]. To this end, the 2D material was secured over micrometer-sized apertures in an original vacuum system that ensured sensitive detection of molecular permeation by means of a mass-spectrometer. The first striking observation was that regular gases like oxygen and nitrogen could not cross the membrane even though their size certainly fits to some of the pores in bilayer silica. Only for the smallest helium atoms, we obtained a measurable permeation rate that was equivalent to one in ten million atoms passing through the membrane. This behavior in sub-nanometer pores is explained by van der Waals interactions between the gaseous molecules and the atoms comprising the 2D material. When an inert particle flies towards a pore, its trajectory is first deflected to the pore rim by long-range attractive forces and then scattered back by short-range repulsive forces.

We found that unlike ordinary gases, vaporous substances such as water are able to stick to the membrane and therefore much more likely to enter angstrom-scale pores. Fig. 3 illustrates a two orders of magnitude difference in the transmembrane flux between helium and water although the applied pressure was 20 times greater in the former case. It means that the probability of water molecules to cross bilayer silica exceeds that for helium atoms by a factor of 3000. At the same time, the permeation rate of water appeared to change dramatically with the vapor pressure which is consistent with its ability to adsorb on the membrane surface. The adsorption-mediated molecular passage in bilayer silica was evidenced by another remarkable finding that methanol had a greater flux than water despite the larger size. This is because of wetting properties of the material that was shown to have lesser chemical affinity to water compared to organic solvents. In other words, the transmembrane flux is proportional to the number of adsorbates which depends on the energetics of gas-surface interactions and is different for water and methanol.

Our innovative measurements with vapors offered a unique way to address the transport selectivity in 2D membranes by varying the size of permeating molecules in a wide range [4]. In addition to methanol, ethanol, propanol and isopropanol as well as tert-butanol were chosen for experiments as their molecular dimensions increase incrementally. The alcohols have similar chemical properties, and we proved spectroscopically that they all readily condense on bilayer silica forming multimolecular layers upon saturation. There is a pronounced molecular sieving effect in the measured transmembrane flux whereas the data for tert-butanol indicates the limit of detection (Fig. 3). The results were supported by quantum chemical calculations that revealed the permeation mechanism and agreed closely with the experiment. It appeared that six-membered ring pores were too small for the organic molecules, and the selectivity between the linear alcohols is due to their different ability to pass seven-membered rings. The latter comprise about 20% of all pores and were found to be too narrow for the branched molecules. According to the computations, isopropanol can

Abb. 2: ALD-Reaktor mit Plasmaunterstützung zur Herstellung von zweidimensionalen Siliziumdioxidmembranen im Zollmaßstab.
Fig. 2: Plasma-enhanced ALD reactor used for obtaining wafer-scale 2D silicon dioxide membranes.

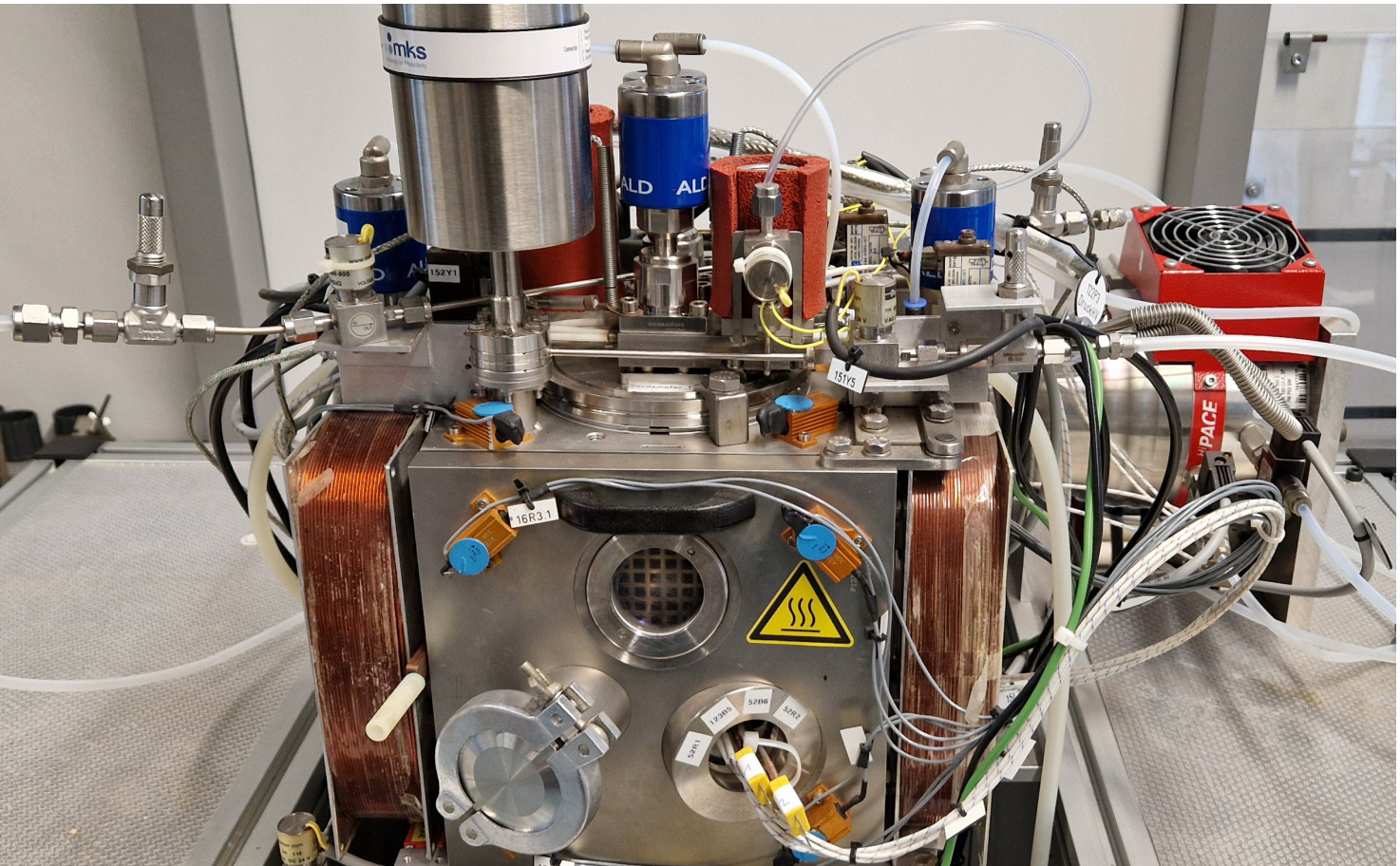

only permeate through eight- and nine-membered ring pores which leads to the significant difference observed for the isomers.

The ultimate pore density, chemical specificity along with size and shape selectivity highlight bilayer silica as an outstanding semipermeable membrane. Given the large surface-to-volume ratio of the 2D material, it is not surprising that interfacial phenomena play an important role in its molecular transport characteristics. In order to test the membrane performance in the liquid phase, microscopic free-standing sheets were exposed to aqueous salt solutions and analyzed by electroanalytical methods [5]. Voltammetric experiments revealed two orders of magnitude decrease in electrical conductance as compared to open apertures of the same size. The finding suggests that ions face a barrier in bilayer silica which is consistent with their bulky hydration shells and can also be related to electric charges on the membrane surface. Further research is needed to explore the prospects of the inherent 2D membrane in real-life separation applications. This includes not only permeation measurements with different substances and their mixtures, but also developing more cost-effective routes for the material preparation.

References

[1] J.-Q. Zhong et al., Chem. Rev. 122 (2022) 11172
[2] G. S. Hutchings et al., 2D Mater. 9 (2022) 021003
[3] D. Naberezhnyi et al., Nano Lett. 22 (2022) 1287
[4] P. Dementyev et al., Small 19 (2023) 2205602
[5] E. I. Altman et al., Catal. Lett. 154 (2024) 1359

Funding

German Research Foundation (DFG), Project PHANTOM (ID 496964156)

Cooperation

[1] Yale University (USA)

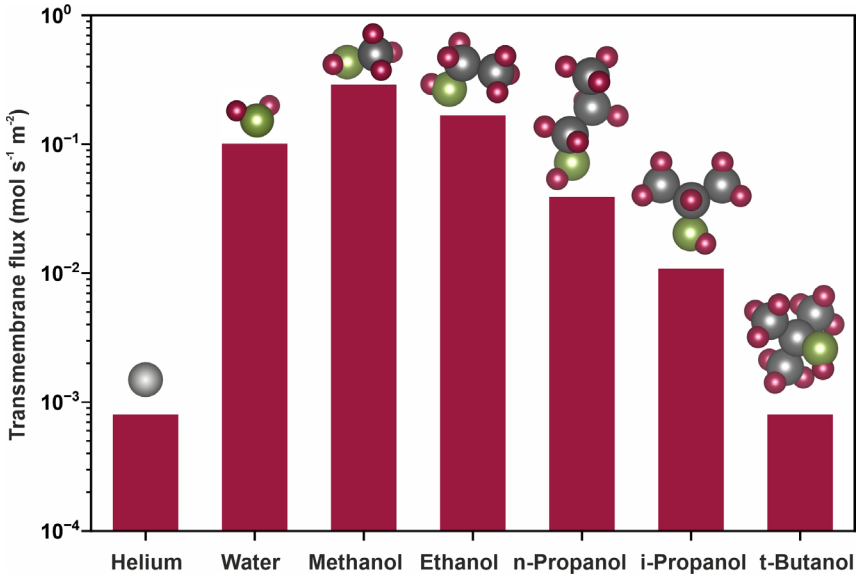

Abb. 3: Transportraten verschiedener gasförmiger und dampfförmiger Substanzen in freistehenden zweidimensionalen Siliziumdioxidmembranen.
Fig. 3: Transport rates of various gaseous and vaporous substances across free-standing bilayer silica membranes.

Current Research Topic 11

Photovoltaic technologies through green materials and processes for sustainable energy generation

Boris Rivkin and Fabian Paulus

Die Erzeugung von Strom aus erneuerbaren Energiequellen, insbesondere aus Sonnenlicht, steht im Mittelpunkt der Transformation der globalen Energieversorgung. Die Herstellung konventioneller Photovoltaikanlagen verbraucht jedoch erhebliche Mengen an Energie und anderen Ressourcen, was ihren positiven Effekt auf Umwelt und Gesellschaft deutlich schmälert. Kürzlich haben Forschende am IFW zur Entwicklung von zwei neuartigen Solarzellentechnologien beigetragen: Quantenpunkte und Metall-Halogen-Perowskite. Es wurde über neue Synthesemethoden mit verringertem ökologischem Fußabdruck berichtet. Diese Entwicklung verdeutlicht die Chancen einer bewussten Material- und Prozesswahl und unterstreicht die Bedeutung, Nachhaltigkeit bereits in der Forschungsphase neuer Technologien zu berücksichtigen.

Energy harvesting from renewable sources, especially from sunlight, is an essential part of the ongoing transformation of global power supply systems. However, manufacturing conventional photovoltaics consumes large amounts of energy and resources, thereby greatly reducing their beneficial effects on the environment and society. Recently, researchers at IFW Dresden have contributed to advancing two different emerging photovoltaic technologies, namely quantum dots and metal-halide perovskites, and reported novel synthetic methods that reduce their environmental footprint. This highlights the opportunities a conscious selection of materials and processes offers and the importance of sustainability considerations already in the research stage of emerging technologies.

Abb. 1: Grüne Elektronik? Inwieweit lassen sich Ressourcen- und Energieverbrauch reduzieren, um elektronische Bauteile nachhaltiger herzustellen?
Fig.1: Green Electronics? To what extent can resource and energy consumption be reduced in order to produce electronic components more sustainably?

In the era of climate change and increasing worldwide energy demand, photovoltaics enable sustainable energy production. The direct conversion of light into electrical energy occurs without greenhouse gas emissions, such as carbon dioxide or other harmful substances. However, producing solar cells often requires substantial amounts of energy. In particular, silicon solar cells require very pure silicon, which has to be produced in complex processes at high temperatures. As a result, the energetic payback time - i.e. the duration after which a silicon solar cell generates more energy than is used to produce it - currently lies around 12-15 months.[1] This often disregards the additional energy required to dispose of the solar cells at the end of their life, further worsening the energy balance. Therefore, research at the IFW focuses on innovative, environmentally-friendly solar cell materials and new manufacturing processes with a significantly lower environmental footprint and reduced energy and resource consumption, thereby enabling solar cell technologies with much shorter payback times.
These efforts are part of the IFW research topics "Photovoltaic Technologies" and "Green Chemistry and Processes". With these investigations, the IFW will make a decisive contribution to sustainable and responsible energy production in the future.

Among emerging photovoltaic technologies, nanocrystal solar cells have attracted significant attention due to their possibility to be fabricated at low temperatures and the absorbance of sunlight in the visble and near-infrared (NIR) region of the solar spectrum. In nanocrystal solar cells, the light-absorbing layer comprises nanometer-sized crystallites of a semiconducting material. By controlling the size of the nanocrystals by chemical means, it is possible to tune the optical and electronic properties of the semiconducting nanocrystals and tailor them to the requirements of a solar cell. Among various and often heavy-metal-based material systems, silver bismuth sulfide ($AgBiS_2$) nanocrystals are considered an environmentally-friendly and non-toxic alternative for future photovoltaics.[2-4] Silver bismuth sulfide is a direct-bandgap semiconductor with a very high absorption coefficient, allowing the fabrication of efficient solar cells with ultrathin absorber layers of just a few dozen nanometers. So far, the synthesis of $AgBiS_2$ nanocrystals relies on the so-called "hot-injection" method, in which the silver (Ag^+) and bismuth salts (Bi^{3+}) are dissolved in oleic acid under vacuum at 100 °C for several hours before a highly reactive sulfur species (bis(trimethylsilyl) sulfide) is swiftly injected into the hot mixture to form the desired nanocrystals. The nanocrystals are collected after precipitation, centrifugation, and washing from the reaction mixture and can be deposited into thin absorber layers of solar cells. However, in this synthetic method, the composition of the resulting $AgBiS_2$ nanocrystals is difficult to control, and the different reactivity of Ag^+ and Bi^{3+} needs to be compensated by a stoichiometric excess of one of the materials.

We invented a novel synthetic route for $AgBiS_2$ nanocrystals that does not require the application of vacuum in the synthesis and is conducted at a temperature of only 50°C.[5] This is made possible by utilizing a novel, reactive, but stable sulfur precursor developed in our group and the cation excess process.[6] To fabricate $AgBiS_2$ nanocrystals, we first synthesized silver sulfide (Ag_2S) nanocrystals. The sulfur precursor lauroyl sulfide allows the synthesis of Ag_2S nanocrystals at room temperature with a nanocrystal size of just 2.8 nm and a very narrow size distribution. In a subsequent step, Ag^+ is partially exchanged by Bi^{3+} in solution at only 50°C. We showed that this cation-exchange process occurs within the first few minutes of the reaction while the original size and shape of the nanocrystals are maintained, typical for such cation-exchange processes. Furthermore, we showed that the cation exchange is fast, but cation homogenization within the nanocrystals is the quality-determining process in this material and requires more time. The resulting and homogenized $AgBiS_2$ nanocrystals exhibit a well-defined composition and a photovoltaic performance of up to 7.35% in thin film solar cells.
Our study shows that by combining novel precursors and the cation exchange reaction, new synthetic paths can be established that allow the fabrication of nanocrystals with lower energy and resource consumption.

Another key research activity at IFW centers on solar cells based on metal halide perovskites (Perovskite solar cells, PSCs). PSCs are expected to contribute decisively to the ongoing transformation of global

energy supply systems. For instance, this emerging photovoltaic technology will increase solar power generation per occupied installation area through more efficient silicon-perovskite tandem solar cells or support a decentralized power grid through lightweight or semi-transparent building integrated PV. However, three key challenges still hold back the wide-scale industrial application of this promising technology to date. These are scalability (the fabrication of large-area PSC), stability (the lifetime of PSC when operated under real-life conditions), and sustainability (the fabrication of PSC using materials and processes that minimize adverse effects on the environment and workers' health). Recently, we focused on the two latter aspects: The development of stable PSCs that are processed in a fashion that promotes safety and environmental friendliness. PSCs suffer from various mechanisms that reduce their lifetime, with their susceptibility to humidity being a key culprit. Quasi-two-dimensional (q-2D) perovskite systems offer a promising strategy to address moisture sensitivity. Here, the optically and electronically active metal-halide crystal lattices are sandwiched between layers of hydrophobic organic cations that repel water on a molecular level and stabilize the compound. While the photovoltaic efficiency of q-2D PSCs is not quite on par with their conventional high-performance counterparts, their stability under real-life conditions positions them as an intriguing alternative in the quest for commercially viable PSCs. However, q-2D perovskites are generally processed using a highly toxic chemical, namely *N,N*-dimethylformamide (DMF), which poses a threat to worker safety and an environmental hazard. Although highly sought-after, alternative "green" solvents remain elusive: Not only do potential compounds have to score points across sustainability-dimension such as biodegradability, toxicity, and resource footprint, but furthermore offer suitable properties regarding reactant solubility, solute-solvent-complex formation, and perovskite film growth. So far, the search for green alternatives is held back by the time-intensive trial-and-error approach that is prevalent in the field.

In contrast, the discovery of green alternative solvents can now be facilitated by the Hansen solubility parameter space analysis method, which Bautista, Vaynzof and co-authors introduced.[7]

Here, chemical compounds were classified sufficiently well by a set of three parameters – their atomic dispersion forces, molecular permanent dipole forces, and molecular hydrogen bonding. This classification allows the identification of groups of compounds with similar properties and helps to isolate promising candidates.
As a result, the identification of chemically suitable yet sustainable solvent systems is accelerated by orders of magnitude. The feasibility of the Hansen-space method for solvent discovery was recently highlighted through the demonstration of the first q-2D PSCs processed exclusively using a green solvent, glycerol-formal (Gly-F), which is conventionally used in the biomedical sector.[8]
Guerrero, Vaynzof, and co-authors, in collaboration with the TU Dresden, reported the fabrication of q-2D PSCs using Gly-F and compared the film properties and PV performance with conventional devices that were fabricated with hazardous DMF. While the "green" devices showed excellent stability and a respectable power conversion efficiency of up to 14.54 %, they were still outperformed by the conventional device in terms of efficiency (up to 18.13%). This mismatch in performance is likely caused by a slightly lower degree of vertical orientation in Gly-F-based perovskite films, as suggested by X-ray diffraction analysis. The vertical orientation of the q-2D structure is critical for efficient transport and collection of photo-current and is thus subject to ongoing optimization. Despite the performance gap, this study emphasizes the potential of sustainable perovskite processing and the potency of a methodologically guided compound discovery.

References

[1] Umweltbundesamt 2021, FKZ 37EV 16 119 0
[2] Nat. Photon. 2016, 10, 521-525
[3] Nat. Photon. 2022, 16, 235–241
[4] J. Mater. Chem. A, 2022,10, 8615-8625
[5] Nanoscale, 2024,16, 9325-9334
[6] Adv. Energy Mater. 2023, 13, 2203965
[7] Chem. Commun. 2023, 59, 10588
[8] Adv. Energy Mater. 2024, 14, 2402916

Funding

BMBF "GreenDots" (FK03XP0422A)
DFG "PERFECTPVs" (424216076) and M-ERA.NET "PHANTASTIC" via TU Dresden

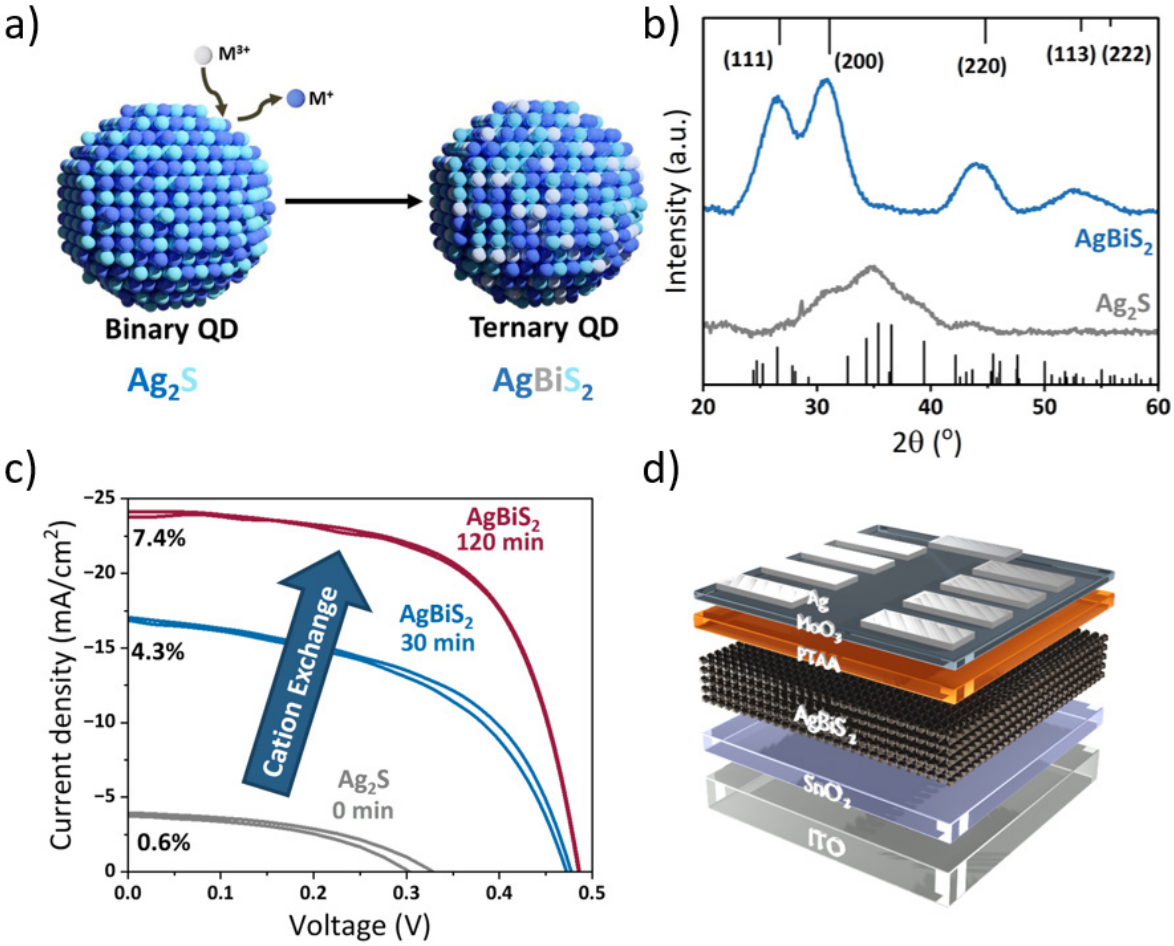

Abb. 2: Kationen-Austausch zur Synthese von Silberbismutsulfid ($AgBiS_2$): a) Schematische Darstellung des Kationenaustauschs zu $AgBiS_2$ an Silbersulfid(Ag_2S)-Nanokristallen. b) Veränderung des Röntgen-Diffraktogramms durch den Kationenaustausch. c) Stromdichte-Spannungskennlinien von Solarzellen mit den $AgBiS_2$-Nanokristallen nach dem Kationenaustausch und unterschiedlich langen Reaktionszeiten. d) Prinzipdarstellung einer Dünnschicht-Solarzelle mit Quantenpunkten.
Fig. 2: Cation-exchange synthesis of silver bismuth sulfide ($AgBiS_2$): a) Schematic representation of the cation exchange reaction to $AgBiS_2$ starting from silver sulfide (Ag_2S)-nanocrystals. b) Change of the X-ray diffractogram upon cation exchange. c) Current-density voltage characteristics of solar cells with $AgBiS_2$ nanocrystals after various reaction times. d) Schematic solar cell architecture of the thin layer device.

Abb. 3: a) Rasterelektronen-mikroskopie-Querschnittsbild von vollständigen Solarzellen, welche mit DMF bzw. Gly-F verarbeitet wurden.
b) Strom-Spannungs-Kennlinie der entsprechenden Solarzellen mit den Abbildungen der jeweils verwendeten Lösemittel.
Fig. 3: a) SEM cross-section comparison of complete solar cells processed using DMF and Gly-F.
b) Current-voltage curves of solar cells processed using DMF and Gly-F with an inset displaying the two solvents used.

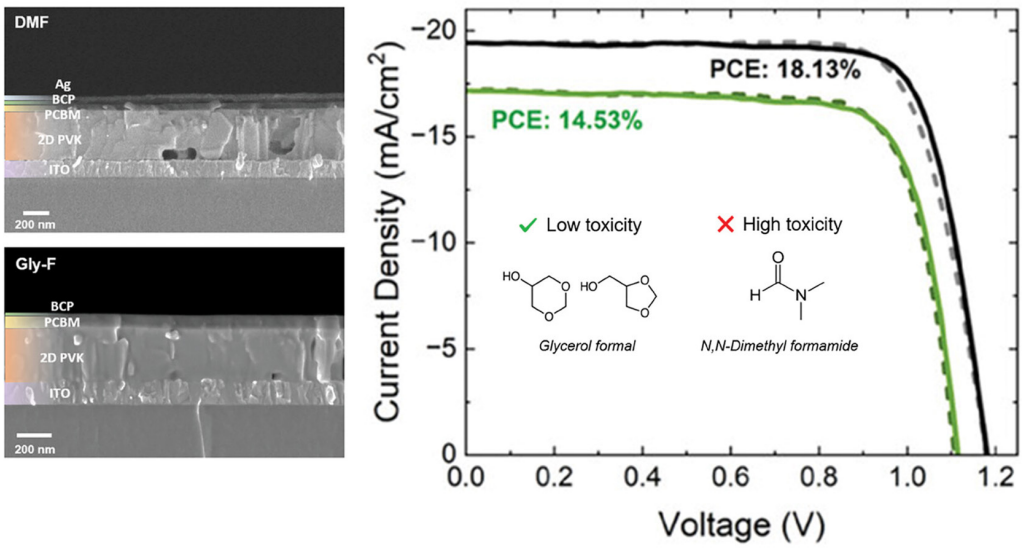

Current Research Topic 12

Towards metal halide perovskite electronics

Yana Vaynzof

Metall-Halogen-Perowskite sind eine neuartige Klasse von Halbleitern mit einem hohen Potential für Anwendungen in der (Opto)Elektronik. Ihre exzellenten physikalischen Eigenschaften ermöglichen eine bemerkenswerte Steigerung ihrer Leistungsfähigkeit als Photovoltaik-Materialien, welche bereits nach nur einer Dekade der Entwicklungszeit jene von etablierten Silizium-Solarzellen übertrifft. Ähnlich beeindruckende Fortschritte wurden im Bereich der Perowskit-Leuchtdioden erzielt, deren Effizienz nun mit der von anderen Technologien vergleichbar ist. Dennoch verzögert sich die Entwicklung der Perowskit-Elektronik, was unter anderem auf die schwierige Dotierung der Perowskit-Materialien zurückzuführen ist. Kürzlich haben IFW-Forschende eine Methode zur elektrischen Dotierung von Perowskiten entwickelt, die erste Perowskit-PN-Diode vorgestellt und so den Weg für die Entwicklung von Perowskit-Elektronik geebnet.

Metal halide perovskites are an emerging class of semiconductors of great interest for application in (opto)electronics. Their excellent properties led to a striking increase in their photovoltaic performance, surpassing that of the well-established silicon solar cells in just a decade. A similarly impressive advance has been made in perovskite light-emitting diodes, whose efficiencies rival those of other technologies. Despite this progress, the development of perovskite electronics lags behind in part due to the challenge of doping perovskite materials.
Recently, IFW researchers developed a method for electrical doping of perovskites, demonstrating the first perovskite PN diode and opening the path for developing perovskite electronics.

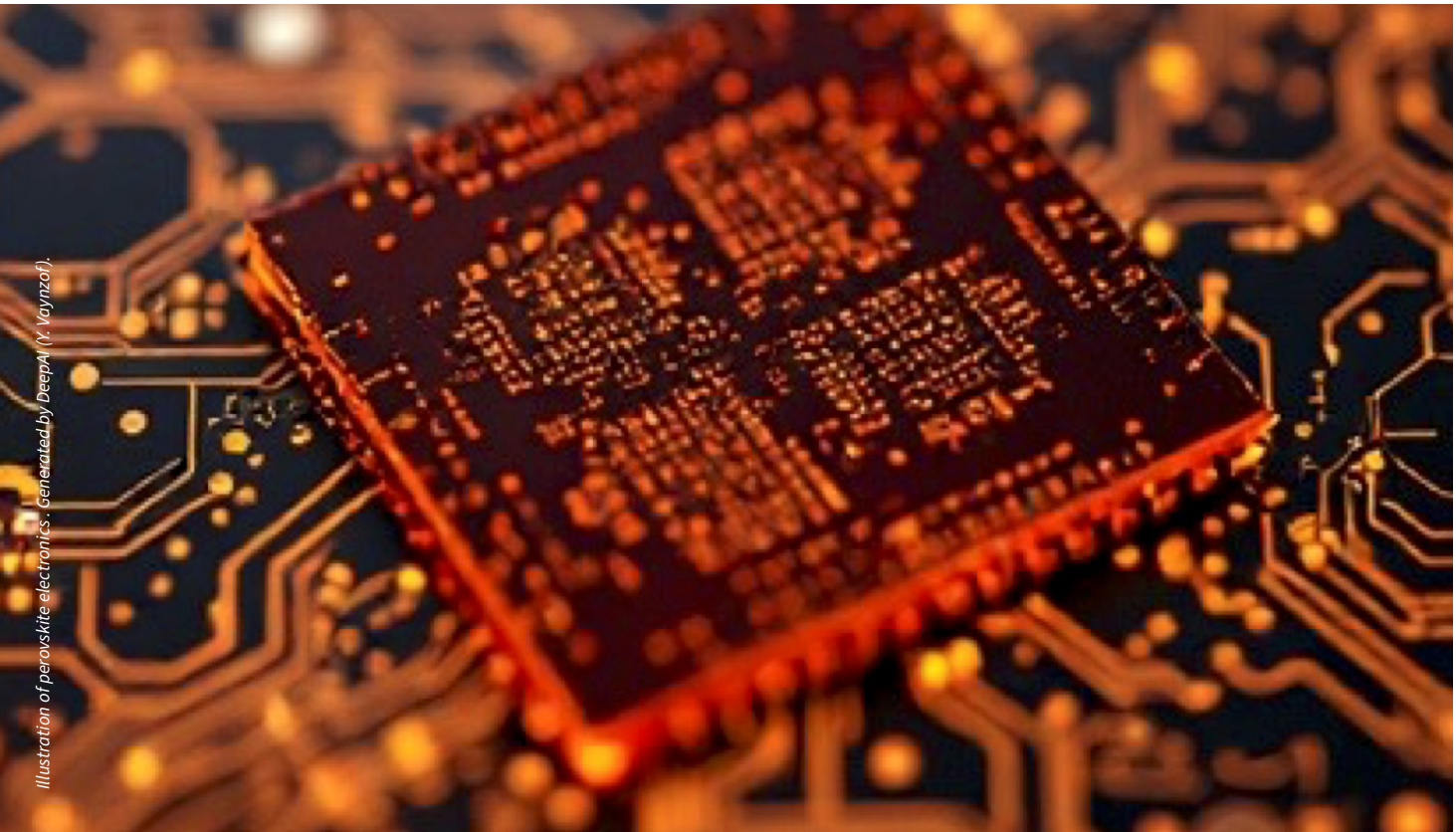

Illustration of perovskite electronics. Generated by DeepAI (Y. Vaynzof).

The doping of crystalline semiconductors (e.g. Si) has enabled the development of modern electronics as it makes it possible to tune their conductivity in a highly controlled fashion. Doping has also been widely demonstrated in other classes semiconductors. [1] An important example is organic semiconductors, where doping either with organic or inorganic dopants has been intensely investigated, enabling technological advances such as organic light-emitting diodes (LEDs) that rely on doped layers to achieve high efficiency. Metal halide perovskites (MHPs) are an emerging class of semiconductors that are of great interest for application in electronic devices due to their excellent electronic properties and compatibility with low-temperature processing. Despite the well-recognized need for developing doping strategies for MHPs, only very few studies have investigated doping. [2] We and others have examined p- and n-type composition-dependent doping in perovskite layers that contain either excess or deficiency of perovskite precursors. [3,4] Specifically, deficiency of MAI in a precursor solution results in n-doped $MAPbI_3$ films, while its excess results in p-doping. This type of composition-dependent doping results from the formation of vacancies and interstitials in the perovskite lattice, and while it has been shown to alter the electronic properties of the perovskite, it also introduces defects that strongly impact the material stability. Moreover, the significant migration of ionic defects in MHPs leads to inhomogeneous composition-dependent doping that will be altered upon applying stimuli such as electric field or light. Consequently, this approach is unsuitable for the controllable doping of MHPs as is required for future applications in electronics.

An alternative approach is based on using molecular dopants, whose energetics enable the transfer of charge carriers from the dopant to the host matrix. Indeed, in the case of solution-processed MHPs, surface doping by organic and inorganic molecular dopants has been demonstrated for selected examples. [5] Importantly, these dopants have been deposited from solution on top of the perovskite layer, thus demonstrating **surface doping** and **not bulk doping** as would be highly desirable. Bulk doping by solution processing is hard to realize since the dopants are likely to be expelled from the perovskite layer during the crystallization process and the solvent drying. For example, bulk doping with F_4-TCNQ has been reported, but the change in the Fermi level position was only on the order of 100 meV, most likely due to the mismatch in the energy levels of F_4-TCNQ and the perovskite layer. [7] Moreover, it was claimed that doping, in particular, affects the interface between the perovskite and the indium tin oxide layer, confirming that it was not homogeneous throughout the MHP layer. These reports highlight that solution processing of MHPs may impede their doping by molecular dopants.

On the other hand, controllable doping of vapour-deposited semiconducting films is well-established, particularly in vapour-deposited organic electronics. [8] Vapour deposition offers several advantages over solution processing, such as its solvent-free nature, scalability and industrial relevance. The deposition of MHPs from vapour is commonly performed by co-evaporating the different perovskite precursors that react to form the MHP on the substrate. This has motivated us to explore the co-evaporation of molecular dopants alongside that of the perovskite precursors (Fig. 1) as a possible strategy towards controllable electrical bulk doping of MHPs. The choice of dopants was motivated by the alignment between the dopant energy levels and those of the host perovskite in order to enable electron transfer to the perovskite for n-doping or electron transfer to the dopant for p-doping (Fig. 1). Beyond the energetic requirements, the chosen molecular dopants should be compatible with vapour deposition and show no chemical interaction with the perovskite host layer. To fulfil these conditions, we selected the dopant tetrakis(hexahydropyrimidinopyrimidine) ditungsten(II) ($C_{28}H_{48}N_{12}W_2$, or in short $W_2(hpp)_4$) since its very low ionization potential (2.4 eV) makes it an ideal candidate for n-doping of three-dimensional perovskites. [9] For p-doping, we chose 2-(7-dicyanomethylene-1,3,4,5,6,8,9,10-octafluoro-7H-pyrene-2-ylidene)-malononitrile (NDP-9) since its large electron affinity of 5.5 eV, [10] should enable electron transfer from the perovskite layer (Fig. 3a).

Exploring the co-evaporation of different amounts of molecular dopants revealed that their presence has only a limited impact on the layer microstructure and crystalline structure. On the other hand, ultraviolet photoemission spectroscopy

measurements revealed that the incorporation of molecular dopants results in the tuning of the Fermi level position of the perovskite layer across 900 meV within the 1.6 eV bandgap (Fig. 3b), effectively demonstrating both n- and p-type doping. [11]

The successful demonstration of doping and the additive nature of thermal evaporation made it possible to realize, for the first time, a perovskite-based PN junction as a key elementary electronic component. The diodes were fabricated in both PN and NP configurations, leading to opposing trends in rectification (Fig. 3c,d). The electrical characteristics were modeled through a collaboration with the group of Professor Nir Tessler at the Technion, Israel Institute of Technology, to reveal that the diode rectification ratios are limited by small lateral inhomogeneities in the doping profile, offering important insights for the future optimization of perovskite-based electronic devices. These inhomogeneities can be eliminated by changing the deposition parameters, such as deposition rate and temperature, or alternatively, by introducing additives into the fabrication process.

These results demonstrate not only that bulk doping of MHPs can be achieved by the co-evaporation of molecular dopants, but also that this strategy enables the fabrication of perovskite-based electronic devices. The work opens a pathway towards the scalable deposition of doped metal halide perovskites and their integration into complementary logic, thus marking an important step towards realizing perovskite electronic technologies.

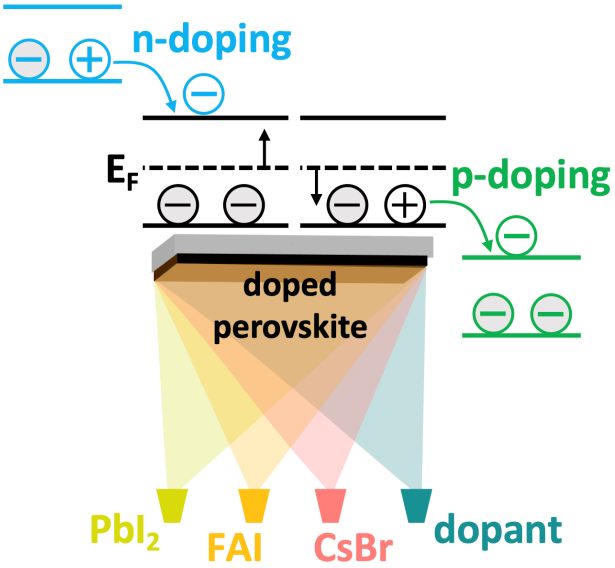

Abb. 1: Schematische Darstellung der Dotierung von Metall-Halogen-Perowskiten durch Co-Verdampfung von molekularen n- und p-Dotierstoffen.
Fig. 1: Schematic illustration of doping of metal halide perovskites by co-evaporation of molecular n- and p-dopants.

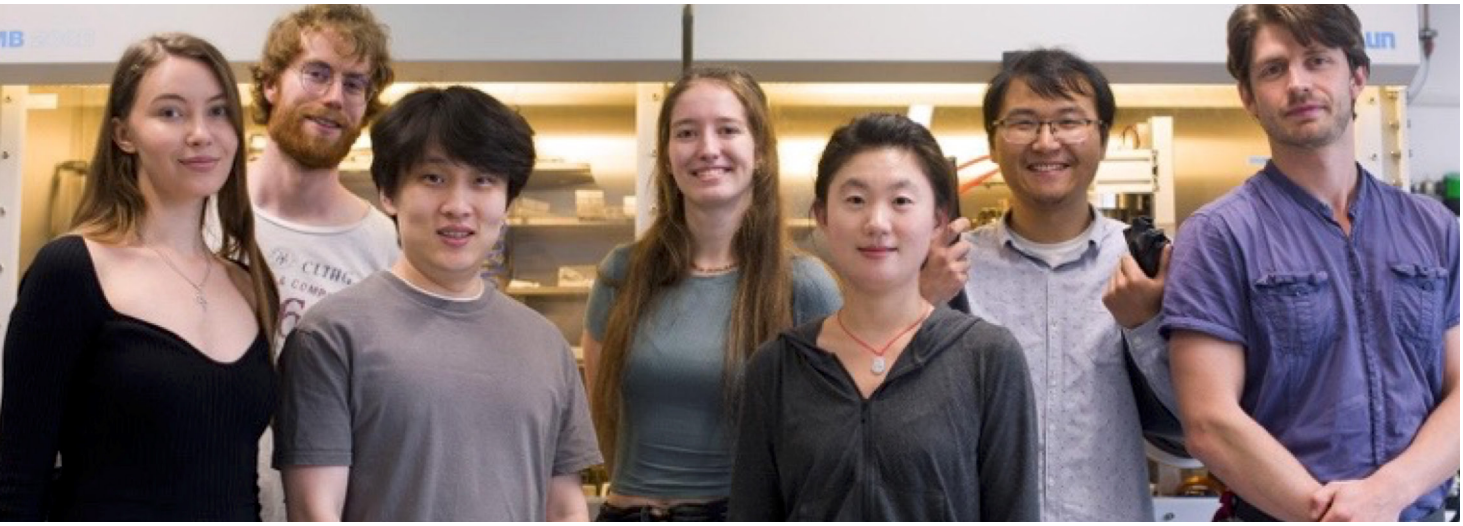

Abb. 2: Gruppe von Studierenden und Postdocs, die am IFW Dresden an der Aufdampfung von Metall-Halogen-Perowskiten arbeiten.
Fig. 2: Students and postdocs working on vapour deposition of metal halide perovskites at IFW Dresden.

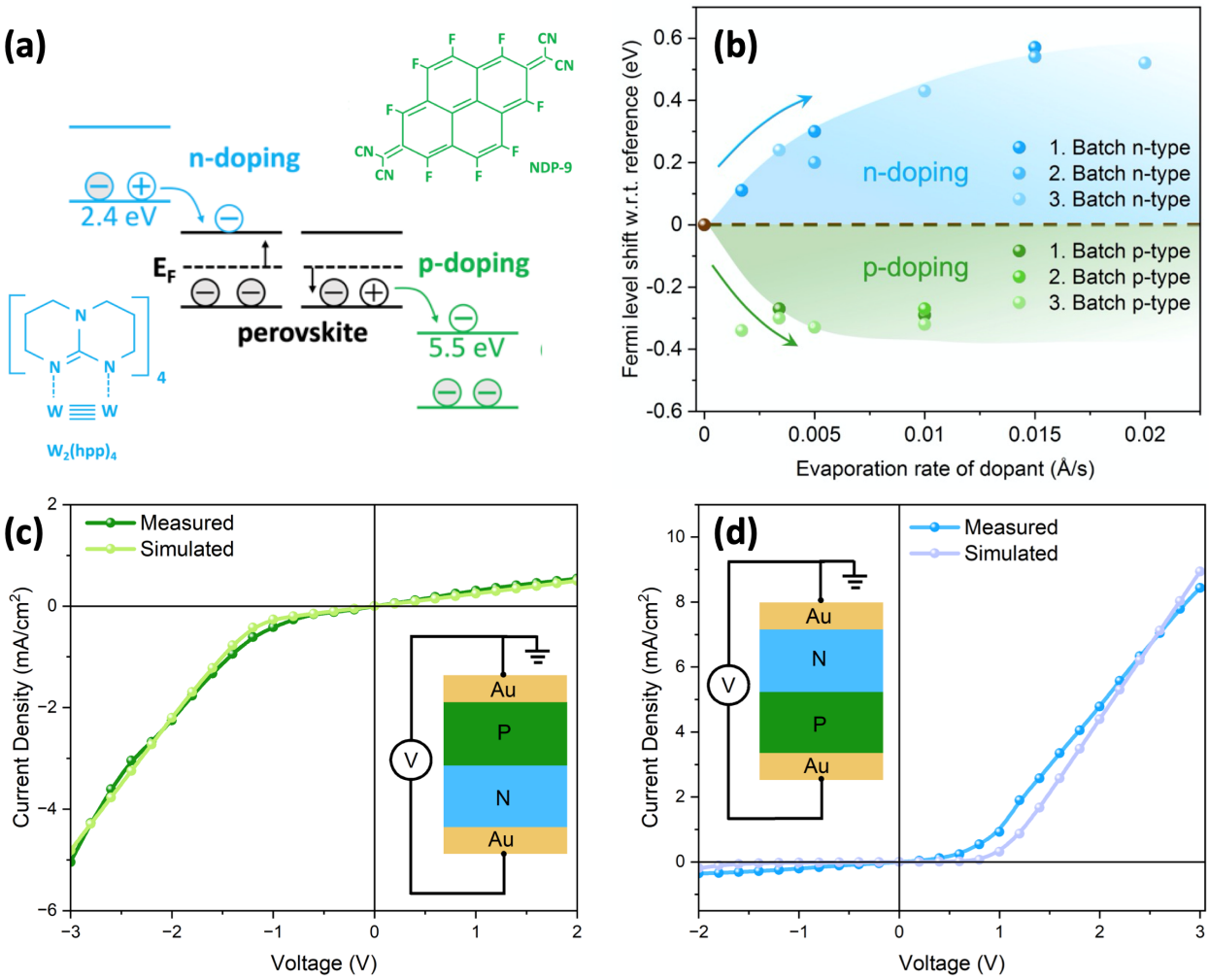

Abb. 3: a) Molekulare Strukturen der für die Dotierung von Perowskiten verwendeten n- und p-Dotierstoffe. b) Zusammenfassung der Weiterentwicklung der Position des Fermi-Niveaus nach Dotierung des Perowskits mit NDP-9 oder $W_2(hpp)_4$ mit jeweils drei Chargen. Gemessene und simulierte Stromdichte-Spannungs-Kennlinien von c) NP- und d) PN-Dioden.
Fig. 3: a) Molecular structures of the n- and p-dopants used for doping perovskites. b) Summary of the evolution of the position of the Fermi level upon doping the perovskite with either NDP-9 or $W_2(hpp)_4$ with three batches of each. Measured and simulated current density-voltage characteristics of c) NP and d) PN diodes.

References

[1] Frontiers Phys. 2016, 11, 117405.
[2] Nat. Rev. Mater. 2021, 6, 531.
[3] Appl. Phys. Lett., 2014, 105, 163508.
[4] Energy Environ. Sci. 2018, 11, 3380.
[5] Adv. Mater. 2018, 1705792.
[6] Adv. Electron. Mater. 2018, 4 (7), 1800087.
[7] Nat. Commun. 2018, 9, 1625.
[8] Chem. Rev. 2007, 107 (4), 1233.
[9] J. Am. Chem. Soc. 2005, 127, 10808.
[10] J. Inf. Disp. 2022, 23, 45.
[11] Advanced Materials 2024, 36 (29), 2314289

Funding

Y. V. acknowledges funding from the ERC through CoG PEROVAP (GA number 101087679).

Cooperation

Prof. Nir Tessler, Technion, Israel

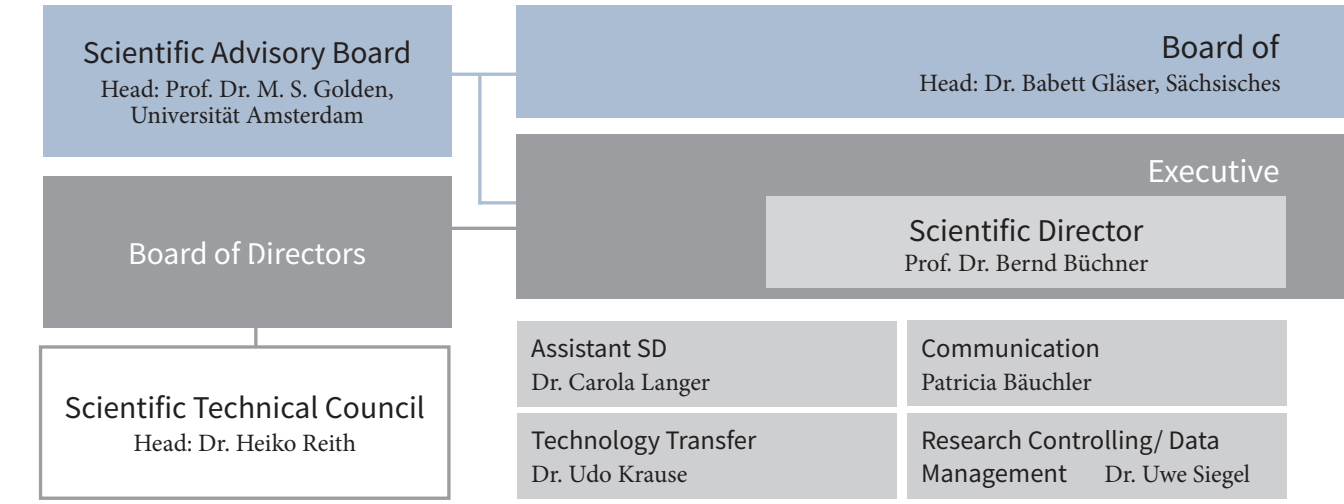

Institute for Solid State Research

Professorship Experimental Physics, TU Dresden

Prof. Dr. Bernd Büchner

- Surface Dynamics / SAWLab
  Dr. Hagen Schmidt
- Transport and Scanning Probe Microscopy
  Dr. Joseph Dufouleur(3)
  Dr. Vilmos Kocsis
  Dr. Thomas Mühl
  Dr. Yulia Krupskaya
- Nanoscale Chemistry
  Dr. Alexey Popov
  Dr. Silke Hampel
  Dr. Evgenia Dmitrieva
- Magnetic Properties
  Dr. Hans-Joachim Grafe
  Dr. Anja Wolter-Giraud
- Electronic and Optical Properties
  Prof. Dr. Martin Knupfer
  Dr. Andreas Koitzsch
  Dr. Aliaksei Charnukha[2]
- Synchrotron Methods
  Dr. Sergey Borisenko
  Dr. Alexander Fedorov[5]
- Crystal Growth and Synthesis of Inorganic Materials
  Dr. Sabine Wurmehl
- Endowed Professorship Electron Optics, TU Dresden
  Prof. Dr. Axel Lubk

Institute for Metallic Materials

Professorship Metallic Materials and Metal Physics, TU Dresden

Prof. Dr. Kornelius Nielsch

- Magnetic Materials
  Dr. Thomas G. Woodcock
- Functional Oxide Layers and Superconductors
  Dr. Ruben Hühne
- Superconducting Nanodevices
  Dr. Nicola Poccia[1]
- Transport in Thermoelectrics
  Dr. Nicolás Pérez Rodriguez
- Micro System Technology
  Dr. Heiko Reith
- Nanograined Bulk Thermoelectrics
  Dr. Ran He[1]
- Interface Engineering of Functional Materials
  Prof. Dr. Kornelius Nielsch
- TE Module Engineering
  Dr. Pingjun Ying
- Surface-Functionalized Materials
  Dr. Amin Bahrami
- Twisted 2D-Materials
  Dr. Golam Haider

Institute for Materials Chemistry

Professorship Materials Chemistry, TU Dresden

Prof. Dr. Anjana Devi

- Molecules to Materials
  Prof. Dr. Anjana Devi
- Structure Analysis
  Dr. Thomas Gemming
  Dr. Ivan Kaban
- Chemistry for Functional Materials
  Dr. Annett Gebert
- Sustainable Nanomaterials
  Dr. Fabian Paulus[4]
- Nanostructured Thin Film Materials
  Dr. Harish Parala
- Alloy Design and Processing
  Professorship Development and Functionalization of Metallic Materials, TU Bergakademie Freiberg
  Prof. Dr. Julia K. Hufenbach
  Dr. Uta Kühn
  Prof. Dr. Jens Freudenberger

Update: March 2025

Trustees
Staatsministerium für Wissenschaft, Kultur und Tourismus

Board

Administrative Director
Juliane Schmidt

Work Council
Head: Dr. Hans-Joachim Grafe

- Assistant AD/ Compliance — Stefan Leipnitz
- Safety and Environment — Uwe Schmiel
- Building Team — Marco Heger
- Data Security Officer — Dr. Heiko Haaz (external)

Institute for Emerging Electronic Technologies

Professorship Emerging Electronic Technologies, TU Dresden

Prof. Dr. Yana Vaynzof[1]

- Perovskite Photovoltaics — Prof. Dr. Yana Vaynzof[1], Dr. Boris Rivkin
- Quantum Dot Photovoltaics — Prof. Dr. Yana Vaynzof[1]
- Magnetic Microstructures and Devices — Prof. Dr. Rudolf Schäfer, Dr. Volker Neu, Dr. Andy Thomas
- Quantum and Topological Photonics — Dr. Libo Ma
- Acoustic Microsystems/ SAWLab — Dr. Andreas Winkler

Institute for Theoretical Solid State Physics

Professorship Theoretical Solid State Physics, TU Dresden

Prof. Dr. Jeroen van den Brink

- Theoretical Solid State Physics — Prof. Dr. Jeroen van den Brink
- Quantum Chemistry — Dr. Liviu Hozoi
- Topological States — Dr. Ion Cosma Fulga
- Computational Methods for Correlated Materials — Dr. Oleg Janson[3]
- Quantum Transport Theory — Dr. Shu Zhang[3]
- Machine Learning for Materials Science — Dr. Dmitrii Cherniavskii
- Numerical Solid State Physics and Simulation — PD Dr. Manuel Richter

Administration
Juliane Schmidt

- Finance and Controlling — Dirk Rehn
- Funding and Cooperation — Dr. Sascha Balakin
- Human Resources — Michael Stritzke
- Purchase and Disposal — Kristin Schwencke
- Library — Jana Sonnenstuhl

Research Technology
Prof. Dr. Dirk Lindackers

- Electrical Engineering — Karsten Peukert
- Mechanical Engineering — Dr. Ralf Voigtländer
- Information Technology — Thomas Fichte
- Building and Facility Management — Veit Köhler

- Ombudsperson — Dr. Manuel Richter
- Representative for disabled employees — Dr. Silke Hampel
- Equal Opportunities Officer — Dr. Anke Kirchner
- Information Security Officer — Benedict Voßbein (external)

[1] ERC Group // [2] Emmy Noether Research Group // [3] Leibniz Junior Research Group // [4] Joint Junior Research group with HZB

Zahlen und Fakten 2024

Das IFW Dresden ist eines der größten Forschungsinstitute Sachsens und Mitglied der Leibniz-Gemeinschaft. Als Leibniz-Institut mit gesamtstaatlicher Bedeutung wird das IFW gleichermaßen vom Bund und dem Land Sachsen gefördert. Wir unterhalten enge Kooperationen mit Universitäten, anderen außeruniversitären Forschungseinrichtungen und Partnern aus der Industrie auf nationaler und internationaler Ebene. Neben dem wissenschaftlichen Auftrag ist die Ausbildung von Nachwuchs im wissenschaftlichen, technischen und administrativen Bereich ein wichtiger Bestandteil unserer Arbeit.

Sowohl Chancengleichheit als auch Familienfreundlichkeit sind erklärte Ziele des IFW Dresden. Im Jahr 2024 lag der Frauenanteil in wissenschaftlichen Positionen bei 33 Prozent und der Anteil von Frauen in wissenschaftlichen Führungspositionen bei 26 Prozent.
Wir unterstützen unsere Beschäftigten dabei, Familienleben und berufliche Anforderungen in Einklang zu bringen. Seit dem Jahr 2007 ist das IFW Dresden mit dem *"audit berufundfamilie"* zertifiziert.

Facts und Figures 2024

IFW Dresden is one of the largest research institutes in Saxony and a member of the Leibniz Association. As a Leibniz Institute of national importance, the IFW is supported by the federal government and the state of Saxony. We maintain national and intenational cooperations with universities, other research institutions and industrial partners.
In addition to the scientific mission, the training of the scientific, technical and administrative staff is an important part of our work.

Equal opportunities and family friendliness are declared goals of IFW Dresden. In 2024, the proportion of women in scientific positions was 33 percent and the proportion of women in scientific management positions 26 percent.

We support our employees in reconciling family life and professional requirements. IFW Dresden has been certified with the *"audit berufundfamilie"* since 2007.

Foto: Jürgen Lösel

2024

4
Research areas

477
Employees

15
Research topics

from
36
Nations

184 female
293 male

5
Institutes

348
journal articles

380
Participants in scientific conferences

3500
Visitors at public events

24
PhD theses

9
Diploma and master theses

3
Bachelor theses

Finanzierung
Financing

Institutionelle Förderung durch Bund und Länder
Institutional funding by the federal government and the federal states

43,1 Mio. EUR
davon Investition Neubau/ including new build investment: 6,2 Mio EUR

Bewilligte Drittmittel
Third party funding

14,7 Mio. EUR

davon/ including:
Deutsche Forschungsgemeinschaft/ German Research Foundation: 6,1 Mio. EUR
Leibniz-Gemeinschaft/ Leibniz Association: 0,8 Mio. EUR
Bund und Freistaat Sachsen/ Federal Government and State of Saxony: 4,2 Mio. EUR
Europäische Union/ European Union: 2,6 Mio. EUR
Industrie/ Industrial contact: 0,8 Mio. EUR
Stiftungen und andere Geldgeber/ Foundations and other donors: 0,3 Mio. EUR

Beschäftigte
Personnel

Gesamtzahl der Beschäftigten: 31.12.2024
Personnell total: 31.12.2024

477
davon/ including:
Wissenschaftliches Personal/ Scientific staff: 298
Wissenschaftsunterstützendes Personal/ Science support staff
(Technisches Personal und Verwaltungspersonal/ Technical and Administrative staff): 167
Auszubildende/ Apprentices[1)]: 12

Doktorandinnen und Doktoranden/ Doctoral students: 90
Stipendiatinnen und Stipendiaten/ Scholarship recipients: 26
Gastwissenschaftlerinnen und Gastwissenschaftler/ Guest scientists[2)]: 81

[1)] 6 verschiedene Ausbildungsberufe sowie Student*innen der Berufsakademie/ 6 different training occupations and students of the training academy
[2)] Eingebunden in die IFW-Forschung, über Forschungskooperationen finanziert/ Integrated in the IFW research, financed by research cooperations

Kuratorium
Board of Trustees

Dr. Babett Gläser
Sächsisches Staatsministerium für Wissenschaft, Kultur und Tourismus, Germany
Vorsitzende / Chair

Peter Hassenbach
Bundesministerium für Bildung und Forschung, Germany

Prof. Dr. Angela Rösen-Wolff
Technische Universität Dresden, Germany

Prof. Dr. Maria-Roser Valenti
Goethe-Iniversität Frankfurt am Main, Germany

Wissenschaftlicher Beirat
Scientific Advisory Board

Prof. Dr. Mark Golden
Universiteit van Amsterdam, Netherlands
Vorsitzender / Chair

Prof. Dr. Robert H. Blick
Universität Hamburg, Germany

Prof. Dr. Andrey Chubukov
University of Minnesota, USA

Prof. Dr. Judith Driscoll (until Sept. 30, 2024)
University of Cambridge, United Kingdom

Dr. Damian Dudek (since Oct. 1, 2024)
VDE, Germany

Prof. Dr. Laura Herz (since Oct. 1, 2024)
Univ. of Oxford, United Kingdom

Prof. Dr. Peter Hirschfeld (since Oct. 1, 2024)
Univ. of Florida, USA

Prof. Dr. David Johnson
University of Oregon, USA

Dr. Yves Küsters
Siemens AG, Germany

Prof. Dr. Silvia Picozzi
University of Milan-Bicocca, Italy

Prof. Dr. Nini Pryds
Danmarks Tekniske Universitet, Denmark

Prof. Dr. Roberto De Renzi
Università di Parma, Italy

Prof. Dr. Artur Zrenner
Universität Paderborn, Germany

Stipendien
Scholarships

Über das Jahr 2024 waren 52 Stipendiatinnen und Stipendiaten am IFW Dresden tätig. Darunter waren zehn Fellows der Alexander von Humboldt-Stiftung.
In 2024, 52 scholarship holders worked at IFW Dresden. Among them were ten scholarship holders of the Alexander von Humboldt Foundation.

Publikationen
Publications

In 2024 haben IFW-Wissenschaftler*innen 348 referierte Zeitschriftenartikel veröffentlicht, eine beträchtliche Anzahl von ihnen in sehr renommierten Zeitschriften.
In 2024, IFW scientists have published 348 refereed journal articles, a considerable number of them in high impact journals.

Eine ausführliche Publikationsliste ist auf unserer Homepage verfügbar:
A detailed list of publications is available on our homepage:

https://www.ifw-dresden.de/research/publications

Rufe
Calls on Professorships

Dr. Nicola Poccia
University of Naples Federico II, Italy

Dr. Shuping Guo
Liaoning University Shenyang, China

Externe Auszeichnungen
External Awards

Prof. Dr. Rudi Hackl
APS Outstanding Referee 2024

Philipp Schulmeyer
W. Terence Coakley Award, Acoustofluidics 2024, Uppsala, Sweden

Interne Auszeichnungen
Internal Awards

Die Ehrenfried Walther von Tschirnhaus-Plakette wird jedes Jahr an Dissertationen mit dem Prädikat summa-cum-laude verliehen. Im Jahr 2024 erhielten diese Auszeichnung:
The Ehrenfried Walther von Tschirnhaus-Medal of the IFW Dresden for excellent PhD theses was awarded to:

Dr. Lotte Mertens

Dr. Johanna Fischer

Dr. Ran Ji

Dr. Miguel Albaladejo Siguan

Dr. Bastian Rubrecht

Dr. Denys Kononenko

Dr. Andrii Kuibarov

Dr. Satyakam Kar

Wissenschaftliche Konferenzen
Scientific Conferences

27. - 28. Februar	Kick-off Meeting MSCA Doctoral Network EIFFEL, IFW Dresden
18. - 20. März	Workshop Microprinting, Bad Schandau
11. - 12. Juli	Quantum Materials Summer School (QMatS 2024, hybrid, Kiew and Dresden)
19. August	Kick-off Additive Manufacturing: Pro Material Lausitz, Zittau/Görlitz University of Applied Sciences
9. - 13. September	Summer School "Advanced Materials", Dresden
1. - 2. Oktober	Teacher training “Quantum physics in grade 12”, IFW Dresden
7. - 11. Oktober	International Workshop Novel Superconducting Materials 2024, IFW Dresden
29. Oktober	EFDS-Fachausschuss „Optik, Elektronik & Energie“, IFW Dresden

Veranstaltungen
Events

8. - 9. März	Wissenschaftsfestival SPIN2030 in den Technischen Sammlungen Dresden
25. April	Girls'Day 2024
25. Mai	Demonstration "Gemeinsam für Demokratie" der Wissenschaft und Kultur in Dresden
30. Mai	Sommertag zum Thema Gesundheit
12. Juni	Teilnahme an der 15. Rewe Team Challenge
14. Juni	Dresdner Lange Nacht der Wissenschaften
04. August	Tag des Offenen Regierungsviertels Dresden
07. Oktober	Ausstellungseröffnung "Material im Fokus", Fotoausstellung im IFW Dresden

Oben: Faszination Wissenschaft beim Tag des Offenen Regierungsviertels im August (links) wie auch zur Dresdner Langen Nacht der Wissenschaften im Juni 2024 (rechts): Das IFW Dresden engagiert sich in vielen Projekten für die MINT-Bildung der jungen und jüngsten Generation.
Unten: Gemeinsam zum Ziel: Sowohl wissenschaftlich als auch darüber hinaus sind wir im Team einfach besser als allein. Unsere glücklichen Läuferinnen und Läufer bei der REWE-Team-Challenge 2024.

Above: Fascination of science at the Open Government Quarter Day (left) and the Dresden Science Night (right): The IFW Dresden is involved in many projects for the STEM education of the young generation.
Below: Reaching the goal together: In science and beyond, we are simply better as a team than alone. Our lucky runners at the REWE Team Challenge 2024.


Noel
Uwe
Stefan
Marietta
Jiang
Titouan
Mostafa
Riccardo

Geistiges Eigentum / Patente
Intellectual Properties / Patents

Zum 31. Dezember 2024 hielt das Leibniz-Institut für Festkörper- und Werkstoffforschung Dresden 67 Patente in Deutschland und 50 internationale Patente.
By 31 December 2024, the Leibniz Institut for Solid State and Materials Research holds 67 patents in Germany and 50 international patents.

Erteilte Patente
Patent grants

DE 10 2024 103 977.9
02.12.2024
Verfahren zur Defektdetektion additiv gefertigter Bauteile mittels in situ Schallemissionsanalyse
invented by Dmitry Chernyavsky, Konrad Kosiba, Denys Kononenko, Julia Kristin Hufenbach, Jeroen van den Brink

DE 10 2019 116 526
08.11.2024
Verfahren und Vorrichtung zur Bestimmung der Position von Objekten
invented by Daniil Karnaushenko, Oliver G. Schmidt

EP 22 216 944.3
03.09.2024
Measurement circuit and method to measure a physical characteristic of a device
invented by Viktor Koenye, Joseph Dufouleur, Cosma Fulga, Jan Budich, Jeroen van den Brink

DE 10 2023 119 113.6
25.07.2024
Modulare Vorrichtung zur Bestimmung von richtungsabhängigen Eigenschaften von Schichten und Schichtsystemen
invented by Hagen Schmidt, Günter Martin

DE 10 2020 118 268
21.06.2024
Verfahren zur Herstellung eines magnetokalorischen Drahts, magnetokalorischer Draht und dessen Verwendung
invented by Maria Krautz, Jens Freudenberger

DE 10 2018 128 438.1
10.06.2024
Verfahren zur Herstellung von einteiligen Gelenken, Aktoren, Sensoren, Hub- und Verstellelementen, Stellgliedern in Regelkreisen oder Federpaketen in Dämpfungssystemen aus Formgedächtnismaterial sowie einteilige Gelenke, Aktoren, Sensoren, Hub- und Verstellelemente, Stellglieder in Regelkreisen oder Federpakete in Dämpfungssystemen aus Formgedächtnismaterial
invented by Simon Pauly, Konrad Kosiba, Uta Kühn

DE 10 2023 107 385.0
29.04.2024
Natrium-Ionen-Sekundärbatterie, Verfahren zur Herstellung einer Natrium-Ionen-Sekundärbatterie und deren Verwendung
invented by Björn Pohle, Alexander Thomas, Daria Mikhailova

Patentanmeldungen
Priority patent applications

EP 24 215334.4
26.11.2024
Vorrichtung zur Detektion von Partikeln im Fluß
invented by Andreas Winkler, Hagen Schmidt, Simon Göllner, Andre C. Stiel

DE 10 2024 124 456.9
27.08.2024
Hochleistungsfähige Aluminiumlegierung für die Fertigung von Leichtbauteilen
invented by Philip Grimm, Julia Kristin Hufenbach, Gianaurelio Cuniberti

EP 24 382802.7
23.07.2024
System and method for detecting ice accretion
invented by Andreas Winkler, Julio Mora Nogués, Paloma García Gallego, Francisco Carreño Puertas, Ana Isabel Borrás Martos, Agustín R. Elipe, Jaime del Moral, Juan Ramón Sánchez Valencia, Víctor Joaquín Rico Gavira, Miguel González del Val

DE 10 2024 119 835.4
12.07.2024
Elektroakustisches Messsystem und Verfahren zur Detektion und Dickenmessung von Eisbeladungen auf aerodynamischen Strukturen
invented by Philipp Schulmeyer, Hagen Schmidt, Manfred Weihnacht, Thomas Rische

DE 10 2024 119 648.3
10.07.2024
Elektroden für mikroakustische Bauelemente
invented by Marietta Seifert, Thomas Gemming, Hagen Schmidt

DE 10 2024 117 629.6
21.06.2024
Verfahren und Vorrichtung zur Erzeugung von Magnetfeldern mit hohen magnetischen Flussdichten
invented by Thomas Mühl, Sathyadharma Prasad Aniruddha, Rachappa Ravishankar

EP 24 172115.8
24.04.2024
Oscillator circuit and method of operating the oscillator circuit
invented by Joseph Dufouleur, Torsten Seidemann

DE 10 2024 110 931.9
18.04.2024
Sensor für Behälterinnenräume
invented by Thomas Windisch, Hagen Schmidt, Dirk Lindackers

DE 10 2024 105 991.5
01.03.2024
Akustofluidische Vorrichtung zur Erzeugung von Aerosolen
invented by Iman Frozanpoor, Mehrzad Roudini, Yara Alsaadawi, Andreas Winkler

DE 10 2024 103 977.9
13.02.2024
Verfahren zur Defektdetektion additiv gefertigter Bauteile mittels in situ Schallemissionsanalyse
invented by Dmitry Chernyavsky, Konrad Kosiba, Denys Kononenko, Julia Kristin Hufenbach, Jeroen van den Brink

EP 22 743 485.9
16.01.2024
Vorrichtung und Verfahren zur elektrischen Charakterisierung von Eigenschaften von Stoffen, Baugruppen und/oder Bauteilen in einer Umgebung mit hoher Temperatur
invented by Thomas Windisch, Hagen Schmidt, Robert Weser, Uwe Biscop

Dissertationen
PhD Theses

Felix Anger
Festkörpereinkristallzüchtung von LaOFeAs und dessen Substitutionsvarianten

Miguel Albaladejo-Siguan
Colloidal Metal Sulfide Quantum Dots for Application in Charge-Generating Devices

Bhargava Balaganchi Anantha Ramu
Imperfections in non-Hermitian topological systems

Melanie Colditz
From chip to Demonstrator - Biological Sample Separation using Surface Acoustic Wave-based Microfluidics

Louis-Philip Doctor
Spectroscopic Investigations of Excitons in Metal-Phtalocyanine Thin Films

Mohamed Sabry Eldeeb
Magnetic interactions in systems with strong spin-orbit coupling

Lukas Fink
Wachstum, Charakterisierung und Funktionalisierung von Schichten für thermomagnetische Mikrosysteme

Johanna Fischer
Biopolymerbasierte Materialien als Precursoren für elektrochemische Anwendungen

Jan-Niklas Huster
Development of Aluminium, Ruthenium and Tin Complexes as New Precursors for Thin Film Processing via Vapor Phase Deposition Methods

Ran Ji
Photovoltaics

Satyakam Kar
Größendefekte in Formgedächtnis-Mikroaktoren

Parmish Kaur
Precursor Engineering for ALD/MLD Processing of Functional Materials

Denys Kononenko
Electronic structure of magnetic cuprates: a machine learning approach

Andrii Kuibarov
Finding routes to topological superconductivity with PtBi2

Yejin Lee
Magneto thermoelectric and magnetoelectric measurements of quantum materials

Lotte Mertens
Breaking Boundaries. Charge Density Waves, Quantum Measurement, and Black Holes in Theoretical Physics

Abdullah Mohamed
Exploring Novel Approaches for Enhancing the Electrochemical Performance of Li-ritch Antiperovskite Cathodes for Li-ion Batteries

Martin Nichterwitz
Magneto-ionic properties of metal/oxide heterostructures in different geometries and electrolytes

Fatemeh Rajabasadi
4D printed microrobots for assisted reproduction

Bastian Rubrecht
Thermodynamic investigation of emergent magnets with aspects of magnetic frustration and/or topology

Sanaz Shokri
Electronic and thermoelectric transport in automatically thin van der Waals cuprate superconductors

Martin Wilken
Chemical Strategies in Vapour Phase Deposition Techniques for Nanostructured Transition Metal Sulfide and Oxide Thin Films

Jan-Lucas Wree
Vapor phase deposition of layered transition metal sulfide and oxide thin films: From precursor design toward nanostructred application

Jun Yang
Ferecrystals based on Atomic Layer Depostion

Studentische Abschlussarbeiten
Graduation theses

Carolin Dellf
Perfusion von biodegradierbaren FeMnCS-Stents, Diplomarbeit

Marcus Dietzel
Entwicklung eines supraleitenden Lagers zur Verlustreduktion in supraleitenden Dynamos, Diplomarbeit

Ariane Reif
Transporteigenschaften bei tiefen Temperaturen von ternären Tetradymit Thermoelektrika Bi2Se3-xTex und Sb2Se3-xTex, Diplomarbeit

Johannes Emil Saske
Einfluss der Anordnung von Permanentmagneten auf die Levitationskräfte von Supraleitern, Diplomarbeit

Nele Kheim
Separation of Extracellular Vesicles from Biological Suspensions using SAW-based Microfluidics, Masterarbeit

Amit Kotadiya
Study of Gold-based thin film transducers for highly efficient SAW-basedaerosool generation, Masterarbeit

Emma Markwardt
Biomedical Applications of Surface Acoustic Waves based acoustofluidics, Masterarbeit

Jorge Isaac Sandoval
Study of Magnetic Bistability and Relaxation Dynamics in Hetero-atomic Endohedral Metallofullerene Magnets, Masterarbeit

Kilian Srowik
Thermodynamical characterization of the topological superconductor candidate γ-PtBi2, Masterarbeit

Radmila Kyrychenko
Symmetry study of superconductor PtBi2 by convergent beam electron diffraction, Bachelorarbeit

Tim Schulze
Lithium NMR Untersuchung von Lithium-Batterie-Materialien (Li2FeSo & Li2FeSeO), Bachelorarbeit

Felix Urban
Die Lösligkeit des Zn in der ferromagnetischen Phase tau-MnAl, Bachelorarbeit

quantum

function

Sustainability

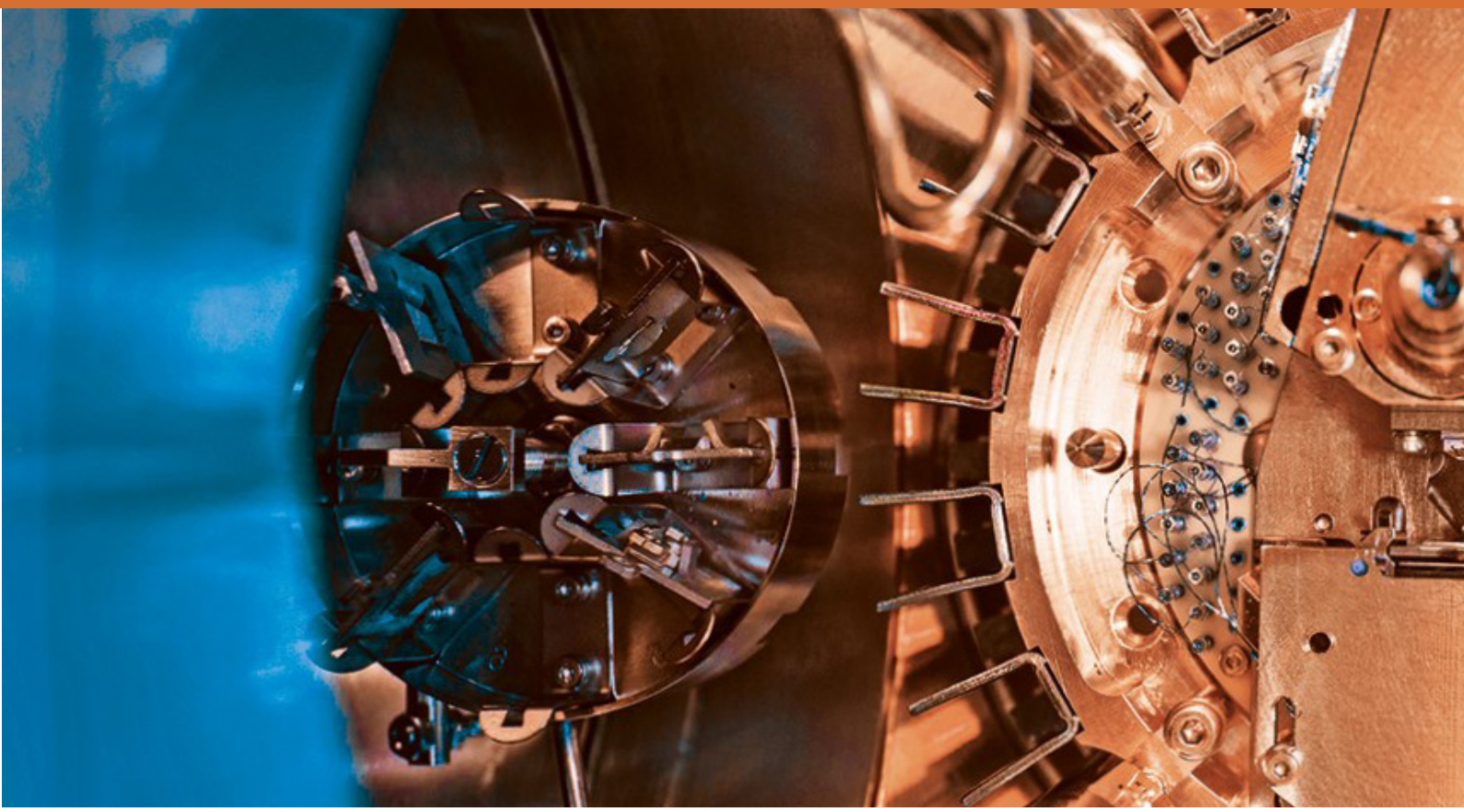

Leibniz Gemeinschaft

SACHSEN

Dieses Institut wird mitfinanziert durch Steuermittel auf der Grundlage des von den Abgeordneten des Sächsischen Landtags beschlossenen Haushaltes.

Zertifikat seit 2007
audit berufundfamilie